DREW UNIVERSITY, MADISON, NJ

Kinetics and Mechanism of Carbonyl Substitution of $Os_3(CO)_{10}(\mu\text{-}I)_2$ by $P(OR)_3$

A Thesis in Chemistry

by

Cristabella R. Fortna

Submitted in Partial fulfillment of the requirements
of an ACS-Approved Bachelor of Science degree
with Specialized Honors in Chemistry

Examining Committee:

Dr. Mary-Ann Pearsall, Advisor, Chemistry Department

Dr. Ryan Hinrichs, Chemistry Department

Dr. Sandra Jamieson, English Department

14 May 2023

TABLE OF CONTENTS

Abstract

The study of catalysis by organometallic compounds is a well-established field that has more recently focused on transition metal carbonyl clusters. While transition metal carbonyl clusters are not inherently catalytically active, they serve as unique structural templates that can be helpful in designing new homo- and heterogenous catalysts. The introduction of halogens onto carbonyl clusters has been shown to activate the cluster towards carbonyl substitution. This study reports the kinetics and mechanism of carbonyl substitution of the dihalo-bridged cluster $Os_3(CO)_{12}I_2$ with $P(OR)_3$ (R = Me, Ph) as a novel structural motif that may be employed or integrated in future homogenous organometallic catalysts. Substitution of the carbonyls trans to the metal-metal bond was found to be first order in cluster and zero order in ligand. This substitution is proposed to proceed through two rate-controlling steps, forming a monosubstituted intermediate compound $Os_3(CO)_9I_2[P(OR)_3]$ before then producing the final compound $Os_3(CO)_9I_2[P(OR)_3]_2$. These steps are proposed to involve the breaking of a metal-metal bond. This reaction was investigated at temperatures of 49-69 ^oC and values of k_1 were found to range from 1.67×10^{-4} to 2.59×10^{-3} sec^{-1}, and k_2 was found to range from 9.31×10^{-5} to 3.47×10^{-3} sec^{-1} with temperature. Propagated error of k_2 is quite large and thus conclusive statements regarding step two cannot be made at this time. Each step was found to be independent of ligand identity, and that the rate of the second step is not affected by the first addition of $P(OR)_3$. The activation energy was found to approximate 120 kJ/mol for the first substitution of each $P(OR)_3$. The propagated error of k_2 prevents conclusive kinetic or thermodynamic analysis of the second substitution of $P(OR)_3$. This investigation provides a kinetic and mechanistic understanding of the behavior of dihalo-bridge transition metal clusters that may prove beneficial as a structural template for the design of new compounds and homogenous catalysts.

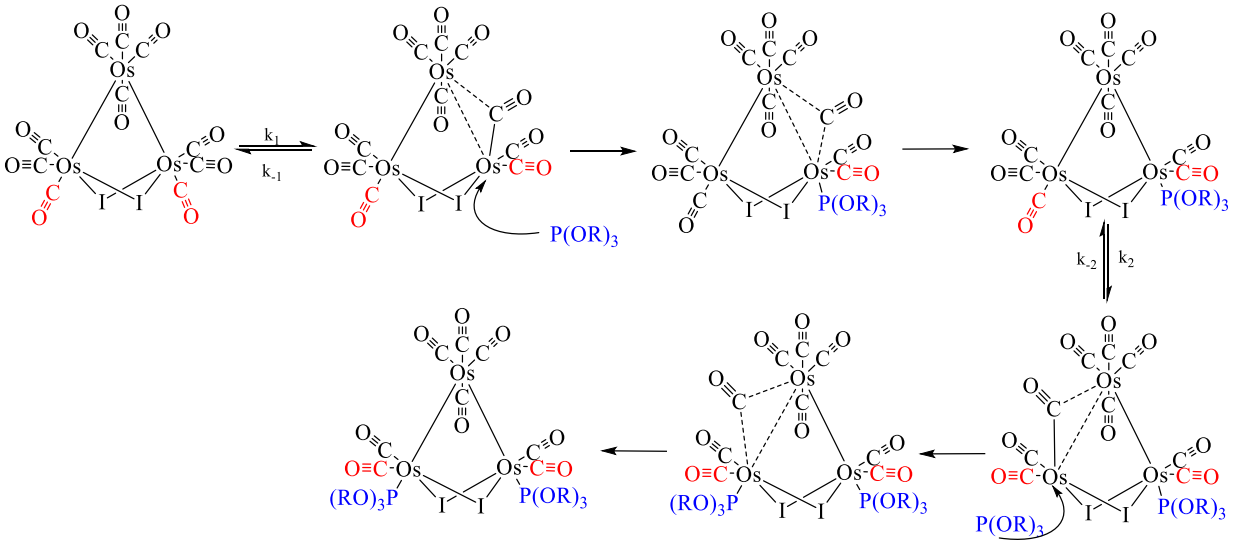

Fig iii. Proposed mechanism of carbonyl substitution by $P(OR)_3$ ligands, consistent with data reported in this study. The rate-limiting step is proposed to be the breaking of the Os-Os bond, which is then partially stabilized by an adjacent CO.

Introduction

Catalysis

Catalysts are substances that increase the rate of a chemical process yet do not undergo chemical change themselves. A catalyst, therefore, is something that increases the rate of reaction, yet is regenerated at the end of the chemical process it facilitates to thus catalyze multiple cycles. While catalytic processes are not essential for all chemical reactions, catalysis is extremely common. Biologically, enzymes catalyze most reactions by bringing and holding substrates in close proximity to one another to react in a specific manner, one that may not otherwise occur. Industrially, catalysts are employed not only to more effectively produce a desired compound, be that faster or lower-energy syntheses, but also to create single products that would not otherwise be produced naturally. In organic chemical synthetic pathways often employed in pharmaceutical production, catalysts facilitate stereoselectivity, the favoring of one chiral center over another, as biological systems—the human body, more specifically—are incredibly stereospecific. Catalysts and catalytic pathways are everywhere.

Catalysts can be described as heterogenous or homogenous. Heterogenous catalysts are those that are in a different phase than the reacting compounds, while homogenous catalysts are in the same phase as the reacting compounds. Heterogenous catalysts, such as a bulk metal surface over which reagents can be passed, can be easily separated from the products[1] but are not very specific in which reactions they facilitate, often encouraging multiple synthetic routes that cannot be controlled. Thus, bulk metals as catalysts are highly reactive but low in reaction specificity.

One example of a common heterogenous, bulk-metal catalyst is Raney Nickel. A porous, Nickel-Aluminum alloy, Raney Nickel is an activated metal surface that is used to desulfurize thioacetals that can reduce ketones through a two-step process[2]. While the mechanism is unclear, the activated Nickel surface has adsorbed hydrogens that attach to an incoming substrate; these hydrogens ultimately replace the sulfur atoms of either the thioacetal substrate or intermediate, resulting in an alkane carbon chain or a ketone. A simplified example of such processes is shown in Figure 1.

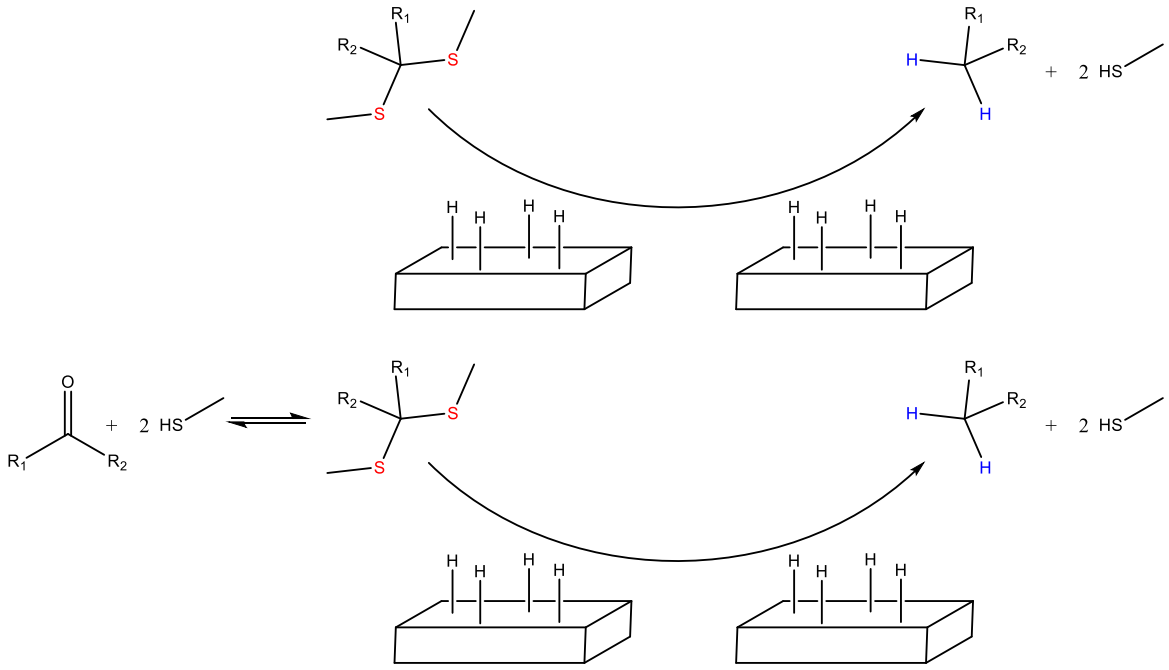

Fig. 1. Top: Desulferization of thioacetal by Raney Nickel surface. Bottom: Reduction of ketone via two-step process involving Raney Nickel. For each, the bulk metal surface is, in essence, unaffected by these processes and thus after an appropriate industrial-scale turnover of product, the Raney Nickel can simply be removed from the reaction solution.

It is important to note that the surface of the bulk metal, and therefore the heterogenous catalyst itself, is unaffected by the reaction it catalyzes and can thus be very easily retrieved from the reaction conditions. Catalysis by heterogenous catalysts like Raney Nickel are not tremendously specific, in both substrate with which it will react and product it will produce.

Homogenous catalysts, however, are often more specific and can provide more mechanistic insight. One of the most common classes of homogenous catalysts are transition metal complexes.

Transition Metal Complexes

Transition metals, those pertaining to the d-block of the periodic table, have unique chemical properties that make them desirable catalysts for many reactions. While many metals are employed as catalysts due to their high reactivity, bulk metal samples leave much to be desired regarding reaction specificity. In contrast, transition metal complexes have covalently bonded ligands and are much more specific in their reactivity as their geometry is confined to the number of available d-orbitals. Catalytic function, therefore, is dictated by the number and location of vacant coordination sites on the metal core.

In order for a transition metal complex to catalyze a reaction in solution, there must exist, or become available, a vacant coordination site. Vacant sites can occur from displacement of solvent molecules, leaving an opening for ligands to bind.[1] Alternatively, already-coordinated ligands can be displaced by heat, creating a vacant coordination site that can be filled by another incoming ligand in solution. Figure 2 depicts the catalytic cycle of hydrogenation of alkenes by Wilkinson's Catalysts, a common industrial homogenous catalyst to reduce double bonds.

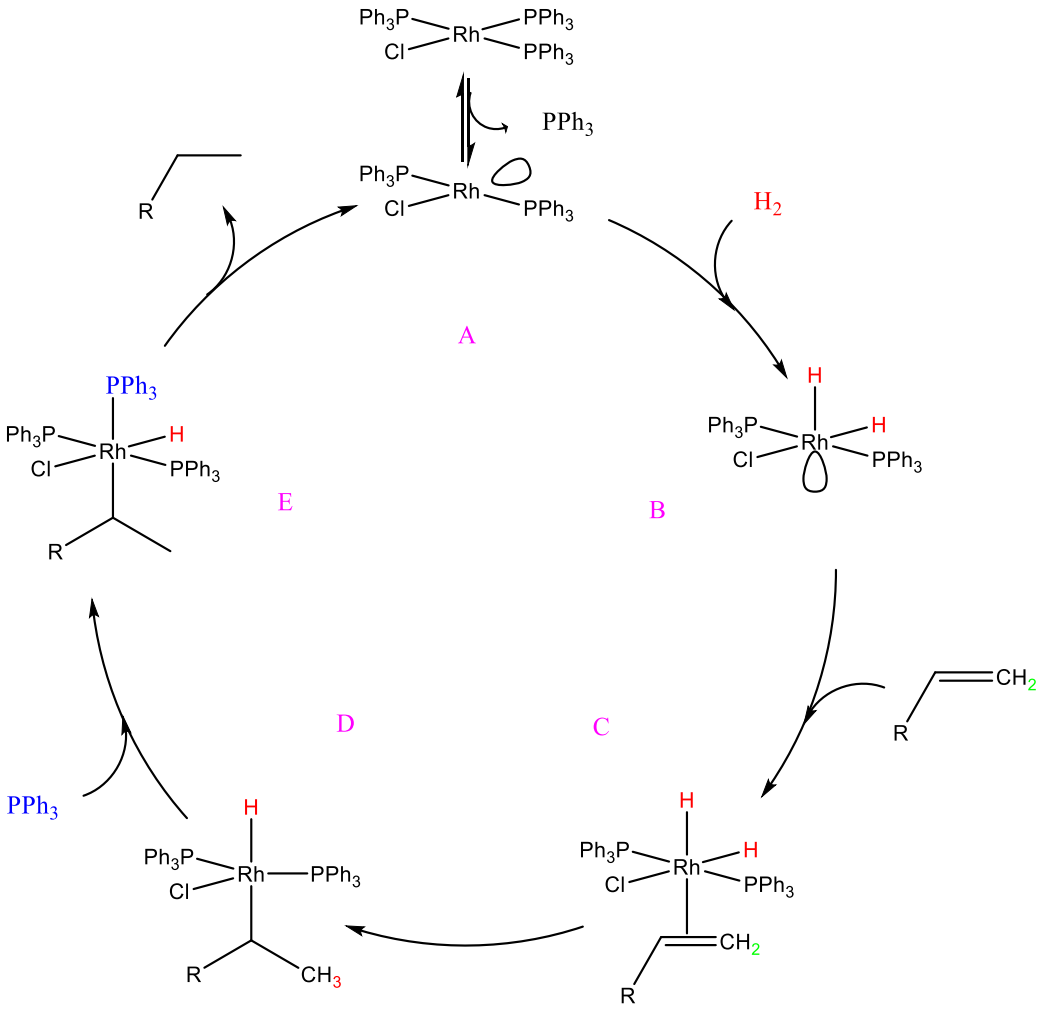

Fig 2 Hydrogenation of an alkene by Wilkinson's Catalyst (A). The coordinatively unsaturated complex A is hydrogenated to B, an alkene can coordinate as shown by C. One of the red hydrogens on the catalyst complex is then added to the alkene in D, creating a CH_3 group rather than the original CH_2. Adding another PPh_3 generates complex E, which then releases the alkane compound to regenerate complex A.

In the cyclical catalytic scheme shown in Figure 2, Wilkinson's Catalyst loses an PPh_3 ligand in solution and becomes the coordinatively unsaturated active catalyst (complex A), which can take on another ligand to reach a maximum allowance of 18 electrons. Complex A is thus hydrogenated (complex B), increasing the electron count but still leaving a vacant site on the transition metal core. This vacant site is where the incoming substrate, in this case an alkene, will coordinate to result in complex C. One of the hydrogens, indicated in red, is then transferred to the alkene (D), changing the green CH_2 to a CH_3, reducing the double bond, and the overall

complex is once again coordinatively unsaturated as the transition metal core has lost a ligand. A PPh_3 ligand then coordinates to form complex E, which then releases the desired product by reductive elimination to regenerate the catalyst, thereby allowing this catalytic cycle to restart.

Within this cyclical mechanism of adding hydrogens to a double bond, the original catalytic complex A is regenerated from complex E by releasing the product through reductive elimination. Note that throughout this cycle, incoming additives could only coordinate to complexes that are coordinatively unsaturated, meaning they have fewer than 18 electrons and/or have a vacant site, like the examples shown in complexes A and B of Fig 2. This is in contrast to the reactions involving Raney Nickel, in which the substrate passes over the surface bulk metal to grab hydrogens from its surface. In the case of homogenous catalysts, like Wilkinson's, the complex is directly involved in the cyclical steps necessary to convert the substrate to product, though the original catalyst is always regenerated in the end, as per the very definition of a catalyst.

Because homogenous catalysts, specifically transition metal complexes, are directly involved in the mechanism of reaction, there is much more specificity in both substrate that coordinates to the catalyst and product that is released from it in the last step. In industrial-scale production of pharmaceuticals, petroleum, and fragrances, for example, greater specificity of the catalyst paired with a wide range of reductive partners results in an incredible variety of available products[3]. Figure 3 presents a comparison of how one catalyst, like Wilkinson's Catalyst, can be employed to produce a wide variety of products that bear their own unique reactivity, thereby exponentially expanding the synthetic applications of such a process.

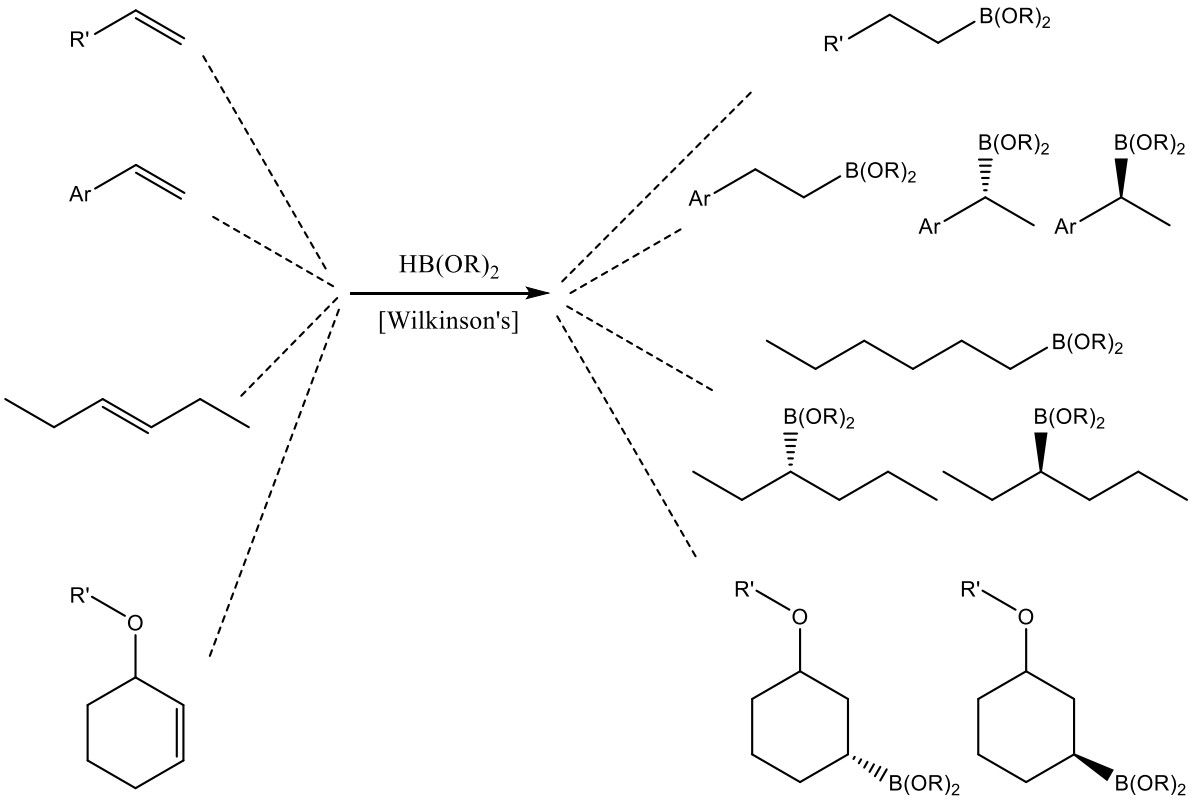

Fig. 3. Non-exhaustive demonstration of the variety of substrates that can react with Wilkinson's Catalyst and the wide variety of their products. Adapted from [*3*]. Note the variety of products obtained from the same reaction conditions but different starting materials.

The hydroboration of alkenes, shown above in Fig 3, is a similar process as described in Fig 2, but the double bond is reduced with the addition of a boron atom rather than a hydrogen. In this case, the use of a homogenous transition metal complex catalyst results in unique products with their own reactivity and selectivity without employing a different catalyst for each synthetic route. This is due to the simple fact that the boron added to the substrate can be distinguished from the hydrogens it already bears, whereas hydrogenation shown in Fig 2 add another hydrogen that cannot be distinguished from the other hydrogens the substrate already has. Looking closely at aryl alkenes, the second row of Figure 3, the $B(OR)_2$ could add to the very end of the molecule, or it can add to the middle; on the middle carbon, $B(OR)_2$ can add to the top and pushing the hydrogen

back (coming out of the page, shown with a bolded wedge), or it can add from below and push the hydrogen forward (going into the page, shown with a dashed wedge). While these are the same possibilities as the hydrogenation shown in Fig 2, there is no difference between adding from the top or from the bottom because the "new" hydrogen cannot be distinguished from the existing hydrogens of the alkene.

Another example of transition metal complexes are those with carbon monoxide (CO) as ligands, referred to as transition metal carbonyl complexes like $Os(CO)_5$ of Figure 4. Many studies have demonstrated that transition metal carbonyl complexes do catalyze some reactions, but such behavior occurs at high temperatures exceeding 100 ˚C[1, 4-6]. Thus, while carbonyl complexes are not inherently catalytic, these complexes are of particular interest due to the unique properties of the carbonyl ligand itself.

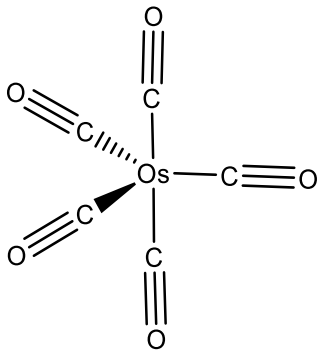

Fig 4. Example of a transition metal carbonyl complex, $Os(CO)_5$

Carbon Monoxide as a Ligand

Free carbon monoxide (CO) is a triply bonded molecule that is described as a strong π-accepting ligand due to the nature of its bonding. Creating any chemical bond can be described as the overlap of electron waves, which are referred to as atomic orbitals. Shown in Figure 5, atomic

orbitals can overlap both in and out of phase with one another to create different molecular orbitals that may, or may not, contribute to the bonding of the molecule.

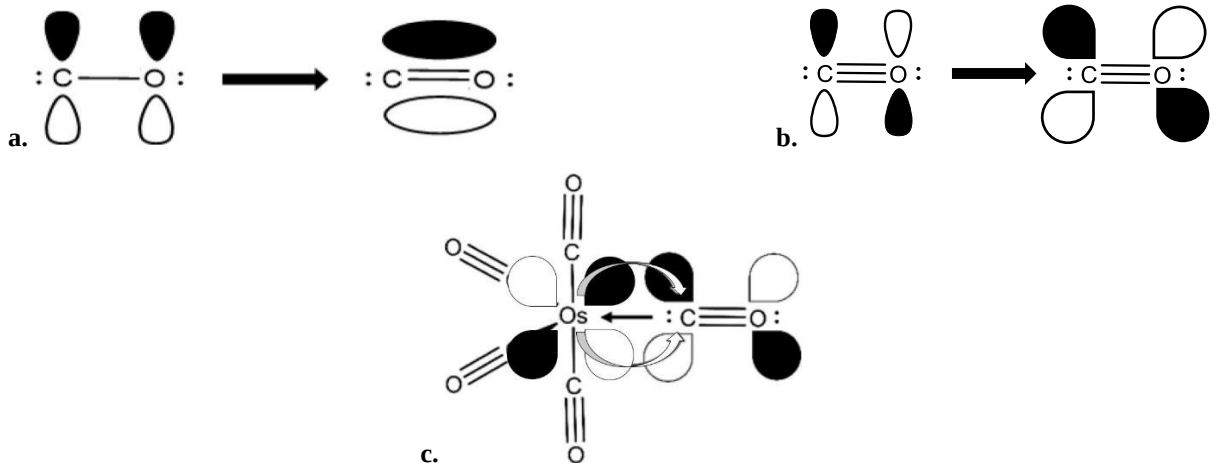

Fig 5 demonstration of electron wave overlap in bond forming events. **a** In-phase overlap of π-type orbital contributing to the triple bond. Additional in-phase overlap of remaining p-orbitals to produce the full triple bond excluded here for demonstrative simplicity. **b** Out-of-phase π-type orbital contributing to the empty anti-bonding orbital. **c** σ-donation from CO and π-acceptance onto the empty anti-bonding orbital.

In forming the triple bond shown between C and O in CO ligands, the p-orbitals of both the carbon and oxygen overlap in-phase, shown as Fig 5a. The electron waves add together, and increase the overall electron density shared between atoms, thereby creating bonding molecular orbital perceived as a bond between the two atoms. Additionally, the electron waves also overlap out of phase (Fig 5b), thereby subtracting mismatched electron density from the sites of overlap, creating an anti-bonding molecular orbital. The anti-bonding molecular orbital does not contribute to the triple bond between C and O because it is empty; should more electrons be added to the system, this is the overall shape they would produce. When CO is coordinated to a transition metal, however, the anti-bonding orbital contributes to the unique qualities of the bonds of the overall molecule.

Depicted in Fig 5c with a black arrow, the lone pair of electrons from the carbon donate to the osmium to create the observed single bond, referred to as σ-donation. Additionally, the osmium can also donate its electrons back onto the empty anti-bonding orbital of the carbon, since the shape of this anti-bonding orbital is compatible with that of the filled d-orbitals on the transition metal center and because they overlap in-phase with one another. This back-donations of osium eletron density back onto the CO ligand shown in Fig 5c is known as π-acceptance. This unique, two-way electron overlap strengthens the Os-C bond, since there are multiple vectors of electron overlap, but weakens that of the C-O triple bond since electron density was added into the higher-energy, less-stable, anti-bonding orbital. This slightly weakened carbonyl bond therefore behaves differently under infrared (IR) light than that of free, unbound, carbon monoxide.

Infrared (IR) Spectroscopy

IR spectroscopy monitors the chemical response to absorption of light in the infrared region, specifically the modes of vibrational stretching of bonds that is induced by the infrared light source. The horizontal axis of IR spectra denotes the wavenumber, which is proportional to the frequency of absorption. Frequency of absorption is related to bond strength; stronger bonds require more energy to vibrate and stretch thus absorb at higher frequencies and appear further left on the IR spectrum. The vertical axis of IR spectra presented within this work is absorbance, which is unitless. The region between 2200 cm^{-1} and 1500 cm^{-1} is where the frequencies of carbonyl vibrational stretching modes of a molecule appear; the exact frequency of absorption reflects the strength of the bond and thus how much energy, supplied by the IR light source within the

instrument, was absorbed in order to excite that vibrational mode. Figure 6 provides a cartoon depiction of many characteristics of CO characterization by IR spectroscopy.

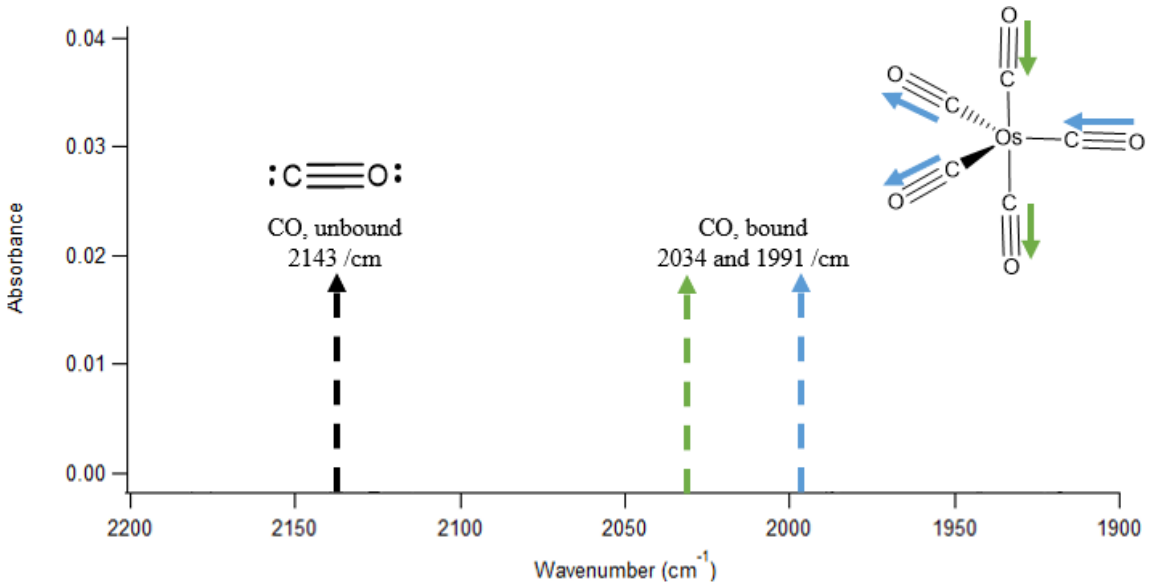

Fig. 6. Cartoon depiction of shifts and splitting of carbonyl peaks of organo-metallic complexes in IR. Free, unbound CO absorbs at a higher frequency than that of coordinated CO, since coordinated CO ligands are weakened by back-donation of the metal. The hypothetical spectrum of $Os(CO)_5$ produces multiple peaks of CO as there are multiple modes of stretching vibrations.

Shown above in Figure 6, free, gaseous CO absorbs in IR at 2143 cm^{-1}. When coordinated to a metal atom, however, the carbonyl triple bond is weakened by the π-acceptance and the absorption is shifted to a lower frequency. Further, when multiple CO are bound to a metal center, many peaks appear as dictated by the symmetry of the molecule. $Os(CO)_5$, in Fig 6 above, has five CO ligands but two peaks as there are two infra-red active modes of vibration of CO bonds. To appear as a peak within an IR spectrum, the vibrating mode must result in a change of the net dipole of the molecule; in the case of $Os(CO)_5$, there are only two modes of vibration that are IR active. The axial (vertical) CO vibrate together, indicated in green in Fig 6, and the three remaining planar CO also vibrate together, indicated in blue in Fig 6. However, the vibration of the axial CO as one mode, and the planar CO as one mode are not equivalent to one another and thus appear as

two distinct absorption peaks at 2034 and 1991 cm^{-1} in Fig 6 above. This pattern of peaks is thus characteristic to the symmetry of the carbonyls of the molecule; as the number of modes of carbonyl vibration are added to the molecule, the number of peaks in the IR spectrum will also increase.

Transition Metal Carbonyl Clusters

Transition metal clusters are compounds that have multiple metal centers bound by at least one covalent metal-metal bond. These differ from complexes with the addition of a metal-metal covalent bond, which is confirmed to exist by the eighteen-electron (18 e^-) rule. The 18 e^- rule is a counting system that accounts for the electrons on the transition metal(s) and those donated by the ligands, much like the octet rule of organic chemistry. The octet rule is often remembered as a simple rule which states that carbon must have eight electrons surrounding it at all times, thereby fulfilling the octet. This is not because eight is some magic number, but rather because carbon atoms only have four valence orbitals, each of which can have two electrons, and thus the maximum allowance of electrons on carbon is eight. Since metals from the d-block have nine available valence orbitals, each of which can hold two electrons, the total quantity of electrons surrounding each transition metal atom will total 18 electrons. This counting system is a method of interpreting bonding of transition metal complexes, but can also be applied to more complicated molecules like di- or tri-nuclear clusters.

In the example shown in Figure 7, there are three osmium centers and twelve associated carbon monoxide ligands. Neutral osmium has eight valence electrons, and each carbonyl contributes two electrons to the osmium atoms, summing to 48 electrons from the formula

$Os_3(CO)_{12}$. However, following the 18 e^- rule, the expected quantity of electrons should total 54 electrons, since there are three osmium atoms that should each be surrounded by 18 electrons. This indicates that the formula $Os_3(CO)_{12}$ is "missing" 6 electrons. Because a standard covalent bond shares two electrons between two atoms, these six "missing" electrons indicate the presence of three metal-metal covalent bonds and thus fulfills the expected 54e^- count as determined by the 18e^- rule.

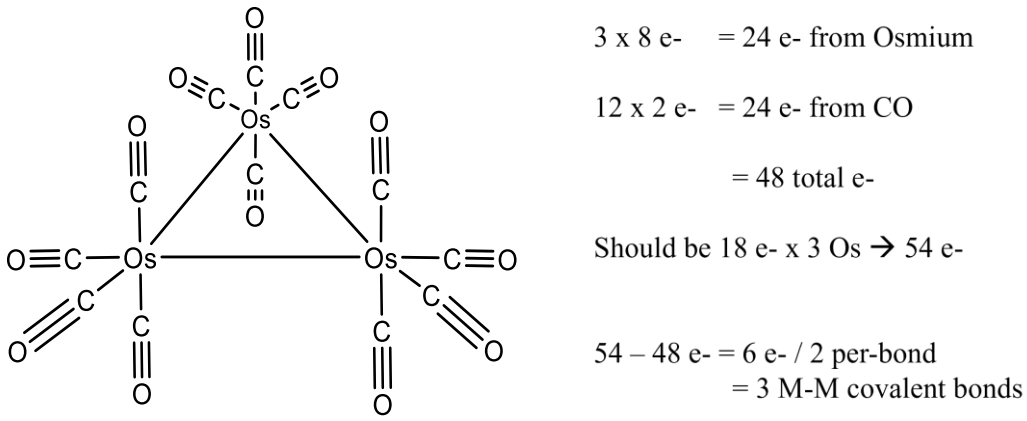

Fig 7 Example of trinuclear metal carbonyl cluster, $Os_3(CO)_{12}$ as an example of the 18 e- rule.

The metal-metal covalent bonds, like those shown in Figure 7, are similar to metallic bonding found in samples of pure metals. This suggests that such covalent bonds have similar reactivity to that of bulk metal. Clusters often have metal-metal bond lengths of similar length of close-packed metal samples and the overall structure of such clusters are often fragmented derivatives of close-packing arrangements.[7]

Reactivity of Triosmium Carbonyl Clusters

In addition to the idea that clusters perhaps have reactivity closer to that of the bulk metal, a comparison of some reactions of triosmium carbonyl clusters reveals their reaction specificity.

Poe and Sekhar investigated the reactions of dodecacarbonyltriosmium with P-donor ligands[5], and obtained a mixture of mono-, di-, and tri-substituted products as summarized in Figure 8 (shown only with $P(OMe)_3$ for simplicity). P-donor ligands refers to any ligand of the type PR_3 or $P(OR)_3$ such that the phosphorous atom is attacking the cluster.

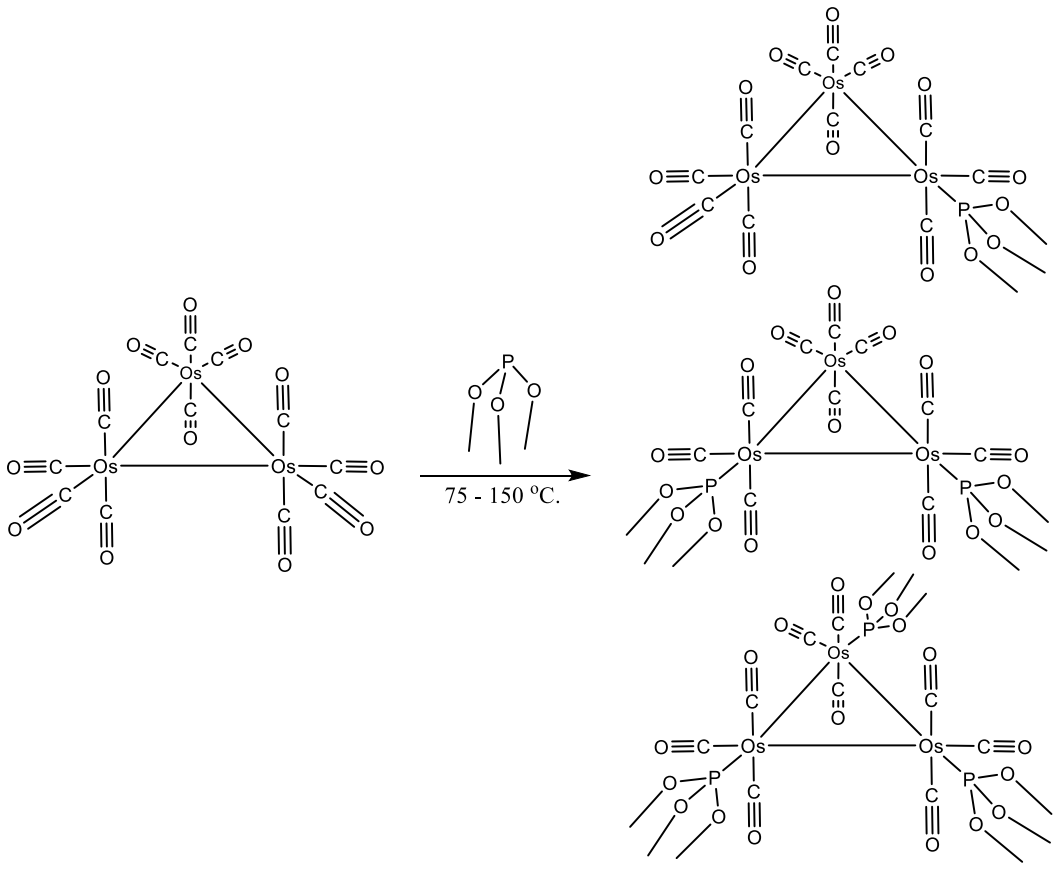

Fig 8 Simplified summary of dodecacarbonyltriosmium ($Os_3(CO)_{12}$) carbonyl substitution by trimethyl phosphite ($P(OMe)_3$) as studied by [5]. $Os_3(CO)_{12}$ reacted at high temperatures and produces a mixture of products.

Reacting dodecacarbonyltriosmium ($Os_3(CO)_{12}$) with P-donor ligands, shown in Figure 8 with trimethyl phosphite ($P(OMe)_3$), produced three products, mono-, di-, and tri-substituted, over a range of temperatures. The lowest temperature investigated by this group was 75 °C in decalin under argon[5]. While this reactivity is a small improvement from that of carbonyl complexes that generally react at 100 °C[1, 4-6], the resulting mixture of mono-. di-, and tri-substituted products

indicates little reaction specificity. This suggests that $Os_3(CO)_{12}$ would be an ineffective catalyst since there is little control over the location of substitution or how many times a substrate would be substituted with a P-donor ligand.

$Os_3(CO)_{12}$ produces three products in solution, but the introduction of just one halide (X = Cl^-, Br^-, I^-) was shown by Shen and Basolo[7] to improve the reactivity and specificity of the resulting cluster $Os_3(CO)_{11}X^-$. Thus, when $[Os_3(CO)_{11}X_2]^-$ was reacted with P-donor ligands, only one major product was obtained. Carbonyl substitution of $[Os_3(CO)_{11}X_2]^-$ is proposed to proceed through a halogen bridged transition state, demonstrated in Figure 9, that is thought to then come undone upon the addition of their ligand of choice, triphenyl phosphine (PPh3). This reaction was carried out in pseudo-first order conditions, meaning that ligand was always in excess, and was monitored at low temperatures (8.5-31.0 ^oC) using a Neslab RTE-s refrigeration circulation bath.

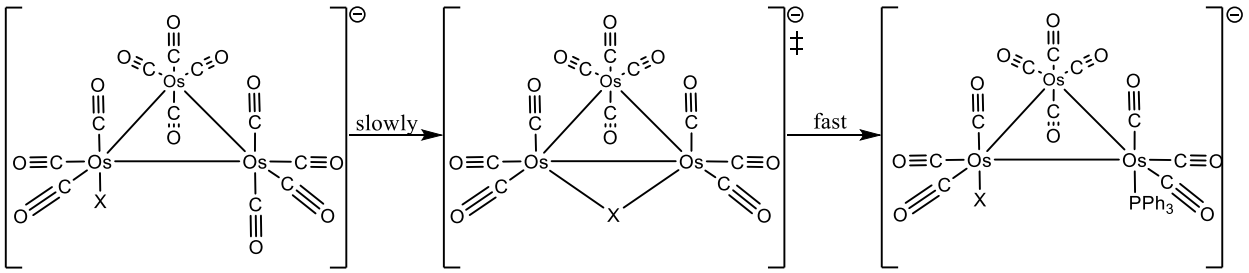

Fig 9 original figure adapted from [*7*], X = Cl, Br, I. One CO of $Os_3(CO)_{12}$ was replaced with X and activated the cluster towards ligand substitution through this proposed scheme. CO geometry left unspecified as the original document did not specify; it would be inappropriate to imply structural specificity beyond what the original paper indicates.

The reactions of $Os_3(CO)_{11}X^-$ were found to be an order of magnitude faster than those of $Os(CO)_{12}$, with small enthalpies of transition and negative entropic values of transition shown below in Table 1.

X	ΔH‡ (kJ/mol)	ΔS‡ (J/mol)
Cl	65.7 ± 1.7	-79.9 ± 5.9
Br	69.5 ± 0.8	-66.1 ± 1.7
I	71.5 ± 0.4	-62.3 ± 0.8

Table 1. Reported enthalpies and entropies of transition for CO substitution by P-donors. Original figure adapted from [*7*], converted from cal/mol for direct comparison to the data reported in this work.

Generally, small enthalpies of transition and negative entropic values—like those reported by Shen and Basolo[7]—are observed in associative pathways, which would be second order overall. A second order process indicates that the rate of reaction depends on the concentrations of both the cluster *and* the incoming ligand. A first order process would mean that the rate of reaction only depends on the concentration of the cluster. While the reported first order kinetics of Shen and Basolo are driven by the vast excess of ligand, hence the phrase "pseudo-first order conditions," a ligand-independent pathway (first order in cluster, zero order in ligand) would suggest a CO dissociative pathway, which would have large entropy and enthalpy of transition. Should first order kinetics and similar thermodynamic data be seen under stoichiometric conditions, both still generally thought to be conflicting, it would be a noteworthy route of mechanistic investigation.

Since halides have three unused lone pairs of electrons, Shen and Basolo[7] hypothesized that the halogen would attack the adjacent metal core as depicted in Fig 7 above. This would eliminate coordinated CO and leave a vacant site for the PPh_3 to attack upon dissociation of the bridge. While the work of Shen and Basolo investigates an anionic, or negatively charged, cluster rather than the neutral compounds of our lab, the comparison of a halogen addition serves as an interesting comparison to an unhalogentated cluster.

Di-halo Bridged Triosmium Carbonyl Clusters

In a similar manner to how the addition of one halide activates clusters towards substitution[7], dihalo-bridging triosmium cluster derivatives show improved reactivity and specificity of carbonyl substitution by P-donor ligands. Shown in Figure 10, reacting $Os_3(CO)_{10}X_2$ with $P(OMe)_3$ produces only one product rather than a mixture of mono- di- and tri-substituted products, as seen with $Os_3(CO)_{12}$, even after prolonged refluxes in excess $P(OR)_3$. Thus, even with excess ligand in solution, only one major product is obtained rather than the mixture of products obtained by the substitution of Poe and Sekhar[5].

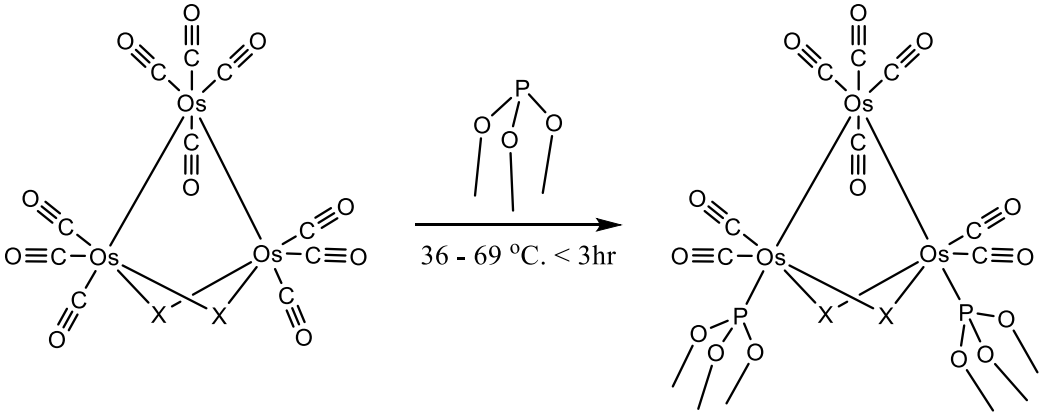

Fig 10 $Os_3(CO)_{10}X_2$ (X = Cl, Br, I) with $P(OMe)_3$. Substitution occurs at lower temperatures ranging from 36 to 69 ˚C with refluxes not exceeding 3 hours.

This substitution occurs at lower temperatures than that of the dodecacarbonyl, ranging from 36 to 69 ˚C with reaction times that do not exceed three hours. This heightened reactivity, evidenced by lower reaction temperatures and reaction times, and heightened reaction specificity, evidence by only one major product in solution, demonstrate the improved potential catalytic properties of dihalo-bridges triosmium cluster compounds with respect to carbonyl complexes. While the compound employed our research lab, $Os_3(CO)_{10}X_2$, is not an anionic cluster like that

of Shen and Basolo[7], it is noteworthy that both clusters see heightened reactivity and specificity upon the addition of halides and/or halogens compared with the "original" $Os_3(CO)_{12}$ cluster.

As demonstrated in Figure 10, the sites of ligand substitution are very specific. While the overall specificity of these clusters is demonstrated by obtaining only one product, the location of substitution is also specific; the incoming ligand only coordinates trans to the metal-metal bond. Carbonyl substitution has not been reported to occur at other CO cites on the cluster.

Years of research with triosmium clusters within our research group has led to a deep understanding of the behavior of these compounds. Figure 11 presents a summary of known reactivity of dibridged triosmium carbonyl clusters conducted within our research group.

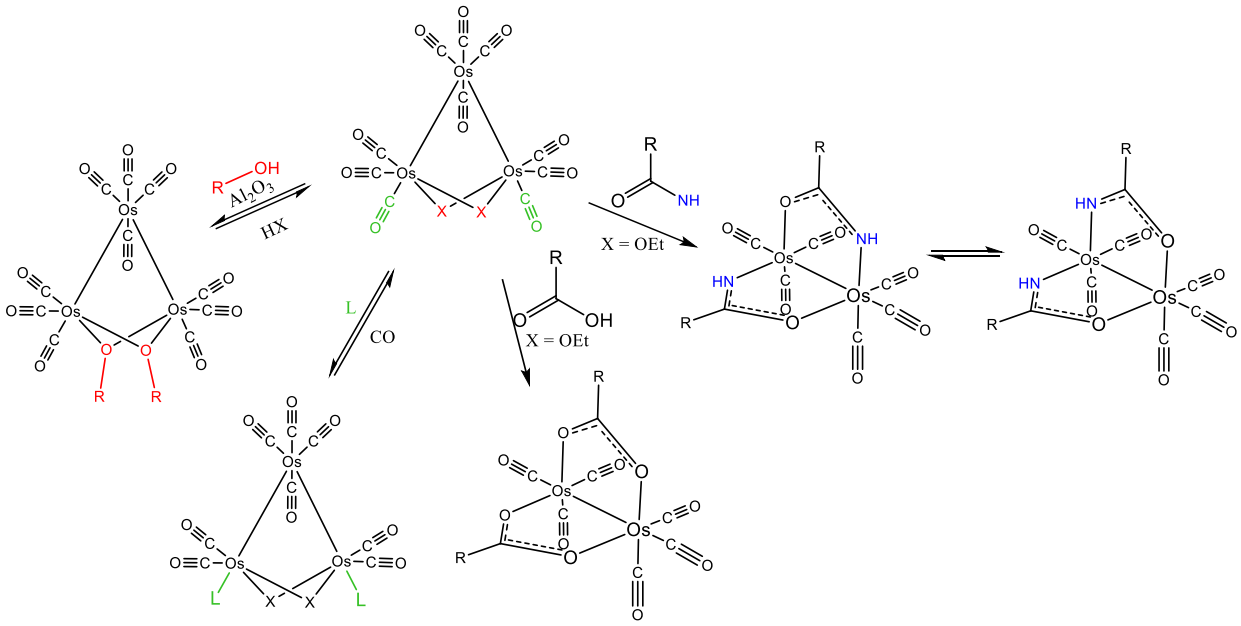

Fig 11 Summary of known categorical reactivity; strong alcohols replace the bridge halides, other ligands replace labile CO, when X = OEt bidentate ligands fragment the complex. Summary compiled from [*8*, *9*]

Alcohols of the type R-OH have been shown to replace the bridging ligands, regardless of the identity of X[8]. Additionally, ligands not of the type R-OH have been shown to replace the labile CO that are trans to the Os-Os covalent bond, also independent of X. Further, when X is ethoxide

(OEt), reacting the dibridged cluster with bidentate π-donor ligands like carboxylic acids, has been demonstrated to fragment the cluster[9]. Additional reactivity has been investigated within this research group, but most lay within these three categories of reactivity.

Most important to this research is that, with each category of reactivity, each synthetic route yields only one major product. This is in contrast to $Os_3(CO)_{12}$, which yields many products, thereby suggesting that the presence of bridging halogens is contributing to the heightened reactivity and specificity of $Os_3(CO)_{10}(X)_2$ clusters. Such unique reactivity, in direct contrast with $Os_3(CO)_{12}$, may therefore be a structural motif of interest that demands kinetic and mechanistic investigation.

The work of Baum and Pearsall[10] investigated carbonyl substitution of $Os_3(CO)_{10}X_2$ with $P(OMe)_3$. As a result of their work, Baum and Pearsall proposed a mechanism as shown in Scheme 1. This proposed mechanism is in agreement with the work of Shen and Basolo[7], which suggested that the halogen bridge creates a vacant site on the osmium where an incoming ligand would coordinate. The bridge then reforms, thereby evicting a carbonyl on the same osmium atom that had been attacked by incoming ligand, $P(OR)_3$. This scheme, then, is the mechanistic conceptualization with which subsequent researchers within this lab had been working for their kinetic and mechanistic works.

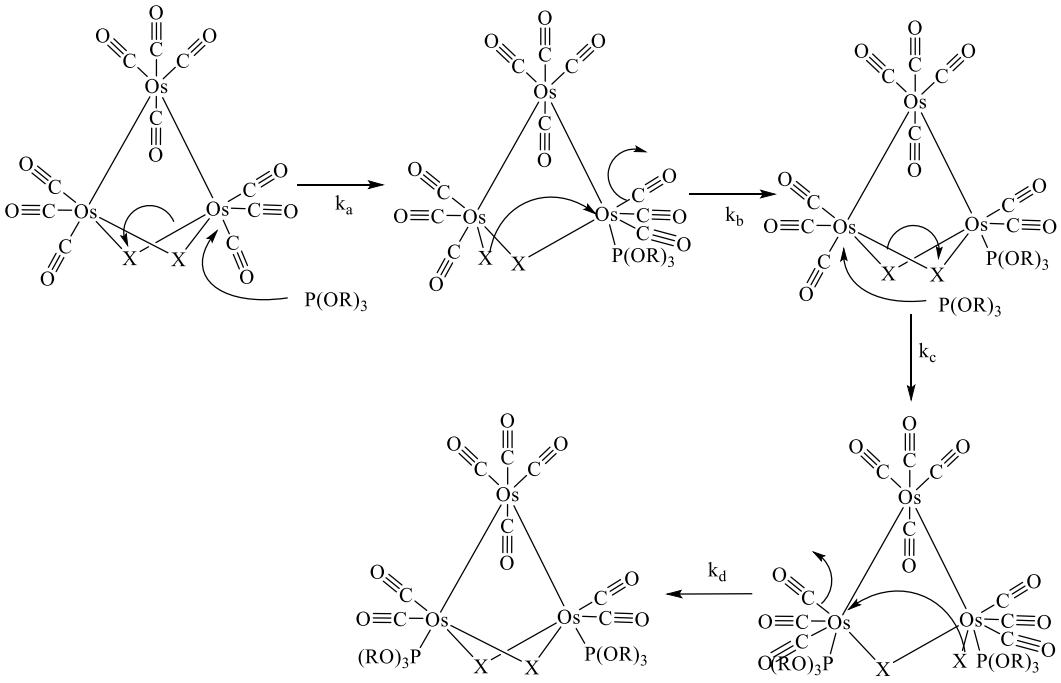

Scheme 1. Proposed mechanism of carbonyl substitution of $Os_3(CO)_{10}X_2$ clusters adapted from [*10*]. The bridged ligand, X, is hypothesized to break, thereby leaving a vacant site on the Os atom where an incoming ligand, shown with $P(OR)_3$ could coordinate; the bridge then reforms and evicts a carbonyl on that same osmium.

Previous Kinetic Works on $Os_3(CO)_{10}X_2$

Previous work of Cavaliere and Pearsall[11] investigated the ligand substitution kinetics of decacarbonyltriosmiumdichloride, -dibromide, and -diiodide ($Os_3(CO)_{10}Cl_2$, $Os_3(CO)_{10}Br_2$, $Os_3(CO)_{10}I_2$) with 300x excess trimethyl phosphite over several temperatures, summarized in Figure 12. Rate parameters were obtained through IR analysis of the highest frequency peak. Transitional energetic values, enthalpy of transition and activation energy, were obtained by Arrhenius and Eyring plots.

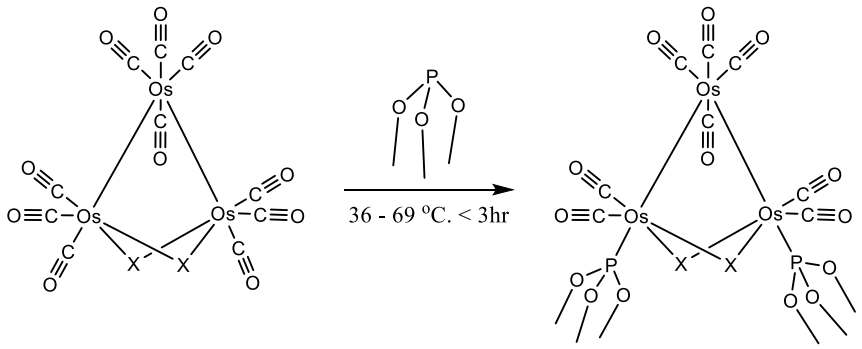

X bridge	k, /s	Ea, kJ/mol	ΔH‡, kJ/mol
Cl	3.97E-03	110 ± 8	108 ± 8
Br	2.41E-03	106 ± 5	103 ± 5
I	9.41E-04	116 ± 11	113 ± 11

Fig 12 summary of Cavaliere and Pearsall's work [*11*] regarding substitution kinetics of $Os_3(CO)_{10}X_2$ (X = Cl, Br, I) with $P(OMe)_3$. Average rate constant for each bridge identity reported in sec^{-1}.

Shown in Fig 12, the activation energy and enthalpy did not change significantly with halogen identity (avg E_A = 111 kJ/mol, avg $\Delta H^{\ddagger}$ = 108 kJ/mol). Overall, the rate of substitution, assessed by the rate constant k, did not change significantly with bridging halogen identity, but shows a small trend where Cl > Br > I. The rate constant for $Os_3(CO)_{10}I_2$ was found to be 9.41 x 10^{-3} sec^{-1}.

Cavaliere and Pearsall's work with trimethyl phosphite $P(OMe)_3$ largely investigated the influence of halogen bridge substitution kinetics, a study that concluded there is only a modest effect. A subsequent preliminary study was done by Bradford and Pearsall[12] to mirror the work of Cavaliere and Pearsall and investigate the effect of ligand identity and concentration on rate of substitution, investigating $Os_3(CO)_{10}I_2$ as it reacts with triphenyl phosphite ($P(OPh)_3$), as shown in Figure 13.

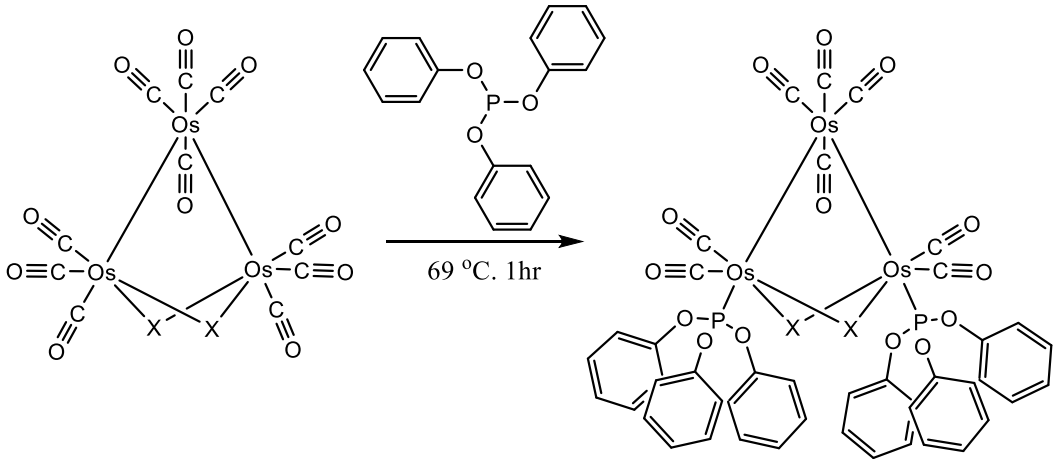

Fig 13 summary scheme of Bradford and Pearsall's study [*12*] in response to that of Cavaliere and Pearsall; ligand substitution kinetics of $Os_3(CO)_{10}I_2$ with 300x excess $P(OPh)_3$ at 69 ˚C

At 300x excess $P(OPh)_3$, k was found to be 0.960 x 10^{-3} per second; under stoichiometric conditions, however, k was found to be 1.65 x 10^{-3} per second. While at 300x excess ligand, conditions that are identical to those of Cavaliere and Pearsall, the rate does not differ statistically from that of Cavaliere and Pearsall's work with $P(OMe)_3$, the difference in rate when ligand concentration is altered is statistically significant. This suggests that the rate increases with decreasing ligand concentration. We now understood, however, that this is most likely due to wet solvents (see "Discussion," p. 71).

Ligand Identity: Parameters that affect the observed rate

The observed rate of carbonyl substitution by P-donor ligands is understood to be related in some manner to both the basicity, and size of the phosphorus-based molecule. Basicity is related to the availability of long pairs on the phosphorous atoms itself, how easily they can be donated to another atom. In extensive studies conducted by Poe et. al of carbonyl substitution of dimanganese

and dicobalt[13], and tetraruthenium carbonyl clusters[14] by P-donor ligands, the rate of carbonyl substitution was found to follow a trend described in Equation 1

$$\log(k_2) = \alpha + \beta(pKa' + 4) + \gamma\lambda(\theta - \theta_{th}) \quad \textbf{(1)}$$

where α is the standard reactivity relative to that of a weak base, as this is how such P-donor ligands behave, and is taken to be pKa' = -4. β is the sensitivity to the σ-basicity of the ligand; this is measured relative to pKa'. The term γ measures the impact on the rate due to the size of the ligand, as estimated by Tolman's cone angles[13], θ.

Tolman's cone angles are the angle of the three-dimensional cone shape produced by phosphine (PR_3) and phosphite ($P(OR_3)$ ligands. This value is measured at a naturally-occurring configuration of the R-substituents where there is zero steric strain, creating an arbitrary cone that just touches the outer boundaries of the substituents and whose apex is 2.28 Å above the center of the phosphorous atom[15]. This is to say that θ is calculated when the R groups are a comfortable distance from one another that does not reduce any degrees of motion of any one R substituent. Figure 14 shows a simplified example where substituents of PR_3 are shown as spheres; one can imagine that as substituent R increases in size or length, the simplified sphere approximation would also increase.

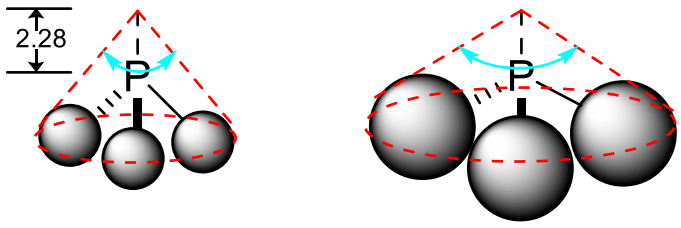

Fig 14. Simplified calculation of cone angle, θ. Substituents are approximated as spheres; a larger group is treated as a larger sphere. The arbitrary cone assignment, red, just touches the spheres, centered 2.28 Å from the center of the P, and θ, blue, is measured between the red cone boundaries not the dihedral angles between R spheres.

In Eqn 1, then, the quantity $\lambda(\theta - \theta_{th})$ therefore represents a switching function dependent upon whether the cone angle of the ligand, θ, approaches or exceeds the steric threshold, θ_{th}, of ~120°[15]. Thus, when $\theta < \theta_{th}$, λ is taken to be 0; this mathematically states that ligands within the steric threshold do not exhibit any steric affects that would be seen in the observed rate constant. The steric threshold, however, does not mean that beyond this cut-off no substitution will occur, but rather it indicates that this is the angle at which steric effects begin to appear and must now be mathematically accounted for.

However, in cases where the P-donor ligand has multiple aromatic or highly conjugated groups, the trend outlined in Eq(1) does not seem to hold[13, 14]. Thus, when investigating the effects of aryl P-donor ligands on the observed rate of substitution, differences in rate should now be described by Equation 2, where

$$\log(k_2) = \alpha + \beta(pKa' + 4) + \gamma\lambda(\theta - \theta_{th}) + \delta(E_{ar}) + \phi(pKa'\pi). \quad \textbf{(2)}$$

The difference of Eq(1) and Eq(2) is the addition of the final two terms that now account for the aryl affect, correlated to the number of aromatic substituents on a ligand, and the ligand's ability to act as a π-acceptor.

With these functions in mind, the rates obtained by Cavaliere, and Bradford suggest that any steric effect due to the difference in cone angle of $P(OMe)_3$ and $P(OPh)_3$ can be considered negligible as both ligands still lie within or around the steric threshold, thus overall steric bulk can be ignored[13-15]. However, it does not appear that even the aryl effect can explain the increase in rate observed by Bradford and Pearsall when comparing the rates under vast excess of $P(OPh)_3$ and no excess $P(OPh)_3$. Overall, the kinetics of substitution with P-donor ligands demand further

investigation, particularly with respect to the effects of ligand concentration on the rate of substitution.

Computational Analysis

Mechanistically, the question comes down to which bond is broken during carbonyl substitution; the metal-metal bond, or the halogen bridge? The work of Shen and Basolo[7] suggests that the halogen bridge would break, and the trend observed by Cavaliere and Pearsall[11] seems to confirm these findings, despite the fact that the differences in observed rate are quite small. In conjunction with the work done by Cavaliere and Pearsall[11], theoretical calculations regarding the molecular orbital energetic approximations of these dihalobridged clusters were investigated by Barnum and Pearsall[16]. As it was previously found that the halogen bridge has a small effect on the rate of substitution[11], this computational work investigated the energies of bonds in addition to the shape and location of bonding molecular orbitals to clarify the observed pattern of reactivity of the $Os_3(CO)_{10}X_2$ series (X = Cl, Br, I).

Table 2 demonstrates Barnum and Pearsall's work through DFT computational analysis examining the effect of bridging halogen on the Osmium metal-metal bonds, the Osmium-halogen "bond," and the false-bond between the Osmium atoms that share the halogen bridge, here denoted as Os(2) and Os(3).

	Os-Os bond		Os-X bond		Os(2)-Os(3)	
	Bond Order	**Distance (Å)**	Bond Order	**Distance (Å)**	Bond Order	**Distance (Å)**
Cl	0.44	**2.93**	0.56	**2.59**	0.09	**3.4**
Br	0.43	**2.95**	0.62	**2.71**	0.1	**3.44**
I	0.42	**2.98**	0.68	**2.89**	0.11	**3.52**

Table 2. adapted from [*16*]. Bond order and inter-atomic distance as it changes with bridging halogen identity. Bond order does not change significantly, any variations are observed entirely in the length of the bond.

Using Gaussian calculations, Barnum and Pearsall were able to conclude that the bond order of the halogen bridges does not change significantly with halogen identity, though any changes thereof are accounted for by the lengthening of the bridged bonds due to halogen atomic radius (Cl < Br < I). This effect is also seen in the lengthening of the "bond" between either osmium that contribute to the multicenter bridging bond (Os(2)-Os(3) bond); there is no true bond between them, as evidence by the incredibly small bond order, but the inter-atomic distance increases with increasing halogen radius. This is to say that while the rate seems to be changing ever so slightly with bridging halide, as per Cavaliere and Pearsall's findings, the strength of the halogen bridge does not appear to be changed with X. This effect alone, therefore, does not seem to account for the observed trends in substitution rate constants as they change with halogen, since, overall, the variance of observed rates is quite small across all X.

Barnum and Pearsall also performed a Gaussian DFT calculation to approximate the electronic character of the bonds as they vary with halogen identity, producing models of the Highest Occupied Molecular Orbital (HOMO) and Lowest Unoccupied Molecular Orbital (LUMO) for $Os_3(CO)_{10}X_2$ clusters, shown in Figure 15. The HOMO shows the regions of electron density of the overall molecule while the LUMO shows where electron density would be added onto the molecule if attacked by an incoming reagent.

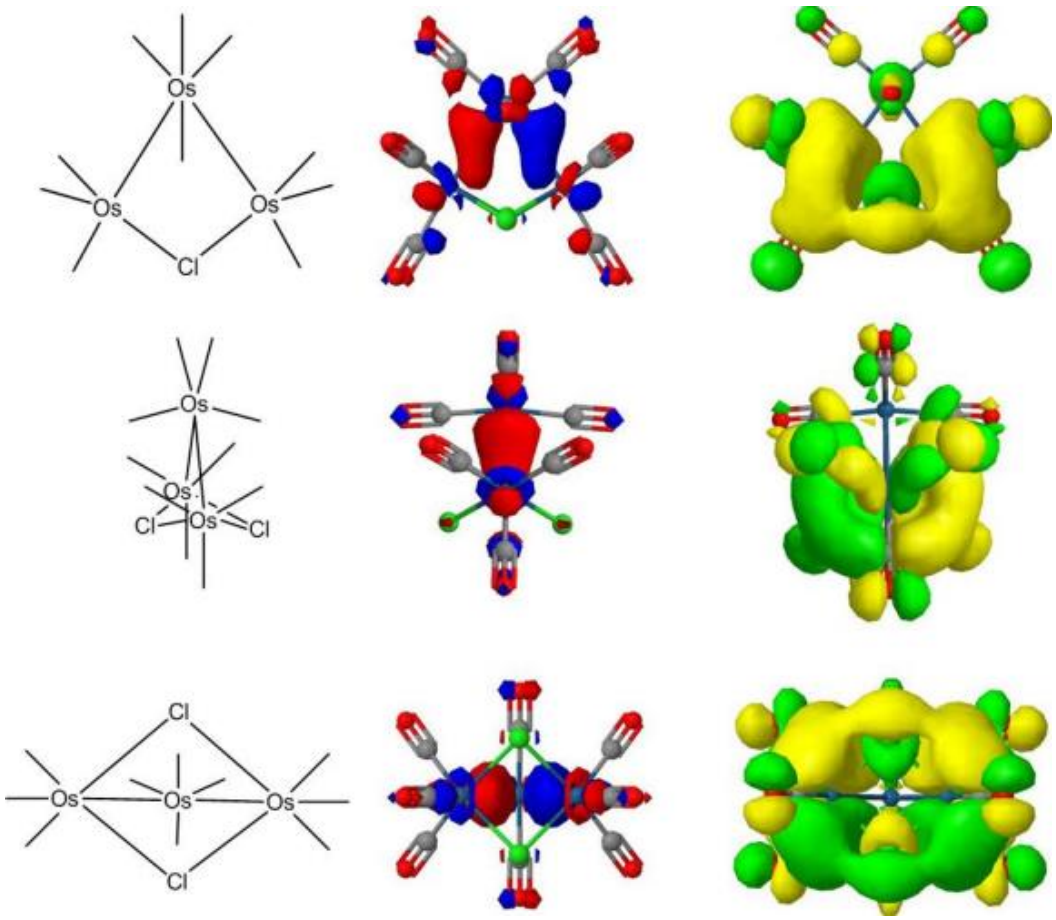

Fig 15. DFT calculations by [*16*] used with permission. The leftmost column shows the orientation of $Os_3(CO)_{10}X_2$ that corresponds to the HOMO (middle, red/blue) and LUMO (right, yellow/green) shown. The HOMO lies along the Os-Os metal-metal bonds while the LUMO lies along the bridge and substituted CO ligands.

Barnum and Pearsall's calculations found that the HOMO lies primarily along the Os-Os metal-metal covalent bond, the strength and length of which was calculated and found not to vary with the identity of X (Table 2). The LUMO lies along the bottom half of the entire molecule, encompassing the Os-X-Os bridges and the CO ligands coordinated to those Os atoms. This data and those presented in Table 2 seem to account for the minimal change in observed rate of CO substitution by $P(OMe)_3$ as observed by Cavaliere and Pearsall[11].

Additionally, Barnum and Pearsall's work determined that the Os-Os covalent bond was found to be the weakest among those incident to the Os atom where substitution occurs. This is to

say that, while the Os-Os bond is not, in itself, a weak bond, it is the weakest bond of the three categorical bonds of the Osmium atom; Os-Os, Os-X, and Os-CO. Therefore, it appears that the most likely to break during the rate-limiting step of substitution is the Os-Os bond, the weakest option. This information, in addition to the activation energy of this process being of the order of an Os-Os bond and statistically unchanging with halogen identity, suggests that the Os-Os covalent bond breaks and reforms during this mechanism, shown in Scheme 2.

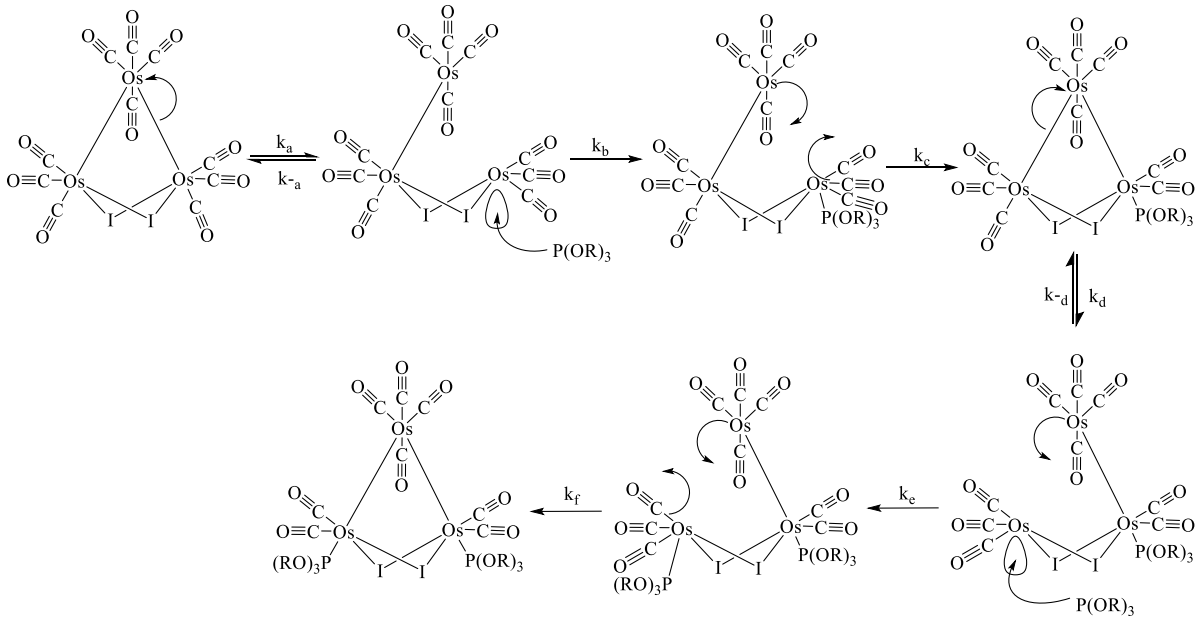

Scheme 2 functioning proposed mechanism of ligand substitution of $Os_3(CO)_{10}X_2$ clusters, adapted from [*17*]. The halogen bridge is not assumed to break during this process, rather the Os-Os covalent bond. This supports the stereospecificity of substitution only trans to the Os-Os bonds.

While it is known that the halogens within this clusters activate the overall compound[7] the statistically unchanged rates and activation energies suggest that the halogen bridge is not involved in the bond-breaking or -forming events of this mechanism, a contrast to the work of Shen and Basolo[7]. However, this proposed mechanism provides a hypothesized explanation as to the stereospecificity of ligand substitution with these cluster derivatives as only the trans CO are substituted.

This investigation therefore continues the work of Bradford[12], Cavaliere[11], Barnum[16] and Pearsall as an investigation of the ligand substitution kinetics and mechanism of $Os_3(CO)_{10}I_2$ with $P(OR)_3$ (R = Me, Ph) to provide insight on the behavior of this structural framework and investigate the mechanistic pathway of carbonyl substitution. This may, in turn, shed light onto the possible catalytic properties of dihalo-bridged trisomium carbonyl clusters. $Os_3(CO)_{10}I_2$ was synthesized from $Os_3(CO)_{12}$ and reacted with varying concentrations of $P(OR)_3$ to analyze the possible effect of ligand concentration on observed rate.

Materials

Compounds

All compounds were received from Sigma Aldrich. Dodecacarbonyltriosmium ($Os_3(CO)_{12}$), anhydrous trimethylamine-N-oxide ($Me_3(NO)$), and ligands trimethyl- and triphenyl phosphite ($P(OMe)_3$ and $P(OPh)_3$), were used as received. All solvents were dried with molecular sieves at least 24 hours prior to use.

Instrumentation and Software

Microwave synthesis was carried out in a CEM Discover Microwave. Infrared (IR) analysis of solutions to monitor reaction progress was conducted in a Thermo Scientific Nicolet iS10 Fourrier-Transform Infrared Spectrometer using a sodium chloride liquid cell with a pathlength of 0.2 mm. IR spectra were taken and analyzed in absorbance mode and fit using IgorPro 8 Multipeak Curve Fitting2 software. Computational and graphical analyses outlined below we conducted in both IgorPro, to define unique fit functions, and Excel, to define calculated columns.

Methods

Microwave Synthesis of $Os_3(CO)_{10}I_2$

200. mg of $Os_3(CO)_{12}$ (0.221 mmol) and 56 mg iodine (0.221 mmol) were placed into a 35-mL thick-walled microwave reaction vessel with 14 mL cyclohexane and a stir bar. The solution was microwaved at 275 psi, 300 W, and 155 ˚C for 13 minutes; the emergent solution was a rich amber color. The reaction vessel was allowed to stand for 45min to allow any unreacted $Os_3(CO)_{12}$ to fall out of solution. The cyclohexane solution was then removed and placed into a clean round-bottom flask (RBF); the microwave vessel was rinsed with cyclohexane thrice to ensure complete transfer of product. Using a stream of nitrogen, the volume of cyclohexane solvent was reduced by half, taking care to swill or scrape any dry product along the walls to keep all product in solution. The concentrated solution was then stored overnight at -20 ºC to crystalize desired product, decacarbonyltriosmium diiodide ($Os_3(CO)_{10}I_2$). When thawed, the impure solution was removed and placed into a clean vessel, as some $Os_3(CO)_{10}I_2$ (R_f = 0.501 in hexanes, characteristic peaks at 2110(w) and 2074 cm^{-1}(s)) still remains in solution with a diosmium by-product, $Os_2(CO)_6I_2$ (R_f = 0.405, characteristic peaks at 2098(m) and 2060 cm^{-1}(s)). The crystals, however, were determined to be pure $Os_3(CO)_{10}I_2$ (45.7% yield). The remaining product was isolated from the impurity solution by column chromatography with silica gel and pure, dry hexanes. Collection flasks were analyzed with TLC and IR before they were appropriately combined in a round bottom flask to remove the hexanes by rotary evaporation. Overall, after both crystallization and column chromatography, microwave synthesis using this isolation method provided $Os_3(CO)_{10}I_2$ (overall 75.3% conversion) with some $Os_2(CO)_6I_2$ byproduct (24.8% conversion) and no unreacted starting material was obtained.

Synthesis of $Os_3(CO)_{10}I_2$ (No Microwave)

In the absence of a microwave reactor $Os_3(CO)_{10}I_2$ can be prepared by a two-reflux process that employs a different synthetic pathway to obtain the desired material. 200. mg of $Os_3(CO)_{12}$ (0.221 mmol) was dissolved in 100 mL cyclohexane and placed into a clean RBF capped with a reflux condenser and a pressure-equalizing separatory funnel. Separately, a dilution of iodine is prepared in cyclohexane and added to the separatory funnel. The $Os_3(CO)_{12}$ solution is brought to reflux while stirring; once boiling, the I_2 dilution is added dropwise until one stoichiometric addition (0.221 mmol I_2) has been added. This can be tracked by TLC, as this first reflux is complete upon the appearance of a baseline spot, and by color change, as the solution will turn the same amber hue as the microwave synthetic route. Upon completion of this first reflux, the cyclohexane is removed by rotary evaporator; the dry product I the RBR is $Os_3(CO)_{12}I_2$, a linear compound rather than a cyclical cluster, characterized by a peak at 2143 cm^{-1}.

The cyclical cluster of $Os_3(CO)_{10}I_2$ is formed by reconstituting the dry $Os_3(CO)_{12}I_2$ in toluene and refluxing for at least 90 minutes. This reaction was tracked by both TLC in hexanes and IR. The reaction is complete upon the appearance of a new spots in TLC (desired $Os_3(CO)_{10}I_2$ R_f = 0.342) and the appearance of $Os_3(CO)_{10}I_2$ peaks, primarily those at 2110 and 2074 cm^{-1}. The toluene is removed by rotary evaporator once more; the dried compound is now an impure mixture of $Os_3(CO)_{10}I_2$ and $Os_2(CO)_6I_2$ as in the microwave synthetic route. The contents of the RBF are dissolved in hexanes and column chromatography in hexane is performed to isolate the desired compound, $Os_3(CO)_{10}I_2$ (80.3% yield) from the impure mixture.

Synthesis of $Os_3(CO)_9I_2[P(OMe)_3]$

An arbitrary dilution of trimethylamine-N-oxide (Me_3NO) was prepared in in a glove box. Anhydrous Me_3NO was massed in a glove box; the vial was capped with a septum prior to removal from the inert environment. Using a syringe, 10 mL dry dichloromethane was added to dissolve the Me_3NO. Additionally, an arbitrary dilution of trimethyl phosphite ($P(OMe)_3$) in dichloromethane was also prepared.

In a 50 mL 3-neck round bottom flask, 20.0 mg $Os_3(CO)_{10}I_2$ (0.221 mmol) was dissolved in 10 mL dichloromethane under nitrogen; the second neck was capped with a glass stopper, and the third covered with a SUBA seal. The reaction vessel was placed in an ice bath with NaCl. While stirring, one molar equivalent of Me_3NO dilution (1.81×10^{-5} mol) was slowly added dropwise. The reaction vessel was then removed from ice and allowed to come to room temperature, monitoring reaction progress with periodic IR and TLC in 50% dichloromethane, 50% hexanes every twenty minutes over one hour. During this process, the solution deepens in color from a bright, vibrant yellow to a richer golden hue. The solvent is then removed by rotary evaporation with no heat. Due to the darkness of the crude solution, the dried product appears black; this would usually indicate decomposition of the cluster, but IR shows that the product did not decompose. IR in hexanes and TLC in 10% dichloromethane, 90% hexanes confirm the near-complete disappearance of starting material $Os_3(CO)_{10}I_2$ (loss of 2110 and 2074 cm^{-1}, loss of R_f = 0.531), yet indicate a mixture of both desired $Os_3(CO)_9I_2[P(OMe)_3]$ and $Os_3(CO)_8I_2[P(OMe)]_2$ products, peaks at 2097 and 2082 cm^{-1} respectively. Products were isolated by Prep TLC in 50/50 dichloromethane/hexanes in which four bands were observed; the top band was determined to be unreacted starting material, $Os_3(CO)_{10}I_2$ (approx. 3mg), the second band was found to be the desired product, $Os_3(CO)_9I_2[P(OMe)_3]$ (approx. 9mg, 42.35% conversion), the third and bottom

bands contained a mixture of compounds and thus true percent conversion to $Os_3(CO)_8I_2[P(OMe)_3]$ cannot be reported.

Kinetics Procedure

This procedure reflects the general form of kinetic refluxes performed throughout the course of this research; a table of solvents, their boiling points, and phosphite volumes employed for an investigation of ligand concentration on rate are provided in Table 3. Unless a particular step is unique to a solvent or phosphite, all steps are referred to in their generic sense.

Solvents Used	
Solvent	bp (˚C)
cyclopentane	49
2-methylpentane	60
hexanes	69

Ligand Volumes for Kinetic Trials			
Ligand Excess	mmols	P(OMe)3, mL	P(OPh)3, mL
300x	5.43	0.641	1.43
50x	0.905	0.107	0.238
2x, Stoich	0.0362	0.00427	0.00952

Table 3. Solvent, boiling points, and volumes of phosphite ligands necessary for each reflux for kinetics assay. For volumes smaller than 0.5 mL, dilutions of ligand in corresponding solvent should be made to ensure accuracy of measurement and complete transfer into reaction solution.

20.0 mg (1.81×10^{-5} mol) of $Os_3(CO)_{10}I_2$ and 10.0 mL solvent were added to a three-neck 50-mL round bottom flask that had been previously rinsed with solvent and flushed with nitrogen gas for two minutes. The 50-mL round bottom flask is equipped with a SUBA seal, reflux condenser, and thermometer to ensure constant temperature throughout the reaction. Phosphite ligand was injected via syringe and the solution was brought to reflux. Once the solution reached reflux, approximately 200-250 μL of reaction solution was withdrawn via syringe and analyzed by IR. This sample was then retrieved from the cell, injected back into the reflux solution, and the NaCl liquid cell was thrice rinsed; first with dichloromethane, then twice more with solvent. This

sampling process was repeated every two minutes until the full disappearance of the peaks at 2110 and 2098 cm^{-1} was confirmed in IR. This procedure was repeated in triplicate for each temperature and each phosphite, thus each data point presented in this paper is the average of at least three kinetic refluxes.

Isolation of Compounds by Stepwise Gradient Column Chromatography

After research was complete, collection flasks of kinetic trials included mixtures of $Os_3(CO)_{10}I_2$, $Os_3(CO)_{10}I_2[P(OR)_3]$, and $Os_3(CO)_{10}I_2[P(OR)_3]_2$. While solvent systems of 20% CH_2Cl_2/hexanes provide the best separation between the three osmium clusters, one remains on the baseline—and would thus be impossible to get off the column—and it was found that the trimethyl and triphenyl phosphite compounds overlap with one another—indicating that at least two columns must be run, one for each identity of $P(OR)_3$. Additionally, there is an unidentified compound that appears with the $P(OPh)_3$ compounds in TLC, assumed to be excess $P(OR)_3$; running a column in 20% CH_2Cl_2 would prove ineffective as separating the first osmium eluant from the blue splodge. Thus, a stepwise gradient system is necessary. The first solvent system is 100% hexanes; it is this system that is used to make the silica gel slurry and load the column. Once the first eluant has come off the column, the column is them maintained with 20% CH_2Cl_2/hexanes to provide greater separation between the second and third yellow, osmium-based eluants. Once the second eluant has been isolated from the column, the baseline eluant can be pushed off with 100% CH_2Cl_2 until it comes off the column. This process was repeated for the second column using the second $Os_3(CO)_xI_2[P(OR)_3]_y$ compounds, and thus a total of six eluants were isolated. Each eluant was dried by rotary evaporation, characterized by IR in hexanes, then characterized

by both ^{1}H and ^{31}P NMR spectroscopy to confirm the exact location of $P(OR)_3$ addition(s) to the clusters (see Spectral Appendix).

Data Analysis

IR spectra were exported as .CSV files to IgorPro 8 to obtain the height, and therefore absorbance, of peaks using the built-in MultiPeak Curve Fitting2 package. The y-axis of the Curve Fitting pop-up window is adjusted to view only the peaks of interest, usually 2120 to 2075 cm^{-1}; this range is kept constant throughout the analysis while the x-axis is adjusted as necessary to allow the pre-programmed software to fit properly. As the 2110 cm^{-1} peak is much smaller than other peaks within the spectra, and therefore becomes indistinguishable from baseline in a larger window, it can be fit individually to minimize error and maximize overall data points. All peaks are fit with a linear baseline before auto-locating peaks and obtaining the produced fit output; only height, which is equivalent to absorbance, and location tags are necessary for this analysis. When the software could not identify a peak, produced a negative height output, or the peak became indistinguishable from background noise at this zoomed range, the reflux is confirmed to be completed and any subsequent spectra were not included in the graphical determination of the order of reaction. Peak heights can also be obtained in OMNIC software using the Peak Height tool. These methods of Peak Height determinations agree with each other and fall well within one standard deviation of one another; there is only 5.1% difference between rates obtained with OMNIC heights and those obtained with IgorPro.

Regardless of acquisition method, the output data is arranged in a table such that peak height can be plotted against time; this is to say that each full IR spectrum is reduced to one point

per peak in this new table. Plots of 2110 cm^{-1} height, natural log of height, and inverse height are plotted against time in unit seconds to determine the order of reaction. Each graph is fit to a line; that with the highest correlation coefficient indicates the order of reaction, not the rate constant. As these reactions were all found to be first order, raw peak heights are once again plotted against time and fit with First Order Sequential Kinetic functions (derived and defined as Equations 7a-c in "Results") to obtain rate constants for this mechanism. To minimize covariance, the values obtained for k_1 from 2110 cm^{-1} curve fitting is held for subsequent fits of intermediate and product peak heights. As kinetic refluxes were done in triplicate, this procedure was also repeated in triplicate; the reported values found in "Results" reflect the average of at least three data points for that specific solvent and phosphite.

Propagation of Error

Standard deviations of each rate constant were obtained from IgorPro's curve fitting analysis. Since all k_1 and all k_2 are averaged for each temperature, a standard propagation of error calculation was performed using the Addition equation published in Analytical Chemistry textbooks. Thus, errors reported for rate constants are the relative error of the whole sample set at that temperature.

While each individual rate constant was used to calculate $\Delta G^{\ddagger}$ for each trial, due to the mathematical manipulations required to convert k to $\Delta G^{\ddagger}$, particularly taking the natural log of k, a simple "conversion" of the standard deviation of k into kJ/mol is inappropriate. This would give larger errors for rate constants that had smaller standard deviations. However, it is appropriate to employ the Logarithmic error propagation equation since constants k_B, h, and R of the Eyring-

Polyani equation can be assumed to have no error. While this assumption may not be wholly accurate, mathematically there is no variance of these *constants* in calculating $\Delta G^{\ddagger}$, only the measures or calculated variance of rate constants. The reported errors for $\Delta G^{\ddagger}$ are the averaged, relative propagated errors from each trial.

Error analysis for natural log-based linear fits has been a popular topic of discussion in academia, particularly because linear regression analyses often do not accommodate the covariance of intercept *and* slope and thus report false approximations of the true error within a mathematical system. Error propagation for the Arrhenius equation has been published, and was calculated using the formula published in Steigel, Sauer, Kleier, and Binsch[18] where

$$\left(\frac{\sigma_{Ea}}{Ea}\right)^2 \approx \frac{2T^2}{(\Delta T)^2}\left(\frac{\sigma_T}{T}\right)^2 + 2\left(\frac{1}{\Delta(\ln(k))}\right)^2\left(\frac{\sigma_k}{k}\right)^2 \quad \textbf{(3)}$$

such that σ_n represents the error of value n, E_a is the activation energy obtained through the slope of the linear fit, T is the temperature at which rate constant k was obtained. Expanding the delta terms to clarify the mathematical term embedded therein, the equation becomes

$$\left(\frac{\sigma_{Ea}}{Ea}\right)^2 \approx \frac{2T^2}{(T_{max}-T_{min})^2}\left(\frac{\sigma_T}{T}\right)^2 + 2\left(\frac{1}{\ln(k_{max})-\ln(k_{min})}\right)^2\left(\frac{\sigma_k}{k}\right)^2 \quad \textbf{(4)}$$

Within this study, propagated error for E_a could not be obtained due to some imaginary values of rate constants with larger errors. However, as the error bars of data presented in Figure 28 are quite tight, the slope of the line is visually confirmed to be quite reasonable (see "Results," p. 72). Thus, even though there is no reported error for E_a in Table 11, since E_a is obtained through the slope of the linear fit, the values reported for k_1 E_a are assumed to have minimal-but-reasonable propagated error.

Morse, Spencer, Wilson, and Girolami[19] modified the above equation to conduct error analysis of Eyring-Polyani linear fits. Because E_a is often substituted for $\Delta G^{\ddagger}$, which is proportional to both enthalpy and entropy of transition ($\Delta H^{\ddagger}$ and $\Delta S^{\ddagger}$ respectively), delta terms for T and ln(k) must be expanded to include ln(k/T), propagating the variance of temperature with the temperature-dependent error of rate constants k. This produces the equations

$$(\sigma\Delta H^{\ddagger})^2 = \frac{R^2 {T_{max}}^2 {T_{min}}^2}{(T_{max}-T_{min})^2}\{(\frac{\sigma_T}{T})^2 \left[(1 + T_{min}\frac{\ln(k_{max}/T_{max})-\ln(k_{min}/T_{min})}{T_{max}-T_{min}})^2 + (1 + T_{max}\frac{\ln(k_{max}/T_{max})-\ln(k_{min}/T_{min})}{T_{max}-T_{min}})^2\right] + 2(\frac{\sigma_k}{k})^2\} \quad \textbf{(5)}$$

for the error of enthalpy, and

$$(\sigma\Delta S^{\ddagger})^2 = \frac{R^2}{(T_{max}-T_{min})^2}\{(\frac{\sigma_T}{T})^2 \left[{T_{max}}^2(1 + T_{min}\frac{\ln(k_{max}/T_{max})-\ln(k_{min}/T_{min})}{T_{max}-T_{min}})^2 + {T_{min}}^2(1 + T_{max}\frac{\ln(k_{max}/T_{max})-\ln(k_{min}/T_{min})}{T_{max}-T_{min}})^2\right] + (\frac{\sigma_k}{k})^2\left({T_{max}}^2 + {T_{min}}^2\right)\} \quad \textbf{(6)}$$

for the error of entropy.

These variances are calculated for each k included on the Eyring-Polyani plot, then averaged to report the overall propagated error of both $\Delta H^{\ddagger}$ and $\Delta S^{\ddagger}$. In some instances, the large error within a given k value produces a negative k_{min}. In these instances, error could not be calculated as the ln(kmin/Tmin) term produces an imaginary result and therefore there is no reported value in the associated table(s).

Results

Microwave Synthesis of $Os_3(CO)_{10}I_2$

While microwave synthesis does not produce 100% yield of desired product, this particular method of improved synthesis[22] and isolation provides the highest yield, and greatest purity, of product with minimal effort. Previous microwave synthesis conducted at 150 C produced greater quantities of by-product $Os_2(CO)_6I_2$ as indicated by peaks at 2098 cm^{-1} shown in Figure 16a. Increasing the temperature of synthesis from 150 ^oC to 155 ^oC improved desired product yield and decreased the production of diosmium byproduct[22].

Additionally, it was found through this work that storage at -20 ^oC brings $Os_3(CO)_{10}I_2$ out of solution. Previous isolation methods from microwave synthesis called for the microwave vessel to rest at room temperature to allow any unreacted $Os_3(CO)_{12}$ to fall out of solution, as it is insoluble at room temperature. However, as solid state $–(CO)_{12}$ and $–(CO)_{10}$ are visibly similar, it was found that the solid that collected at the bottom of the vessel had been misinterpreted as unreacted starting material and had therefore been discarded. Upon cleaning the vessel, the solid dissolved in hexane and dichloromethane, indicating that the solid was $–(CO)_{10,}$ the desired product. Using this to our advantage, crashing out desired product by cooling at -20 ^oC provided a method to obtain the majority of the synthesized $Os_3(CO)_{10}I_2$ without column chromatography, as the collected precipitate was determined to be pure. A column is still necessary to isolate the remaining $Os_3(CO)_{10}I_2$ from the impure solution, a mixture of $Os_3(CO)_{10}I_2$ and $Os_2(CO)_6I_2$, but a column does not need to be done immediately as $Os_3(CO)_{10}I_2$ and $Os_2(CO)_6I_2$ are both stable in solution when capped at benchtop conditions. This updated microwave synthesis, therefore, improved both efficiency of synthesis and isolation, as well as product yield and purity.

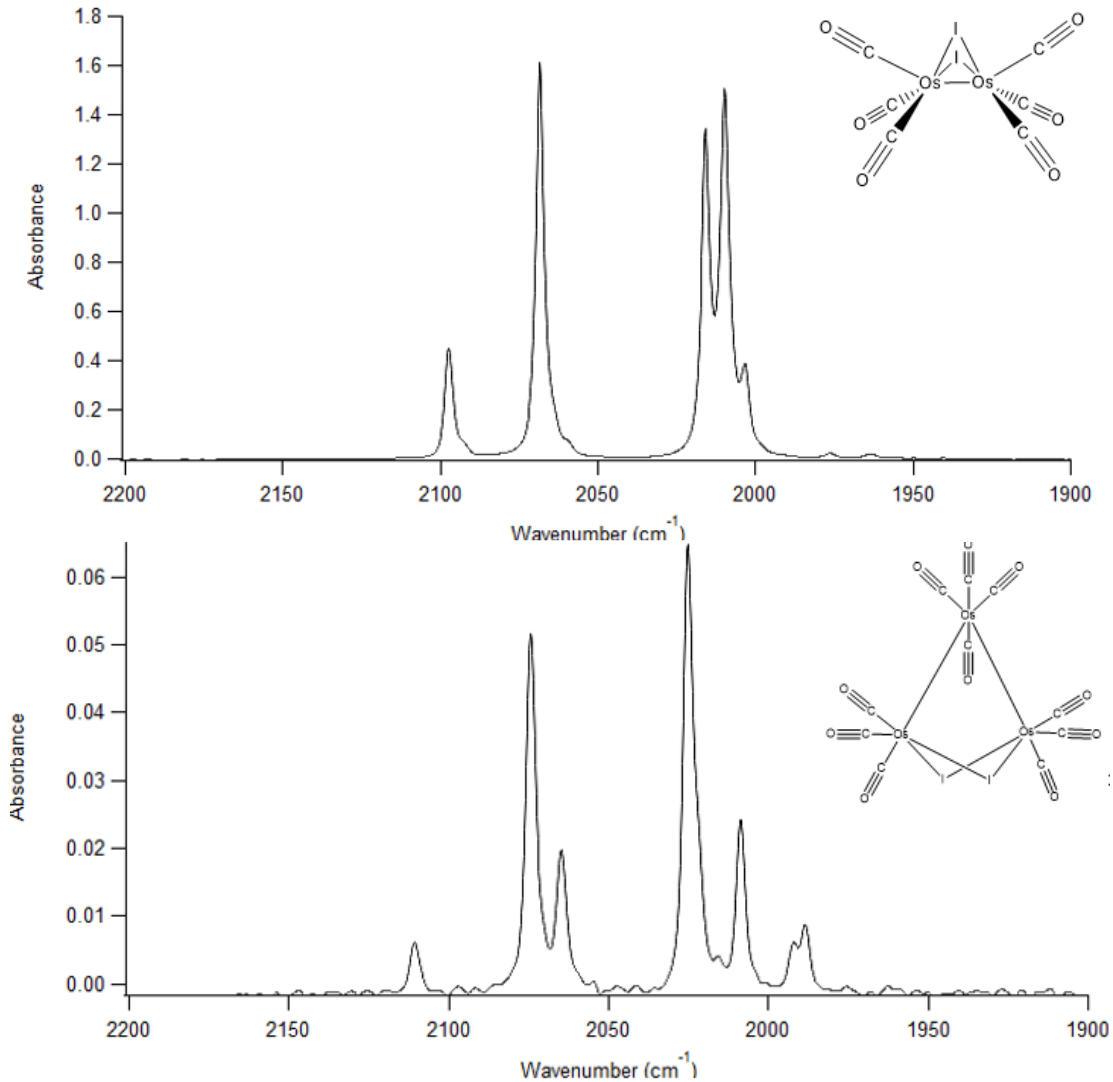

Fig 16 (a) IR of $Os_2(CO)_6I_2$ in hexane, peaks at 2097, 2068, 2016, 2009, 2003, 1976, 1963 cm^{-1}. Top spot in TLC, first to elute in columns. (b) IR of desired product $Os_3(CO)_{10}I_2$ in hexane, peaks at 2110, 2075, 2064, 2025, 2008, 1991, 1988 cm^{-1}.

Order of Reaction

The desired $Os_3(CO)_{10}I_2$ was determined to be of good quality by IR, shown in Fig 16b, and was then refluxed with $P(OR)_3$ at 60 ˚C in 10 mL 2-methylpentane for at least 90 minutes. IR spectra were taken every two minutes once the system had reached reflux. IgorPro analysis of each spectrum within each 90-minute reflux produced peak height estimations by way of curve fitting, an example of which is shown in Figure 17.

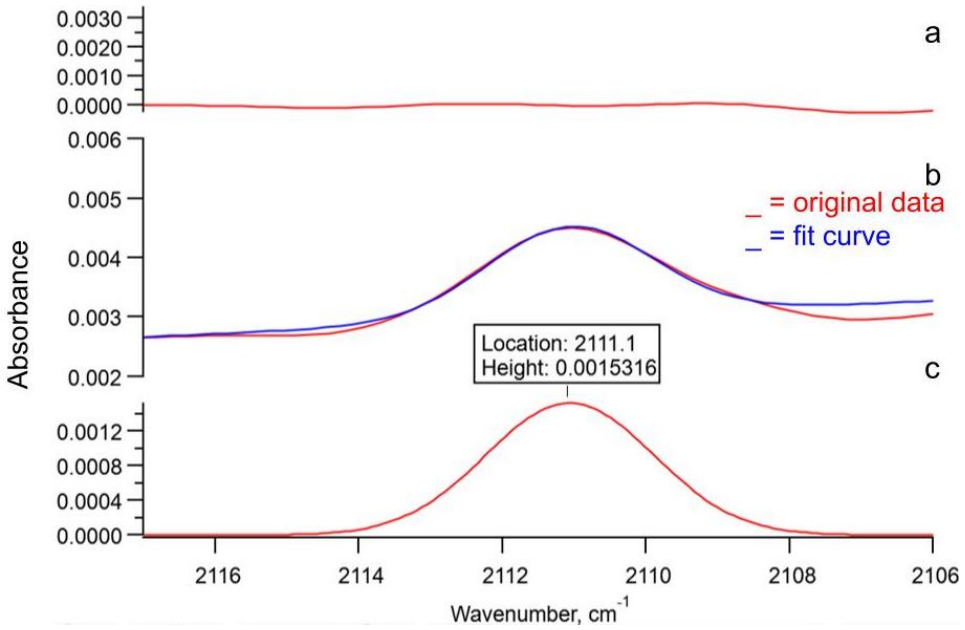

Fig 17 IgorPro curve fitting output for 1:2 Reflux #1 at 48 min. (a) Residual curve, the difference between (b) blue fit curve and red raw IR curve. (c) individual peak obtained by IgorPro with tags for peak location and height.

The raw data, shown in red, is zoomed into a window where only the necessary 2110 cm^{-1} peak is shown. This portion of the IR is fit with a linear baseline to accommodate any noise in the baseline overtime; while the baseline should remain constant with a slope of zero in an ideal spectrum, the introduction of heat may produce a linear sloped baseline rather than a constant 0. The disappearance of the 2110 cm^{-1} peak demands changing the resolution of the fit window as necessary, as the software may no longer detect a peak under heights of 0.001 units within the recommended window Zoom of 2120-2105 cm^{-1}.

The software auto locates any peaks within the defined window range and provides peak results in the form of a summative graph (Fig 17), providing information such as the residual curve and individual peaks in addition to the overall fit function as defined. The residual curve is the difference between the raw IR peak and the IgorPro-obtained fit peak; with an ideal IR spectrum, the fit curve would be identical to the raw data, and the residual curve would therefore be constant

at 0. The residual is not necessary for chemical analysis, but it is a helpful qualification of the confidence in the peak height output from IgorPro, shown as tags on the individual peak on the bottom of this summary graph.

The order of reaction for a given mechanism is determined by the overall quantity of n in Equation 7a, where

$$\text{Rate} = \text{k}[\text{A}]^{\text{n}}, \text{n} = 0, 1, 2 \quad \textbf{(7a)}$$

such that k is the rate constant and [A] is the concentration of reactant. The overall rate is governed by the rate-determining step of the mechanism and, therefore, the order of reaction is given by n. If n = 0, the mechanism is zero order with respect to A, and therefore independent of reactant concentration; n = 1 is first order and dependent on the concentration of reactant; n = 2 is second order and governed by the squared concentration of reactant. In reactions where the concentration of more than one compound is involved in the rate-determining steps, Equation 7a can also be expressed such that

$$\text{Rate} = \text{k}[\text{A}]^{\text{n}}[\text{B}]^{m}[\text{C}]^{l} \ldots [\text{Q}]^{i} \quad \textbf{(7b)}$$

where the order of reaction is given by the sum of the exponents. For example, if the rate of ligand substitution of $Os_3(CO)_{10}I_2$ by $P(OR)_3$ is dependent on both the compound and the ligand, a rate order of two is expected as the order is the sum of exponents, and the rate would thus be described as

$$\text{Rate} = \text{k}[\text{compound}]^{1}[\text{ligand}]^{1}.$$

Integrating the overall rate law (Eqn 7a, for simplicity) for zero, first, and second order reactions produced the Integrated Rate laws as Equations 4a-c

$$n = 0, \qquad [A]_t = -kt + [A]_0, \tag{8a}$$

$$n = 1, \qquad \ln([A]_t) = -kt + \ln([A]_0), \tag{9b}$$

$$n = 2, \qquad \frac{1}{[A]_t} = kt + \frac{1}{[A]_0} \tag{10c}$$

where $[A]_t$ is the concentration of reactant at time t, $[A]_0$ is the initial concentration of reactant, and k is the rate constant. These integrated rate laws allow for linear plots of data over time so that, in each case, the slope of the trendline is ± k.

Due to the absence of peak broadening throughout these reactions, absorbance, or peak height, is used to monitor the rate of reaction for any given overall rate order even if the rate is found to be independent of initial concentration of reactant. Peak heights can be used rather than rote concentration in accordance with Beer-Lambert's Law which states that

$$A = \varepsilon lc \tag{11}$$

where A is the absorbance, or peak height, and is equal to the product of the ε, the extinction coefficient, l, the path length of the IR cell, and c, the concentration. Because ε and l are constants, as ε is a property of the molecule itself and the same IR cell is used for each spectrum, there exists a direct correlation between the change in peak height and the change in concentration. This is not to say that the peak height *is* the concentration, but that the *change* in peak height is proportional to the *change* in concentration. To determine the order of reaction, then, the peak heights from IgorPro are then plot against time as either raw height, natural log of height, or inverse height in accordance with the integrated rate laws of Eqn 8. Each plot is then fit with a linear trendline as

the true overall order of reaction will produce a linear graph; the strongest correlation coefficient, R^2, is used to quantitatively determine the order of reaction in addition to qualitative analysis of linear fit curve.

At 300x excess $P(OPh)_3$, the concentration of ligand at any time throughout this reaction is so much greater than reactant $Os_3(CO)_{10}I_2$ that it can be considered constant throughout the progression of this reaction. This application of the Steady State Approximation therefore eliminates any possible contribution of $P(OPh)_3$ from the overall rate, thereby allowing investigation of the observed rate with respect only to $Os_3(CO)_{10}I_2$. Figure 18 shows three integrated rate plots for 300x excess $P(OPh)_3$ at 60 ^oC.

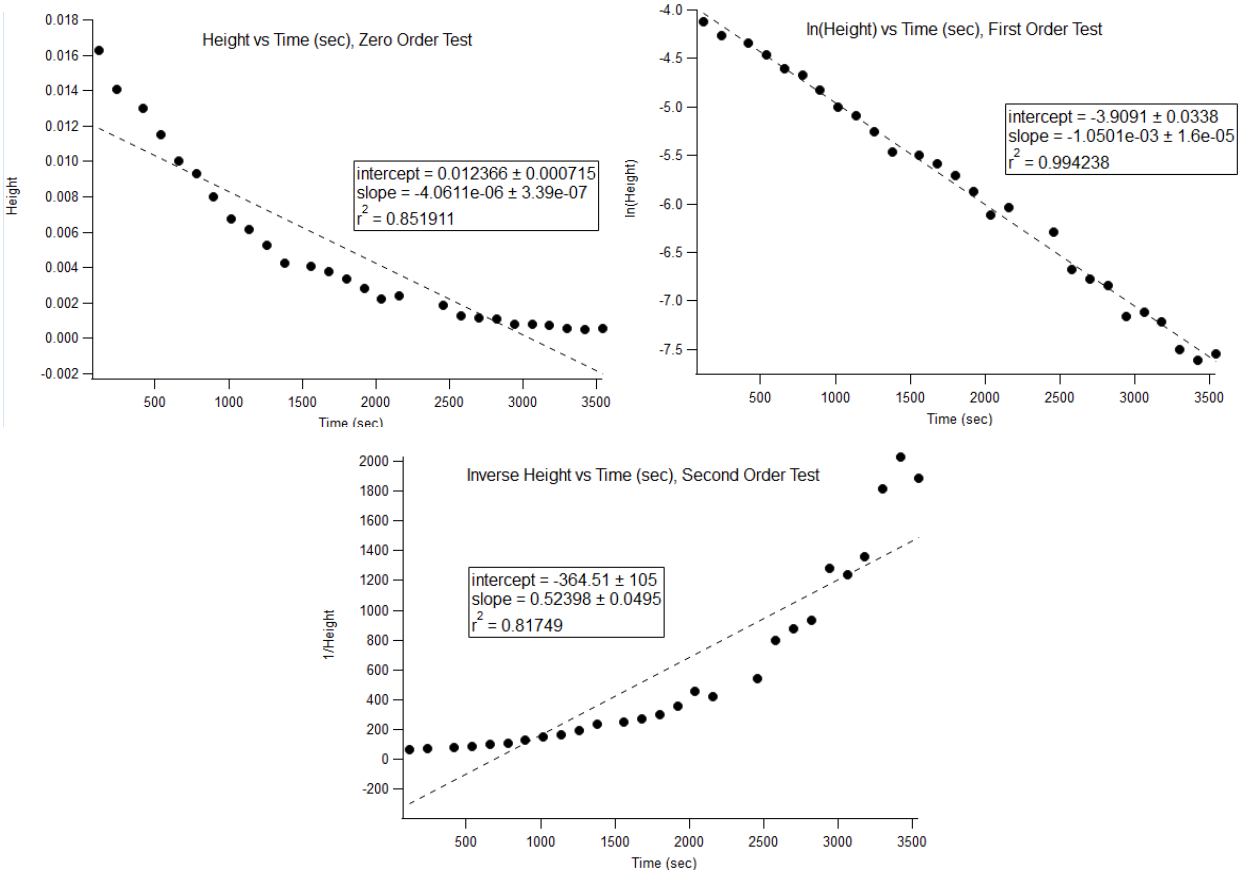

Fig 18 Integrated Rate plots of 1:300 Reflux #1 at 60 C over time to determine order of mechanism (a) Height vs Time, Zeroth Order, R^2 = 0.851911, (b) Natural Log of Height vs Time, R^2 = 0.994238, k = 1.0501 x 10^{-3} ± 0.016 /sec (c) Inverse Height vs Time, R^2 = 0.81749.

This trial is first order as evidenced by the R^2 of Natural Log of Height vs Time (R^2 = 0.994238, k = 1.0501 x 10^{-3} sec^{-1}). Each set of conditions was repeated in triplicate, the average rate constant for 300x excess $P(OPh)_3$ was found to be 1.295 ± 0.305 x 10^{-3} sec^{-1}.

As previous preliminary research suggested that rate increases with decreasing ligand concentration[12], this procedure was then repeated in triplicate at both 50x excess and 2x excess (stoichiometric) conditions to introduce an intermediate comparison, rather than a direct comparison of 300x to one 1:2 reflux as conducted in Bradford's study. The average rate constant of the 1:50 $Os_3(CO)_{10}I_2$:$P(OPh)_3$ was found to be 9.183 ± 0.495 x 10^{-4} sec^{-1}. Even at stoichiometric conditions, 1:2 $Os_3(CO)_{10}I_2$:$P(OPh)_3$ shown in Figure 19 this reaction was found to be first order (R^2 = 0.9912, k = 9.603 x 10^{-4} sec^{-1}) and suggests that this process is zero order with respect to ligand.

The data under stoichiometric conditions confirms that this reflux truly is first order with respect to $Os_3(CO)_{10}I_2$, and zero order with respect to ligand as the Steady State Approximation of 300x excess can no longer be applied in the absence of vast excess ligand. Thus, the overall average rate constant for substitution by $P(OPh)_3$ at 60 ^oC was found to be 9.618 ± 0.937 x 10^{-4} sec^{-1}. Further, as the rate was found to be independent of ligand and ligand concentration, all subsequent data was collected only at stoichiometric (1:2) conditions in triplicate, and these steps necessary for determination of order of reaction did not need to be repeated with each new temperature.

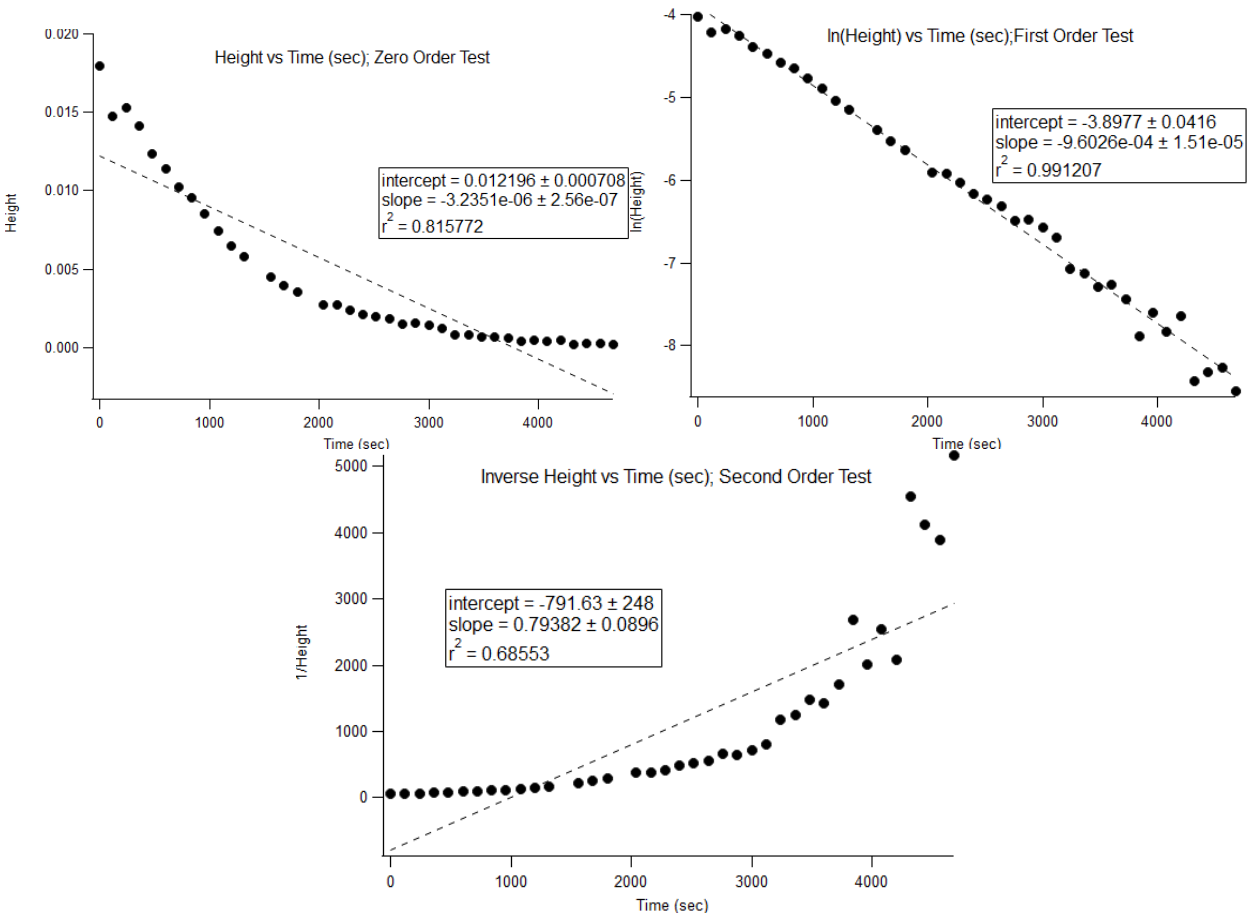

Fig 19 Integrated Rate plots of 1:2 Reflux #1 at 60 C over time to determine order of reaction (a) Height vs Time, Zeroth Order, $R^2 = 0.8158$ (b) Natural Log of Height vs Time, First Order, $R^2 = 0.9912$, $y = -9.603x10^{-3}(x) - 3.898$ (c) Inverse Height vs Time, Second Order, $R^2 = 6.855$

Kinetic Analysis: Multipeak Analysis

While independent analysis of 2110 cm^{-1} peak is useful to determine the overall order of reaction, further investigation of spectral overlays and fitting of additional peaks indicates a mechanistic pathway of at least two steps. An overlay of all spectra, an example of which is shown in Figure 20, captures snapshots of the change of the peaks within the carbonyl region with arrows indicating direction of change, much like an artist's flip book. Disappearing peaks are indicative

of loss of reactant, $Os_3(CO)_{10}I_2$, while new appearing peaks are those correlated with the production of $Os_3(CO)_8I_2(P(OR)_3)_2$.

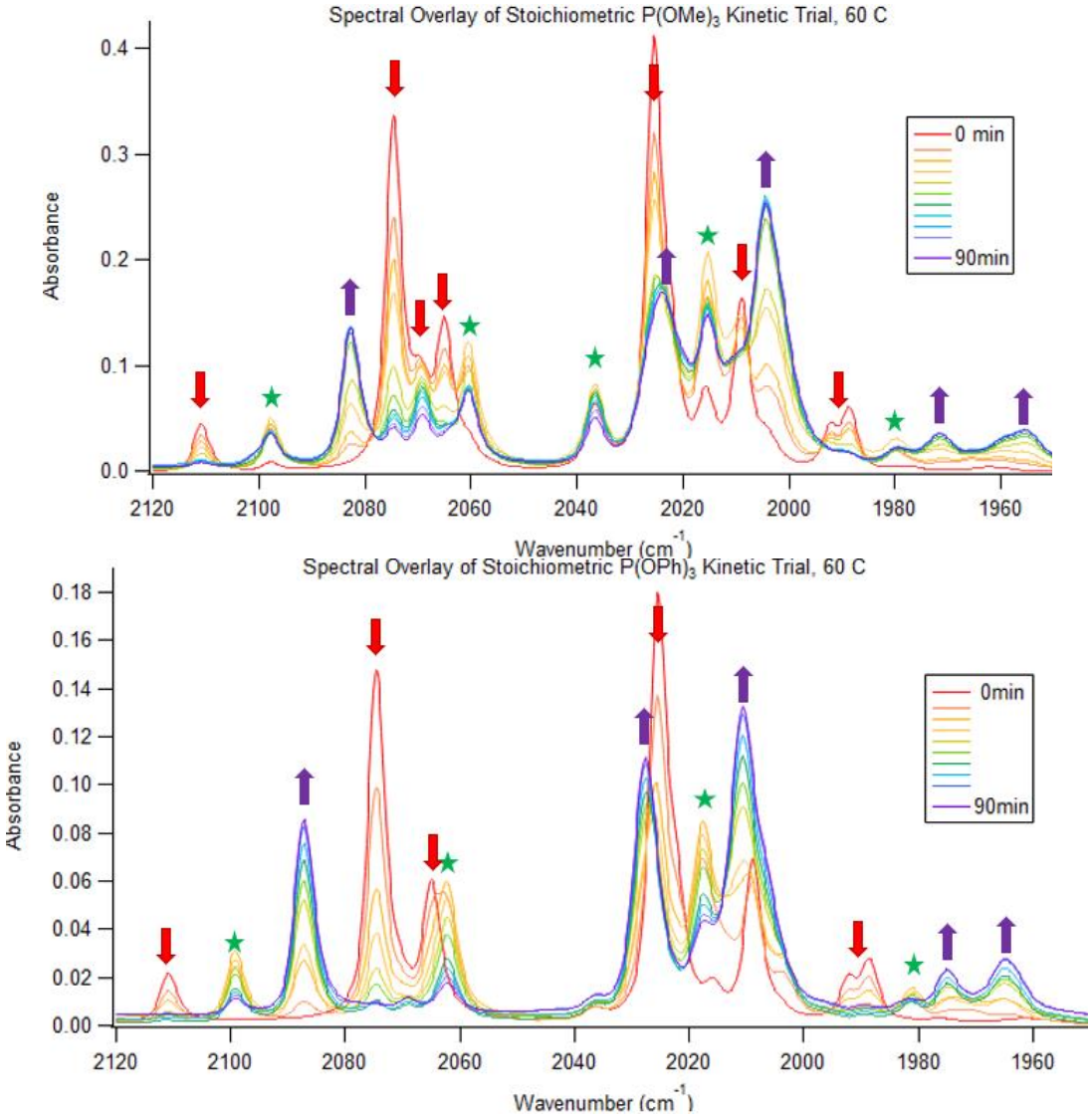

Fig 20 Full 90 min, 60 C reflux overlays, spectra taken every two minutes. Arrows mark dis- and appearing peaks; stars mark compound that comes in at a maximal height then disappears. (a) -$P(OPh)_3$ reflux, (b) -$P(OMe)_3$ reflux. Starred peaks at 2098, 2060, 2015, 1980 cm^{-1} for both phosphite ligands.

In each reflux, regardless of ligand or concentration thereof, there were peaks that are not a part of the initial reactant spectrum nor the final product spectrum, yet grow in to a maximal height then disappear before the termination of the reflux, more clearly shown in Figure 21, where

the dashed purple spectrum represents the maximum height of the starred peaks. These starred intermediate peaks are 2098, 2060, 2015, and 1981 cm^{-1} for both ligands.

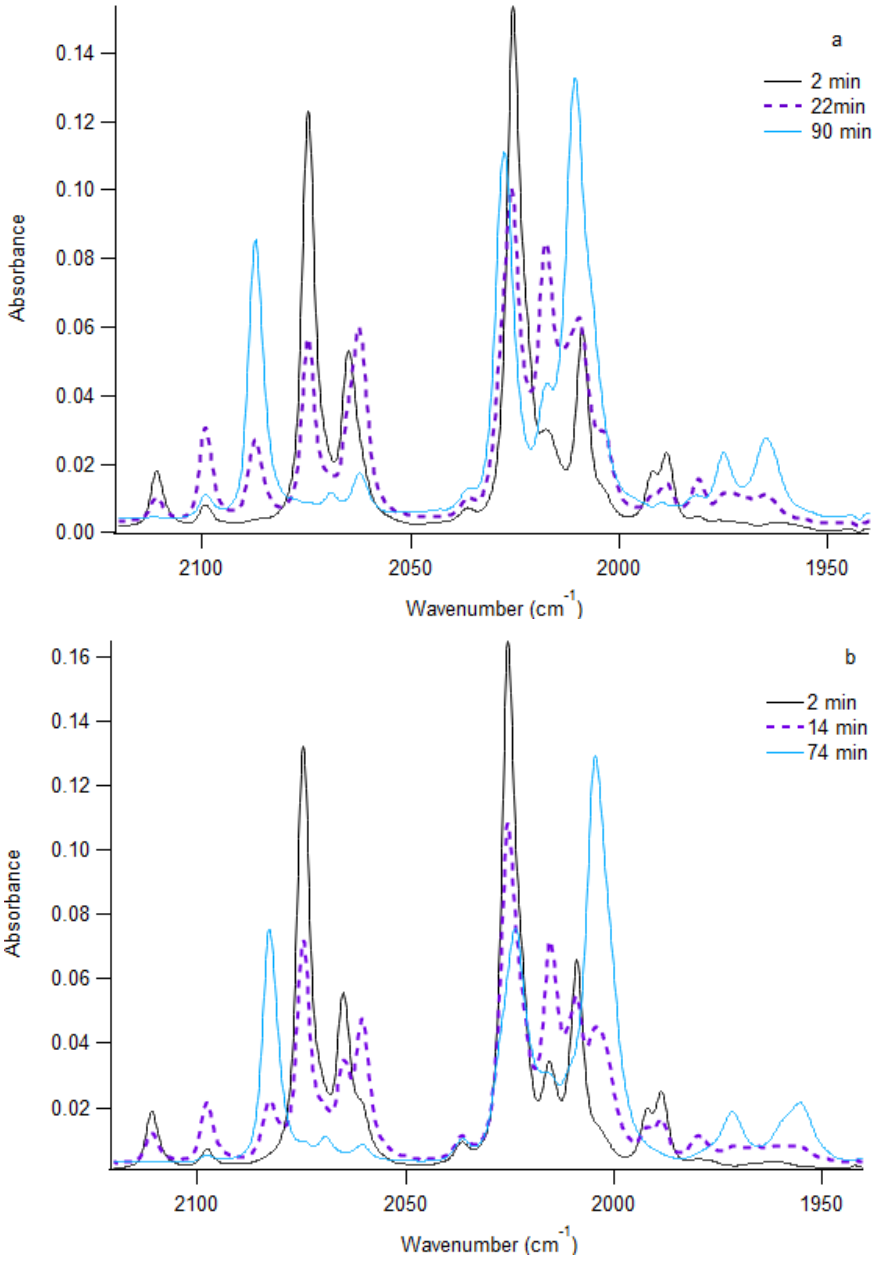

Fig 21. Initial, Final, and Intermediate Max IR overlay of (a) $P(OPh)_3$ and (b) $P(OMe)_3$ at 60 °C. The dashed, purple spectrum includes the starred intermediate peaks indicated in Fig 20a-b at their maximal height, more clearly demonstrating that these peaks are neither reactant nor product.

Figure 22 presents a full spectral overlay as a 3D waterfall for the stoichiometric kinetic trial of $P(OPh)_3$ in 2-methylpentane (60 °C). This 3D display more clearly shows the peak at 2098 cm^{-1} that is not part of the starting material, grows in to a maximal height, then disappears as more starting material is converted to product. The first spectrum, 0min, is in the back; time progresses forward, out of the page, toward the final spectrum taken at 90 minutes.

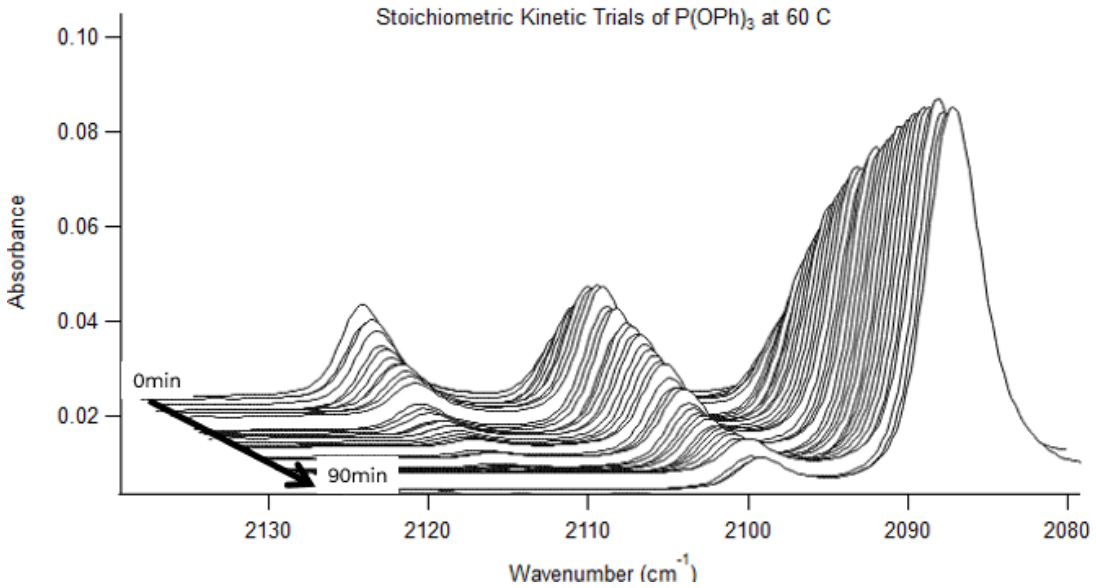

Fig 22. 3D Waterfall plot of all $P(OPh)_3$ IR spectra taken for 90min at 60 °C. One spectrum was taken every two minutes; the first spectrum is in the back, with the last spectrum at the front. Note how the peak at 2098 cm^{-1} is not part of the starting material pattern, yet grows into a maximal height, then disappears once more.

At 300x excess ligand, these peaks could be easily explained as some impurity reacting with excess ligand, but at stoichiometric conditions, as shown above, the presence of these peaks can no longer be disqualified as impurity interacting with excess ligand and is therefore determined to be an intermediate compound, which is proposed to be $Os_3(CO)_9I_2[P(OR)_3]$. However, as none of these intermediate peaks overlap or interfere with the 2110 cm^{-1} peak, kinetic analysis by way of monitoring peak disappearance at 2110 cm^{-1} is still appropriate and unaffected.

Figure 23 shows the final product spectra of both $Os_3(CO)_8I_2[P(OPh)_3]_2$ and $Os_3(CO)_8I_2[P(OMe)_3]_2$. These compounds have the same number and pattern of peaks but can be differentiated by wavenumber shift; the triphenyl phosphite variant has higher wavenumbers than that of the trimethyl phosphite variant.

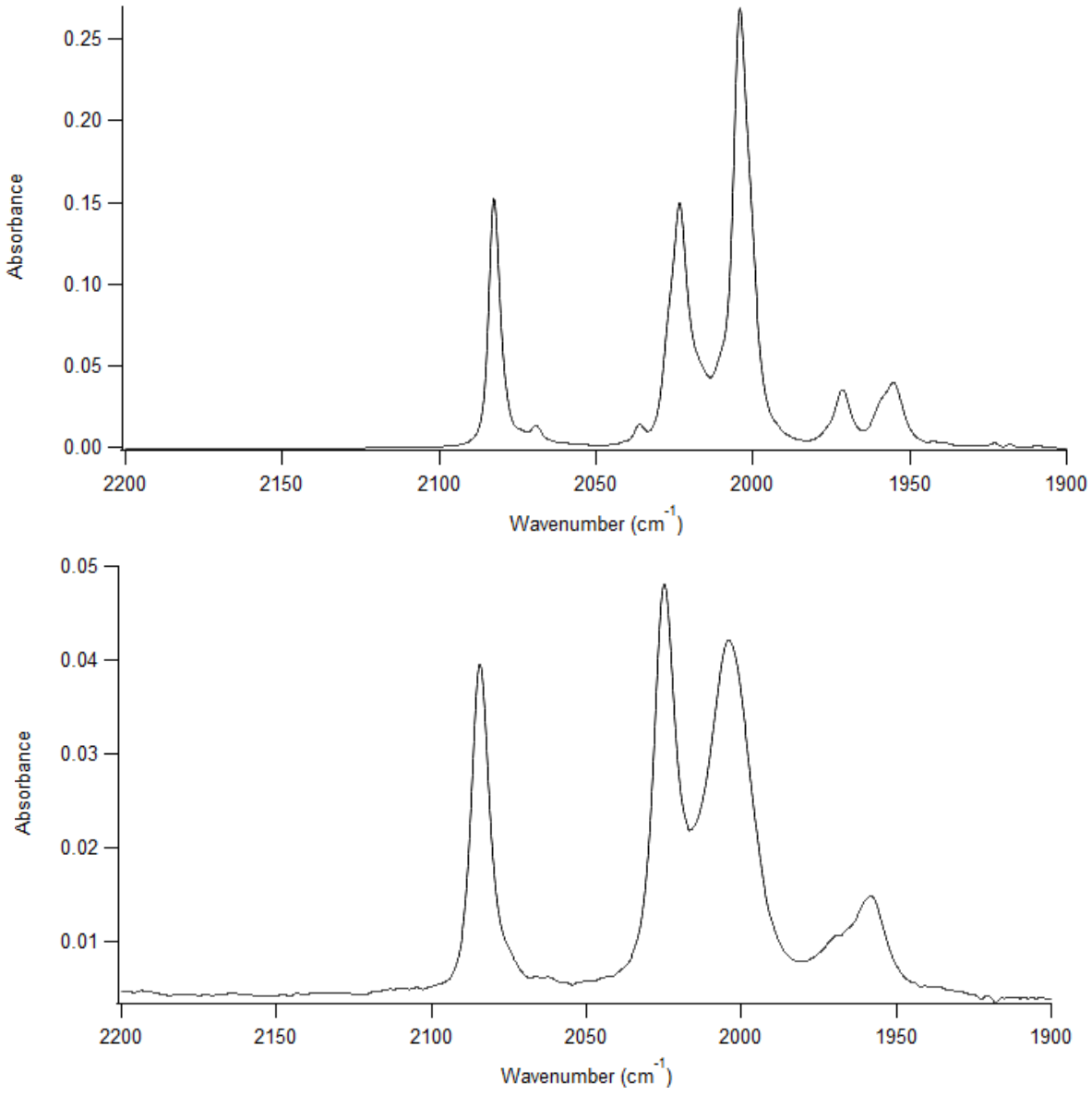

Fig 23. Final products of refluxes. Each have the same number and pattern of peaks but can be distinguished by wavenumber shifts. (a) $Os_3(CO)_8I_2[P(OPh)_3]_2$, peaks at 2086, 2028, 2010, 1975, and 1965 cm^{-1}. The peak marked at 2062 is indicative of unreacted intermediate, not the final product. (b) $Os_3(CO)_8I_2[P(OMe)_3]_2$, peaks at 2082, 2023, 2003, 1970, and 1955 cm^{-1}.

Kinetics Analysis: Two-Step Investigation

With the determination of first-order kinetics at all concentrations of $P(OR)_3$, the conclusion that changing $P(OR)_3$ concentration did not affect the rate and is thus zero order with respect to ligand, and the presence of intermediate peaks even at stoichiometric conditions, a secondary IgorPro graphical analysis was performed to investigate the possibility of a two-step mechanism following Scheme 2.

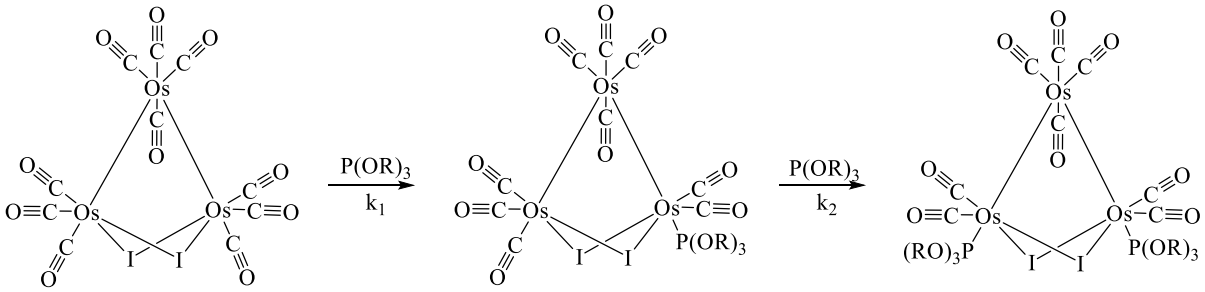

Scheme 3 proposed two-step process of the reaction of $Os_3(CO)_{10}I_2$ with P-donor ligands, here demonstrated with $P(OPh)_3$.

The rates of each step in Scheme 3 can be monitored by the change in concentration of each molecule; R for reactant $Os_3(CO)_{10}I_2$, I for intermediate, and P for product $Os_3(CO)_8I_2(P(OPh)_3)_2$. The rates of each step, then, can be written as Equations 12a-c since ligand is not involved in the observed rate, such that

$$\frac{d[R]}{dt} = k_1[R] \qquad \textbf{(12a)}$$

$$\frac{d[I]}{dt} = k_1[R] - k_2[I] \qquad \textbf{(12b)}$$

$$\frac{d[P]}{dt} = k_2[I] \qquad \textbf{(12c)}$$

Sequential Kinetics, while mechanistically two-steps, occur simultaneously; in the reflux solution, one cannot identify the point at which step one is “complete” and step two “begins” as

the intermediate compound is immediately converted into product upon its creation in solution. This chemical understanding indicates that traditional Integrated Rate Law equations and plots (Eqn 8a-c and Fig 18) will not provide sufficient information.

To obtain kinetic information, then, Eqn 12a-c must be modified and rewritten in terms of reactant R to calculate the rate constants of each step with raw absorbance analysis in IgorPro. Equation 6a requires no substitution, as it is already in terms of [R]. Integration of this equation yields the function

$$[R] = [R]_0 e^{-k1(t)} \quad \textbf{(13a)}$$

and allows for the calculation of k_1 in terms of reactant concentration.

To rewrite Eqn 6b to fit the intermediate peak height data, Eqn 6a is substituted for the term [R]. The entire function is then differentiated and integrated to yield the final form

$$[I] = \frac{k1}{k2-k1}[R]_0(e^{-k1(t)} - e^{-k2(t)}) \quad \textbf{(13b)}$$

which then produces calculated values for both k_1 and k_2.

Similarly, as equation 6c is written in terms of both [I] and [R], both of which are now known as Equations 7a and 7b, those functions substituted for their respective terms [R] and [I], which now leaves the entire function in terms of [R]. This equation is then differentiated and integrated as before to yield

$$[P] = [R]_0\left(\frac{k_1 e^{-k_2(t)} - k_2 e^{-k_1(t)}}{k2-k1} + 1\right) \quad \textbf{(13c)}$$

Equations 7a-c allow for calculation of rate constants k_1 and k_2 by way of analysis of absorbance, or peak height, over time under the mathematical assumptions that (1) both steps are

first order with respect to reactant, $Os_3(CO)_{10}I_2$, and that (2) k_1 and k_2 are numerically different values. This is to say that for the IgorPro to fit these data appropriately, the initial input terms, or "guesses," as IgorPro calls them, for k_1 and k_2 must be different, even if the final output is chemically equivalent (e.g., "guesses" of 0.0001 and 0.00011 are allowed, even if those rates would be called "equivalent" overall).

The heights of peaks 2110, 2098, and 2086 cm^{-1} provide insight to the change in concentration over time of reactant, intermediate, and product respectively and provide calculated values for k_1 and k_2. The same raw peak height data is plot against time, and the fit functions are manually defined in IgorPro. To minimize covariant error of k_2, as this method of calculation produces one k_2 from intermediate peaks and another k_2 from product peaks, the calculated value of k_1 from the reactant data is held for what IgorPro refers to as the initial input term for both the intermediate data and product data fits. Since the consumption of reactant is *only* dependent on the initial concentration of reaction, or in other terms, since k_1 is *only* related to the consumption of reactant, that value can be considered true, and thus allows for the guess-and-hold usage of k_1 in subsequent fits demonstrated in Figure 24.

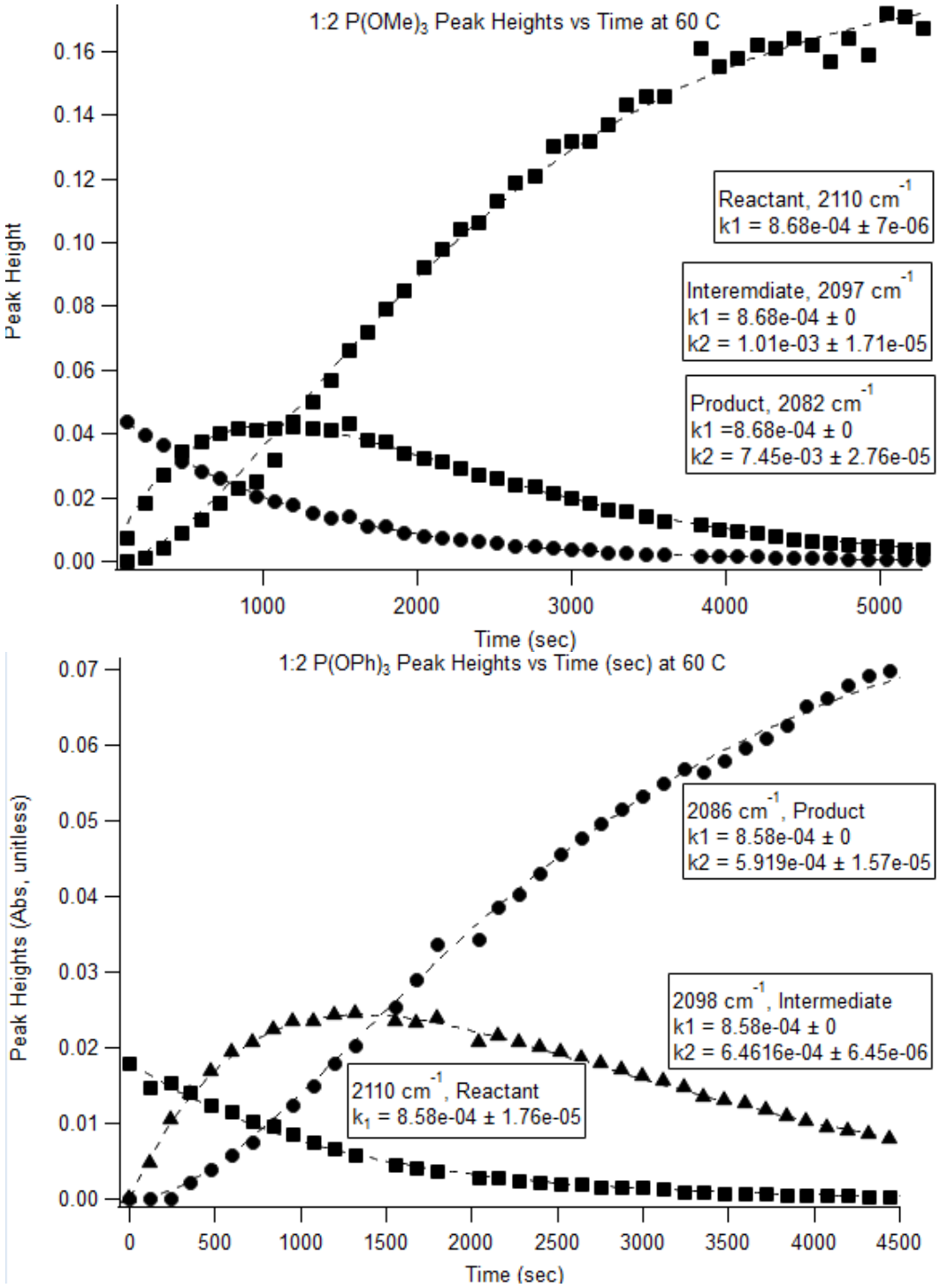

Fig 24 sequential kinetic analysis of stoichiometric refluxes of $P(OMe)_3$ [top] and $P(OPh)_3$ [bottom] ligands both at 60 ºC. Peak heights of reactant, intermediate, and product monitored over time by IgorPro multipeak fit. Data was fit to the corresponding equations 13a-c. The k_1 obtained from the reactant fit is then held for intermediate and product fits to minimize covariance of curve fitting, as demonstrated by the error of 0 for those k_1 terms.

The rate constants for steps one and two, indicated as k_1 and k_2 from each concentration of ligand at 60 °C are compiled in Tables 4 and 5 to analyze the effect of ligand concentration on both observable steps of this reaction.

300x Excess P(OMe)3					
Reactant		Intemediate		Product	
k1, /sec	**± error**	**k2, /sec**	**± error**	**k2, /sec**	**± error**
9.2E-04	0.1E-04	1.08E-03	0.02E-03	6.5E-04	6E-05
9.47E-04	0.09E-04	1.13E-03	0.02E-03	5.2E-04	5E-05
9.6E-04	0.1E-04	1.09E-03	0.01E-03	5.0E-04	3E-05
9.4E-04	0.2E-04	**1.10E-03**	0.03E-03	**5.6E-04**	0.9E-04
50x Excess P(OMe)3					
Reactant		Intemediate		Product	
k1, /sec	**± error**	**k2, /sec**	**± error**	**k2, /sec**	**± error**
9.4E-04	0.1E-04	1.24E-03	0.01E-03	7.4E-04	0.2E-04
8.3E-04	0.1E-04	9.7E-04	0.3E-04	5.3E-04	0.4E-04
8.2E-04	0.1E-04	8.8E-04	0.2E-04	5.9E-04	0.4E-04
8.7E-04	0.2E-04	**1.03E-03**	0.04E-03	**6.2E-04**	0.6E-04
2x Excess, Stoichiometric P(OMe)3					
Reactant		Intemediate		Product	
k1, /sec	**± error**	**k2, /sec**	**± error**	**k2, /sec**	**± error**
8.44E-04	0.17E-04	1.05E-03	0.04E-03	6.60E-04	0.36E-04
8.71E-04	0.09E-04	1.08E-03	0.01E-03	7.34E-04	0.32E-04
8.68E-04	0.07E-04	1.01E-03	0.02E-03	7.45E-04	0.28E-04
8.612E-04	0.21E-04	**1.048E-03**	0.05E-03	**7.131E-04**	0.56E-04

Table 4. Calculated rate constants for $P(OMe)_3$ at 60 °C from IgorPro multipeak fitting using equations 7a-c with associated standard deviations. Final row reports the average of the triplicate data set with propagated error.

300x Excess P(OPh)3					
Reactant		Intemediate		Product	
k1, /sec	**± error**	**k2, /sec**	**± error**	**k2, /sec**	**± error**
8.6E-04	0.2E-04	6.46E-04	0.09E-04	5.9E-04	0.2E-04
8.97E-04	0.08E-04	6.1E-04	0.1E-04	5.6E-04	0.3E-04
9.7E-04	0.2E-04	6.2E-04	0.2E-04	4.6E-04	0.3E-04
9.1E-04	0.3E-04	**6.3E-04**	0.2E-04	**5.4E-04**	0.4E-04
50x Excess P(OPh)3					
Reactant		Intemediate		Product	
k1, /sec	**± error**	**k2, /sec**	**± error**	**k2, /sec**	**± error**
9.23E-04	0.09E-04	6.8E-04	0.2E-04	4.1E-04	0.3E-04
9.6E-04	0.3E-04	4.9E-04	0.4E-04	3.6E-04	0.9E-04
8.63E-04	0.07E-04	6.69E-04	0.06E-04	2.1E-04	0.5E-04
9.2E-04	0.4E-04	**6.1E-04**	0.4E-05	**3E-04**	1.1E-04
2x Excess P(OPh)3					
Reactant		Intemediate		Product	
k1, /sec	**± error**	**k2, /sec**	**± error**	**k2, /sec**	**± error**
9.7E-04	0.2E-04	7.6E-04	0.2E-04	5.5E-04	0.2E-04
1.0E-03	0.1E-04	7.6E-04	0.2E-04	6.4E-04	0.8E-04
1.2E-03	0.2E-04	5.7E-04	0.1E-04	3.3E-04	0.3E-04
1.1E-03	0.3E-04	**7.0E-04**	0.3E-05	**5.1E-04**	0.9E-05

Table 5. Calculated rate constants for $P(OPh)_3$ at 60 °C from IgorPro multipeak fitting using equations 7a-c with associated standard deviations. Final row reports the average of the triplicate data set with propagated error.

Demonstrated within these tables, rate constants of each step did not vary with ligand concentration, and k_1 was found to be independent of phosphite ligand (avg $k_1 = 9.618 \times 10^{-4}$ sec^{-1} for $P(OPh)_3$, 8.897×10^{-4} sec^{-1} for $P(OMe)_3$). However, there were two distinct values of k_2 calculated from the Intermediate and Product peak heights. This is to say that while k_1 was held constant within each ligand's curve fitting process, the values of k_2 from the intermediate peak fit are statistically different from the k_2 of the product peak fit, an unexpected occurrence since they represent the same chemical process. These distinct values of k_2 do not vary with ligand

concentration but do appear to differ with phosphite identity. This variation, though unclear in chemical origin, is more clearly shown in Table 6, which presents the overall kinetic summary of each ligand—the average of nine rate constants for each ligand and the standard deviation of the population at 60 ^{o}C.

Overall Kinetic Summary of P(OMe)3					
Reactant		Intemediate		Product	
k1, /sec	**± error**	**k2, /sec**	**± error**	**k2, /sec**	**± error**
8.9E-04	0.3E-04	1.06E-03	0.07E-03	6E-04	1.19E-04

Overall Kinetic Summary of P(OPh)3					
Reactant		Intemediate		Product	
k1, /sec	**± error**	**k2, /sec**	**± error**	**k2, /sec**	**± error**
9.6E-04	0.6E-04	6.5E-04	0.6E-04	5E-04	1.47E-04

Table 6. Kinetic Summary of $P(OMe)_3$ and $P(OPh)_3$ at 60 ^{o}C. All nine rate constants of Tables 4 and 5 were averaged and error of each k was propagated.

Table 7 presents the minimum and maximum values of k_2 once the standard deviation is taken into account. This is to say that the minimum values are the reported k_2 from Table 6 minus the standard deviation; the maximum value is the same k_2 plus the standard deviation. This same data is also presented on a number line as Figure 25.

	Intermediate Peaks			Product Peaks		
	k2 ± std dev, /sec	min k2	max k2	k2 ± std dev, /sec	min k2	max k2
P(OMe)3	**1.06** ± 0.07E-03	0.99E-03	1.13E-03	**6** ± 1.19E-04	4.81E-04	7.19E-04
P(OPh)3	**6.5** ± 0.6E-04	5.9E-04	7.10E-04	**4** ± 1.47E-04	2.53E-04	5.47E-04

Table 7. Min/Max ranges of k_2's obtained by Intermediate (2097, 2908 cm^{-1}) and Product (2082, 2086 cm^{-1}) curve fits in IgorPro8 for both phosphites at 60 ^{o}C.

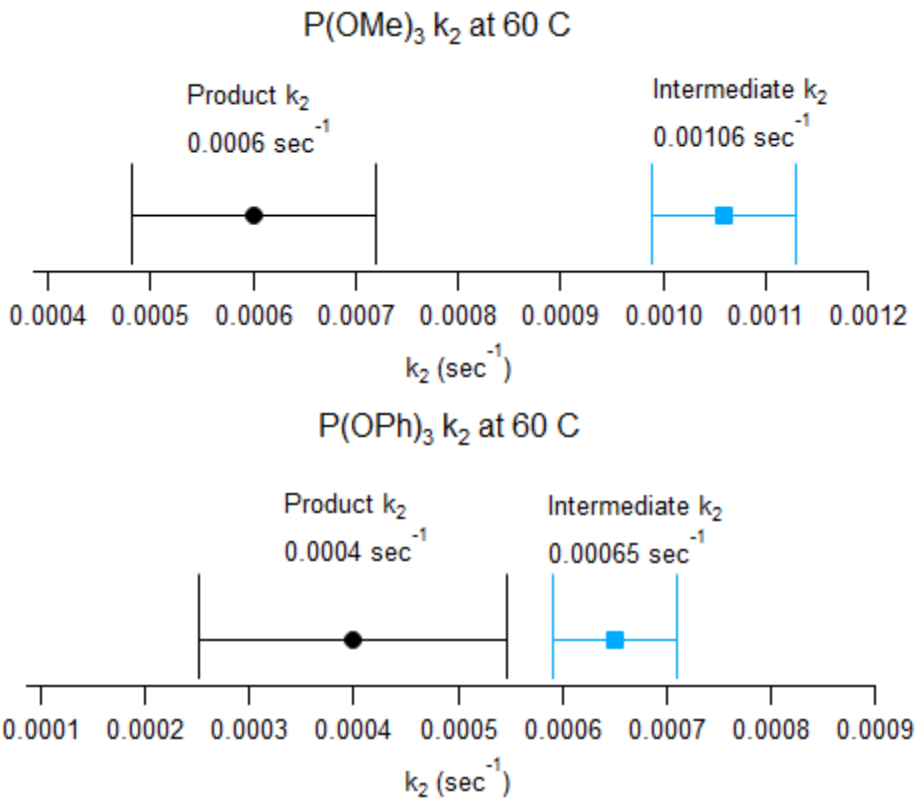

Fig 25. Box plots of variance of k_2 from intermediate and product fits of both $P(OMe)_3$ and $P(OPh)_3$ at 60 °C. The vertical lines represent the min/max, one propagated error margin on either side of the reported value, indicated by a solid marker. Note the complete absence of overlap of these values.

With this condensed comparison of kinetic data, the statistically significant differences between Intermediate and Product k_2's become more apparent as there is no overlap of these values for either $P(OR)_3$. At this point, however, it is unclear if this is a purely mathematical phenomenon because IgorPro as a computer software is not aware of the chemical implications of these data, or if this is an error in the chemical assumptions which were made in order to use these equations. This is to say that it is possible that, though these statistical errors appear quite large on a number line, they may average to an appropriate amount of error when interpreted chemically.

As alluded earlier, mathematically or numerically different values may not always correspond to chemical differences. The previous example, regarding k inputs of 0.0001 and 0.00011, expresses that numerically different values may correspond to identical chemical

applications as the study of mathematics is not bound by the physical and chemical laws of the universe. To investigate whether these different values of k_2 are chemically different, rather than mathematically different as evidence by the standard deviations presented in Table 6 and 7, the activation energy as represented by the Gibbs Free Energy of transition ($\Delta G^{\ddagger}$) was calculated from each k_2 for both ligands using the Eyring-Polyani Equation. While the equations of Sequential Kinetics employed here do rely on the mathematical and chemical assumption that these are the same k_2, additional calculations using these values may begin to demonstrate that the error is systematic and/or mathematical in origin rather. If the values of $\Delta G^{\ddagger}$ obtained from both the intermediate-obtained k_2 and the product-obtained k_2 are mathematically equivalent, then the values of k_2 can be averaged as they represent the same chemical process with some mathematical error.

The Eyring-Polyani equation states that

$$k = \frac{k_B T}{h} e^{\frac{-\Delta G\ddagger}{RT}} \quad \textbf{(14)}$$

where k is the rate constant, k_B is Boltzmann's constant (1.307×10^{-23} J/K), h is Plank's constant (6.26×10^{34} J x sec), R is the universal gas constant (8.3145 J/Kmol) and T is the temperature at which that rate constant was obtained, in units Kelvin. Thus, values of k_1 and k_2 can be used to obtain values of $\Delta G^{\ddagger}$ for each step using Excel, a summary of which is provided in Table 8 for both $P(OR)_3$ ligands.

P(OMe)3 k2's and ΔG‡'s			
From Intermediate Data		From Product Data	
k2 (/sec)	ΔG‡ (kJ/mol)	k2 (/sec)	ΔG‡ (kJ/mol)
1.05E-03	101	6.60E-04	102
1.08E-03	101	7.34E-04	102
1.01E-03	101	7.45E-04	102
	101		**102**

P(OPh)3 k2's and ΔG‡'s			
From Intermediate Data		From Product Data	
k2 (/sec)	ΔG‡ (kJ/mol)	k2 (/sec)	ΔG‡ (kJ/mol)
7.6E-04	102	5.5E-04	102
7.6E-04	102	6.4E-04	102
5.7E-04	102	3.3E-04	104
	102		**103**

Table 8. Gibbs Free Energy of Transition, or Activation Energy, for k_2 obtained from intermediate peaks and product peaks of both ligands at 69 ^{o}C to determine if the mathematical differences in rate constants correspond to a chemical difference in activation energy. As $\Delta G^{\ddagger}$ for both k_2's of both ligands are not mathematically different, the k_2 pool of data can be averaged into one final k_2 value with some associated error.

The values of $\Delta G^{\ddagger}$ from the intermediate-obtained k_2 and the product-obtained k_2 were found to agree, as demonstrated in Table 8. Thus, though the values of k_2 appear different they can still be averaged as they correspond to the same chemical application. Therefore, average k_2 for $P(OMe)_3$ was found to be 8.439×10^{-4} sec^{-1} ($\pm 2.41 \times 10^{-4}$) and average k_2 for $P(OPh)_3$ was found to be 5.542×10^{-4} $ssec^{-1}$ ($\pm 1.51 \times 10^{-4}$).

An additional manner through which to demonstrate that, despite the mathematical isolation of intermediate- and product-k_2's, these are the same values that correspond to the same chemical process, is to hold each "guess" term and hold it for both the intermediate and product fits overall to qualitatively assess the error embedded in this representation of averaged k_2

values. Figures 26a-c fit data for $P(OPh)_3$ at 60 °C with both intermediate-obtained and product-obtained k_2 fits for an overall qualitative assessment of embedded error.

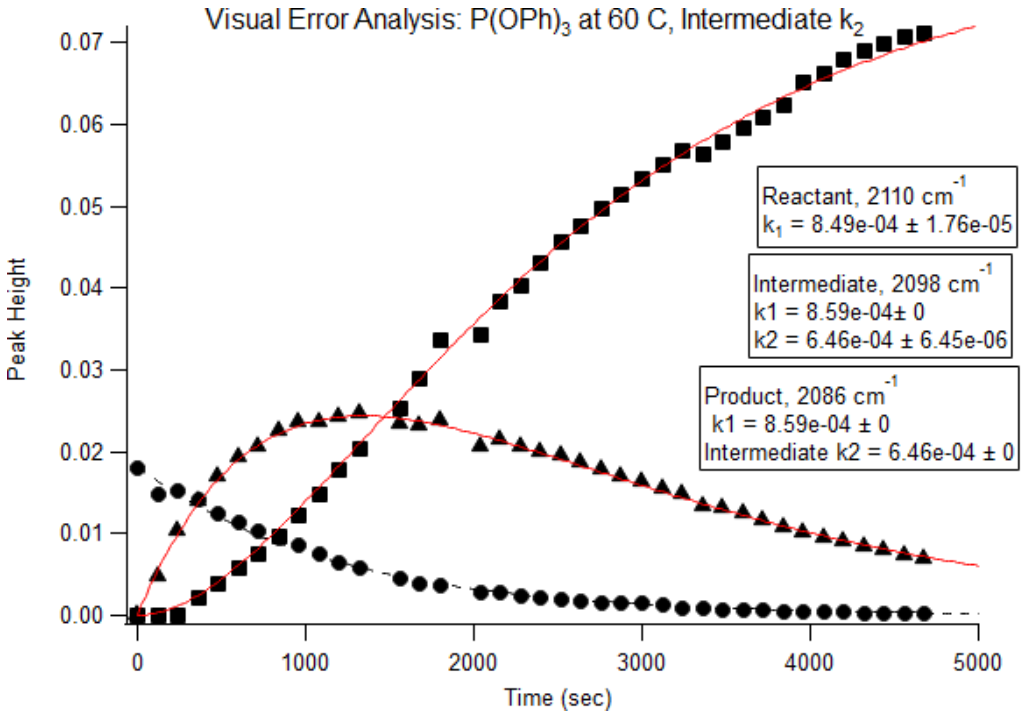

Fig 26a. Intermediate-obtained fits of both intermediate and product data, indicated in red. Intermediate-obtained $k_2 = 6.46 \times 10^{-4}$ sec^{-1}.

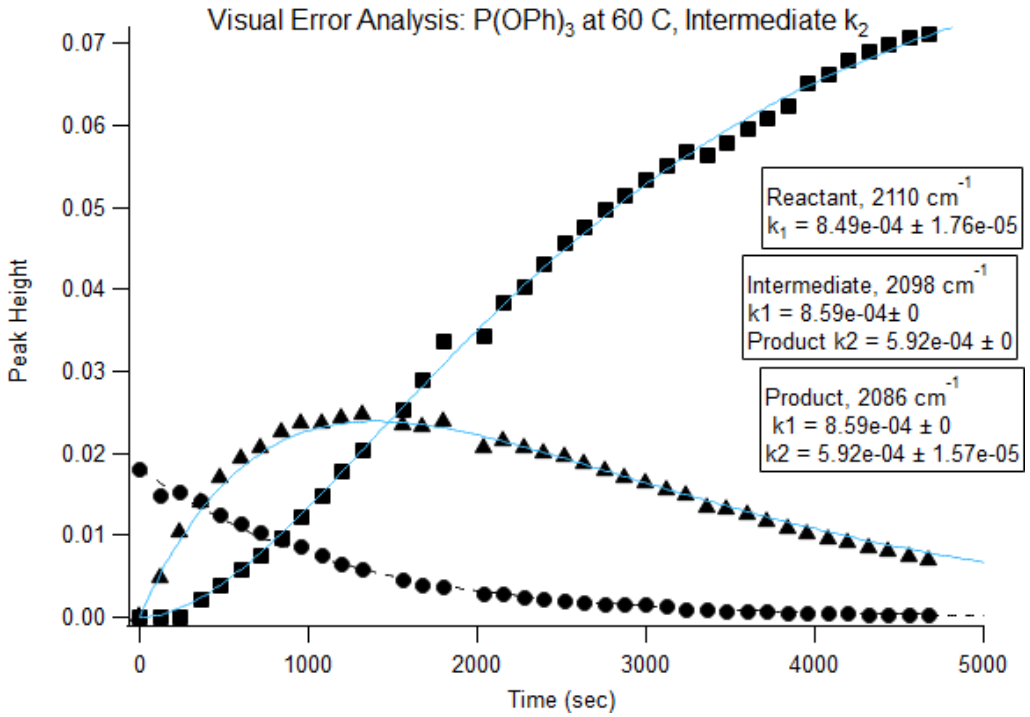

Fig 26b. Product-held fits of both intermediate and product data, shown in blue. Product-obtained $k_2 = 5.91 \times 10^{-4}$ sec^{-1}

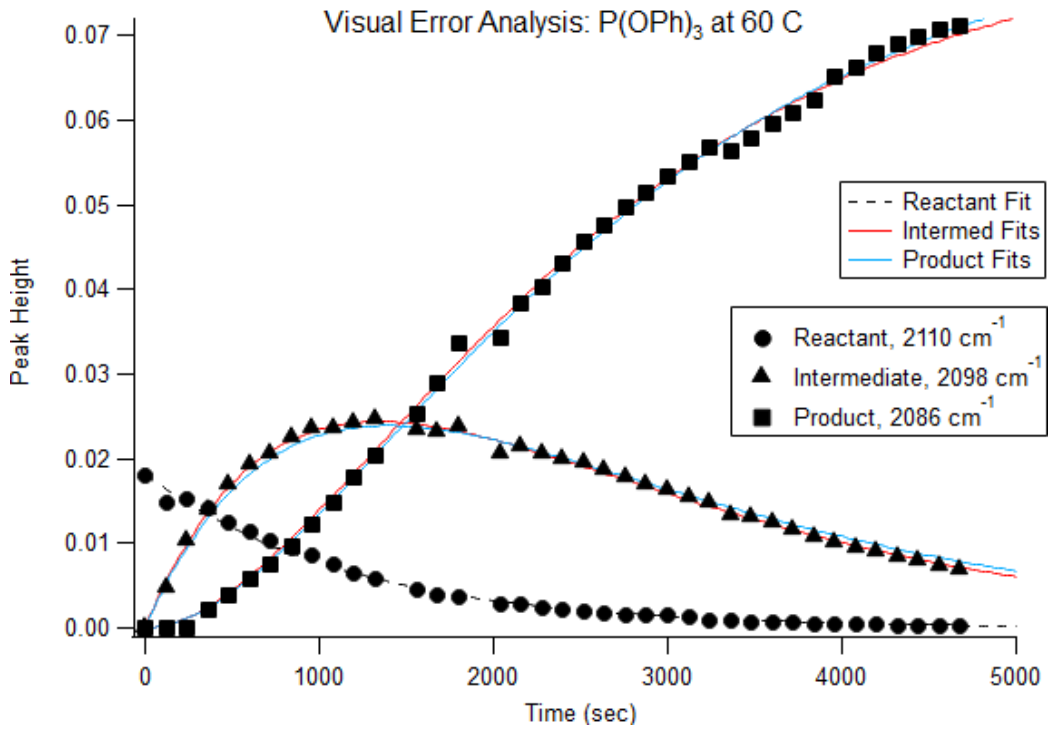

Fig 26c. Overlay of product-held (blue) and intermediate-held (red) fit functions, almost indistinguishable from one another.

Shown most convincingly in Fig 26c, the Intermediate- and Product-obtained values for k_2 are almost indistinguishable from one another when overlayed. Both the red and blue fit curves appropriately fit the raw data set, qualitatively and visually confirming what was mathematically proven in calculating $\Delta G^{\ddagger}$; while mathematically different, both k_2 values correspond to the same chemical process within an appropriate margin of error and can, thus, be averaged. Table 9 presents the average rate constants for each reaction at temperatures that range from 49-69 ^{o}C, and Table 10 reports the Gibbs Free Energy of transition for both steps of both $P(OR)_3$ substitutions at all temperatures investigated in this study. The reported errors of both tables are the propagated errors of rate-constants that have been carried through thermodynamic calculations. Some errors are quite large due to the standard deviations of those rate constants; the propagated error of $\Delta G^{\ddagger}_2$, for example, is not a typo.

Kinetic Summary of P(OMe)3				
T (˚C)	**k1 (/sec)**	± error	**k2 (/sec)**	± error
49	**1.7E-04**	0.1E-04	**1E-04**	5.09E-04
60	**8.9E-04**	0.3E-04	**8E-04**	1.36E-04
69	**2.6E-03**	0.1E-03	**3.5E-03**	0.8E-03

Kinetic Summary of P(OPh)3				
T (˚C)	**k1 (/sec)**	± error	**k2 (/sec)**	± error
49	**1.96E-04**	0.03E-04	**9E-05**	5.22E-05
60	**9.6E-04**	0.6E-04	**6E-04**	1.58E-04
69	**2.6E-03**	0.1E-03	**2.4E-03**	0.5E-03

Table 9. Kinetic summary of carbonyl substitution by $P(OMe)_3$ and $P(OPh)_3$. Average rate constants for k_1 and k_2 at various temperatures and their propagated errors.

ΔG‡ for P(OMe)3				
T (˚C)	**ΔG‡1 (kJ/mol)**	± error	**ΔG‡2 (kJ/mol)**	± error
49	**102**	3.4	**104**	513
60	**101**	1.3	**101**	3.4
69	**101**	2.4	**100**	7.1

ΔG‡ for P(OPh)3				
T (˚C)	**ΔG‡1 (kJ/mol)**	± error	**ΔG‡2 (kJ/mol)**	± error
49	**101.9**	0.7	**108**	9.8
60	**101**	1.8	**102**	3.3
69	**101**	2.4	**101**	6.7

Table 10. Activation energies for carbonyl substitution of $Os_3(CO)_{10}I_2$ by $P(OMe)_3$ or $P(OPh)_3$. Errors reported here are propagated; unfortunately, error of $\Delta G^{\ddagger}_2$ is not a typo.

Thermodynamic Investigation

It is known thus far in this investigation that the carbonyl substitution of $Os_3(CO)_{10}I_2$ by $P(OR)_3$ (R = Me, Ph) is a first order process in compound, zero order in ligand—and therefore independent of both ligand concentration and ligand identity—and occurs through two observable steps, with the proposed production of intermediate compound $Os_3(CO)_9I_2[P(OR)_3]$. Thus far, these findings agree with similar studies that investigate carbonyl substitution of transition metal clusters by phosphites[4, 6, 7, 14, 20, 21]. To elucidate thermodynamic parameters of these two steps, such as enthalpy and entropy of transition ($\Delta H^{\ddagger}$ and $\Delta S^{\ddagger}$ respectively), this kinetic and analytical procedure was repeated at various temperatures.

With kinetic data over various temperatures, thermodynamic parameters of these reactions can be obtained by further manipulation of the Eyring-Polyani equation (Eqn 8). This equation relates the calculated rate constant to the free energy of transition, also referred to as the activation energy. Additionally, it is known that

$$\Delta G^{\ddagger} = \Delta H^{\ddagger} - T\Delta S^{\ddagger} \quad \textbf{(15)}$$

which can be substituted into equation 8 to yield

$$k = \frac{k_B T}{h} e^{\frac{\Delta S^{\ddagger}}{R}} e^{\frac{-\Delta H^{\ddagger}}{RT}} \quad \textbf{(16)}$$

In order to isolate values of entropy and enthalpy from the rate constants for each step, equation 9 is rearranged algebraically to the form

$$\ln\left(\frac{k}{T}\right) = \frac{-\Delta H^{\ddagger}}{R}\left(\frac{1}{T}\right) + \ln\left(\frac{k_B}{h}\right) + \frac{\Delta S^{\ddagger}}{R} \quad \textbf{(17)}$$

which approximates the form of a line when ln(k/T) is plot against the inverse temperature.

The slope of the line contains the enthalpy of transition such that

$$\text{slope} = \frac{-\Delta H‡}{R}\left(\frac{1}{T}\right) \quad \textbf{(18a)}$$

while the intercept contains the entropy of transition shown as

$$\text{intercept} = \ln\left(\frac{k_B}{h}\right) + \frac{\Delta S‡}{R} \quad \textbf{(18b)}$$

Though values of k_1 and k_2 have been averaged thus far to simplify the data presentation, only raw data at stoichiometric conditions are plotted for the Eyring-Polyani plots shown in Figure 27. Each plot contains the raw, unaveraged data for k_1 (filled markers, solid line) and k_2 (hollow markers, dashed line) that are each fit to Eqn 11 to obtain the slope and intercept. With values for both the slope and intercept of these data, $\Delta H^‡$ and $\Delta S^‡$ can be obtained from these values using Eqns 11a and 11b respectively, compiled in Table 11.

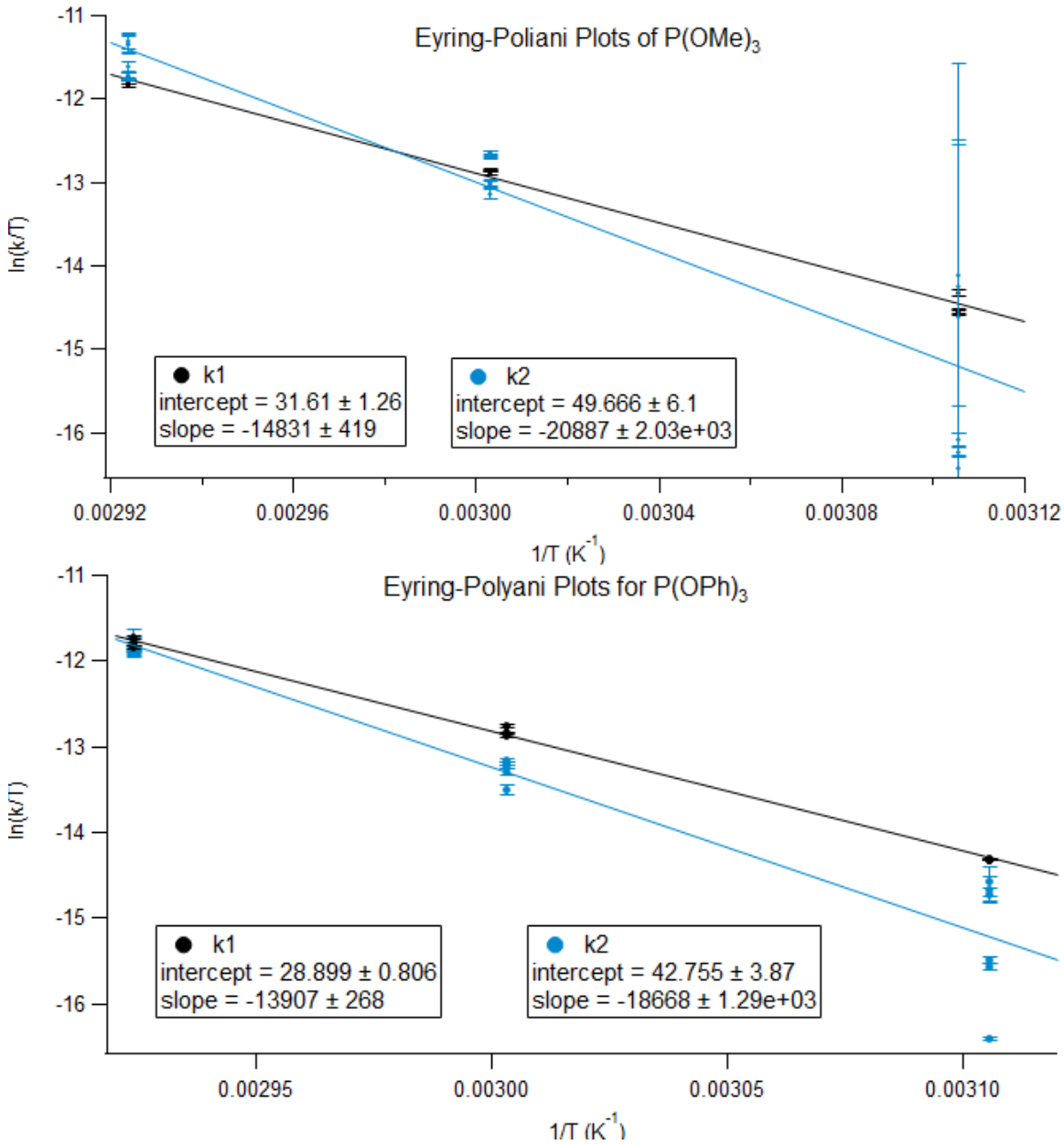

Figure 27. Natural log of (k/T) plotted against inverse temperature and fit to the linear form of the Eying-Polyani equation (Eqn 11). The data in black are k_1 for both ligands, while the data in blue are k_2 for both ligands. The top plot is for that of $P(OMe)_3$ while the bottom plot is that of $P(OPh)_3$. The slope contains $\Delta H^{\ddagger}$ while the intercept contains $\Delta S^{\ddagger}$, both of which are presented in Table 11. Error bars present the propagated errors of k.

Additionally, the Activation Energy for each step can be obtained through linear fit of the Arrhenius Equation,

$$k = Ae^{\frac{Ea}{RT}} \quad \textbf{(12)}$$

where k is the rate constant, A is the pre-exponential or frequency factor, E_a is the activation energy, T is the temperature at which that k was calculated or observed, and R is the universal gas constant. Taking the, much like the Eyring-Polyani equation, takin the natural log of this equation produces a function that can be fit to a line such that

$$\ln(k) = \frac{Ea}{RT} + \ln(A) \quad \textbf{(19)}$$

When ln(k) is plot against inverse temperature, the slope of the line contains the activation energy and the intercept contains the value of the frequency factor. For this analysis, we are most interested in the activation every of this process as determined by the plots in Figure 28 where

$$\text{slope} = E_a/R$$

and therefore the activation energy, E_a, is the product of the slope and gas constant.

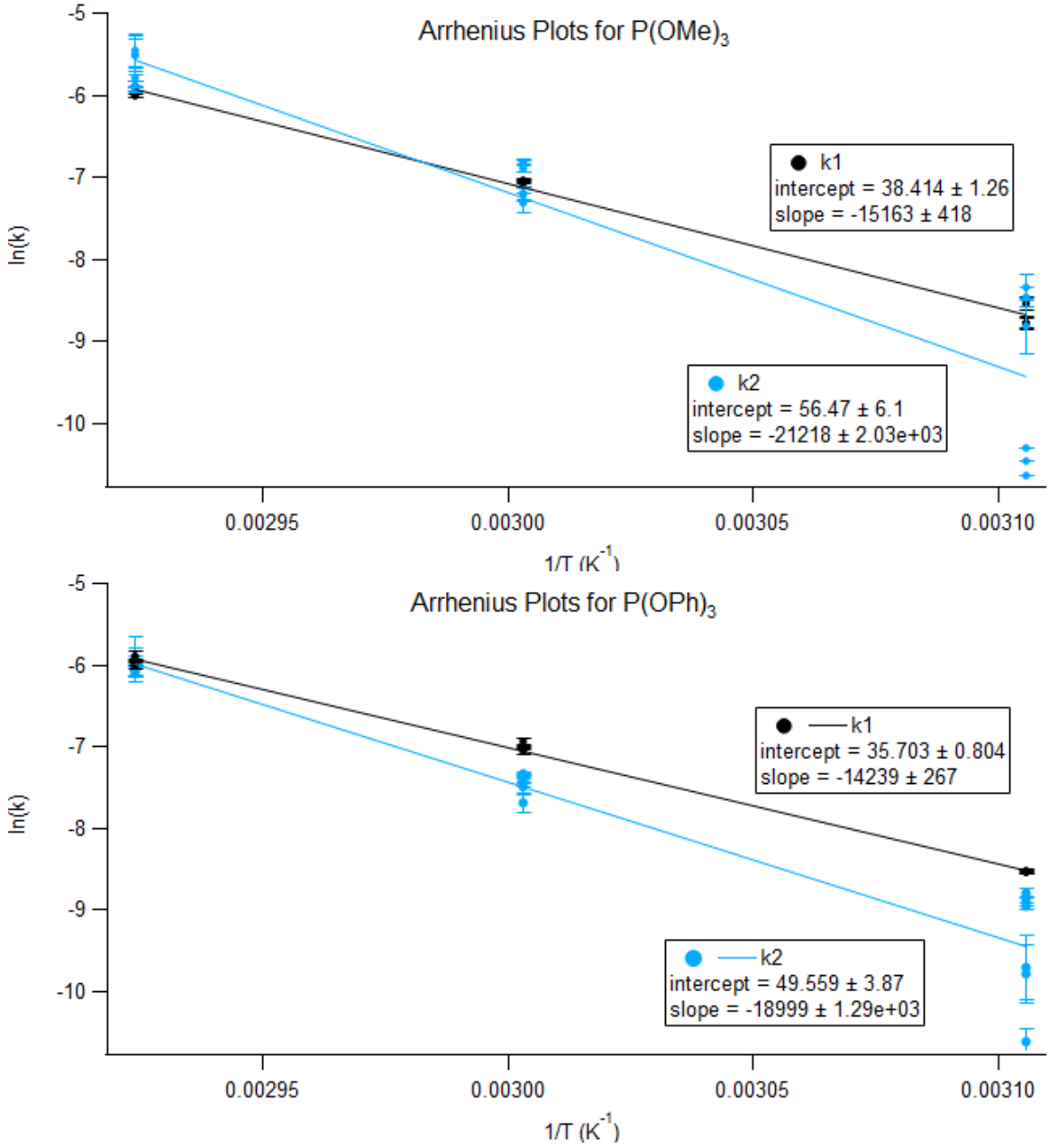

Fig 28. Arrhenius plots for both $P(OMe)_3$ and $P(OPh)_3$ kinetic trials. The slope contains the activation energy, E_a.

Thermodynamic results as calculated by both Eyring-Polyani and Arrhenius equations are summarized in Table 11, with reported propagated errors.

Thermodynamic Summary P(OMe)3				
	k1		k2	
	value	± error	value	± error
$\Delta H^{\ddagger}$ (kJ/mol)	**123**	42.5	**174**	*
$\Delta S^{\ddagger}$ (J/mol)	**66**	128	**216**	*
Ea (kJ/mol)	**126**	*	**176**	*

Thermodynamic Summary P(OPh)3				
	k1		k2	
	value	± error	value	± error
$\Delta H^{\ddagger}$ (kJ/mol)	**114**	30.6	**155**	113
$\Delta S^{\ddagger}$ (J/mol)	**39**	91.1	**158**	343
E_a (kJ/mol)	**118**	*	**158**	*

Table 11. Thermodynamic summary of carbonyl substitution by $P(OMe)_3$ and $P(OPh)_3$. Enthalpy ($\Delta H^{\ddagger}$) and entropy ($\Delta S^{\ddagger}$) obtained from Eyring-Polyani plots of temperatures ranging from 49 to 69 °C with propagated errors. *error of k_2 and all E_a is not reported due to imaginary values obtained during error analysis.

The thermodynamic values reported in Table 11 are unexpected, particularly when comparing the values obtained from k_1 against those obtained from k_2. Comparing, for example, $\Delta H^{\ddagger}$ from k_1 to k_2, there is a difference of over 40 kJ/mol between step one and step two for both $P(OMe)_3$ and $P(OPh)_3$. Were these calculated values accurate, this would indicate that the addition of one $P(OR)_3$ from step one alters the electron density of the molecule so much that it becomes more difficult to substitute the second $P(OR)_3$, resulting in a larger enthalpy of transition. This would likely result in a noticeable change in the rate of the second substitution as well, which was not observed in this study. Taking the propagated errors of these values into account, the error of k_1 does extend to the calculated values of $\Delta H^{\ddagger}$ of k_2, which would usually indicate that the reported value is not statistically different and can be taken as reasonable, but the error of $\Delta H^{\ddagger}$ of k_2 indicates

that that value in and of itself is largely inaccurate. This becomes more apparent with $P(OMe)_3$, where the error of some of the k_2 is so great that that error cannot be propagated (see "Propagation of Error" in Methods, p. 43).

Additionally, crystallographic data of $Os_3(CO)_{10}X_2$ and $Os_3(CO)_8X_2[P(OR)_3]_2$ agrees with the assessment that such a large difference in thermodynamic data between k_1 and k_2 data is unexpected, and, perhaps, untrue. Figure 28 compares the bond lengths of the Os-Os metal-metal covalent bonds for both the unsubstituted chlorinated cluster (28a), and the final, disubstituted chlorinated cluster (28b). Because the metal-metal bond is most likely the rate-controlling bond-breaking event, comparing the bond lengths of the initial and final clusters gives insight into the expected relative values of $\Delta H^{\ddagger}$, which itself is analogous to the bonds broken during substitution steps. Though these figures depict the bond lengths of $Os_3(CO)_{10}Cl_2$, not $Os_3(CO)_{10}I_2$, the comparison sheds light on the effects on bond length due to substitution by $P(OR)_3$, rather than the effects due to exchange of X as calculated by Barnum and Pearsall through DFT calculations[16], and these effects are expected to be identical between X = Cl, Br, I.

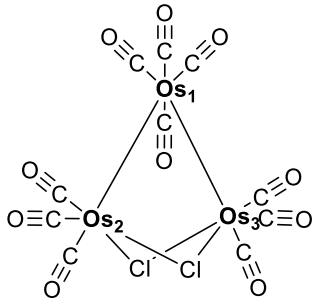

Fig 28a. $Os_3(CO)_{10}Cl_2$ inter-atomic distances, retrieved from the Cambridge Crystallographic Data Centre (CCDC) database

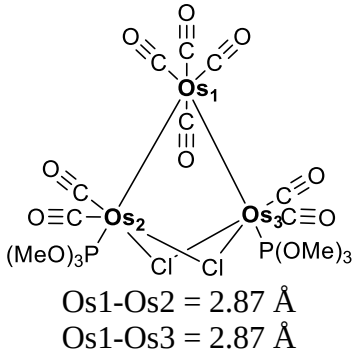

Fig 28b. $Os_3(CO)_8Cl_2[P(OMe)_3]_2$ inter-atomic distances. Data obtained by Mary-Ann Pearsall.

The metal-metal bond length does not vary significantly between the unsubstituted and the disubstituted cluster. The initial bond length of the Os-Os bond is 2.85 Å, and the bond length of the disubstituted cluster is 2.87 Å. Together, these data indicate that a change in enthalpy of transition is not expected because the bond lengths do not vary significantly within the overall substitution process. In fact, these data suggest that if a change in $\Delta H^{\ddagger}$ were observed, the $\Delta H^{\ddagger}$ may decrease slightly since the addition of $P(OR)_3$ lengthens the metal-metal bond just slightly. Thus, the crystallographic data of the initial and final clusters provide addition support that the calculated $\Delta H^{\ddagger}$ values are likely inaccurate due to large error within the system. Phrased differently, if the calculated $\Delta H^{\ddagger}$ values reported in Table 11 were accurate, we would expect to see a dramatic bond *shortening* between the initial and final clusters. Because this is not observed, and because the propagated error is tremendous for k_2-obtained values, the reported values of $\Delta H^{\ddagger}_2$ and $\Delta S^{\ddagger}_2$ are inaccurate at best and cannot be chemically interpreted.

Comparison to Literature

Cavaliere and Pearsall's study[11] examined the carbonyl substitution by excess $P(OMe)_3$ at similar temperatures and various halogen bridges. Their relevant data is compiled and summarized in Table 12, where rate constants have been averaged from their assigned temperatures. The data presented here was found to agree with the data of Cavaliere and Pearsall for rate constants and enthalpy of transition, in addition to the order of reaction with respect to both cluster and ligand. Cavaliere and Pearsall do not report a value for entropy of transition due to large error within the associated plots, and thus there is no direct value to which to compare.

Kinetic		Thermodynamic	
T (°C)	avg k, /s	Ea, kJ/mol	ΔH‡, kJ/mol
49	3.90E-04	116 ± 11	113 ± 11
60	1.32E-03		
69	3.83E-03		

Table 12. Summary tables of $P(OMe)_3$ data compiled from Cavaliere and Pearsall's work [*11*]. No $\Delta S^{\ddagger}$ was published in this study due to the large error within the related thermodynamic plots. Rate constants presented in this table have been averaged from the data in Cavaliere and Pearsall's study.

While Cavaliere and Pearsall did not investigate a two-step process for this carbonyl substitution by $P(OMe)_3$, as presented here, this does not discount a comparison of k_1 as both studies analyzed the disappearance of the 2110 cm^{-1} peak in the starting material spectrum. Much like how k_1 can be held as guesses for the intermediate and product fits within this study, the observed rate of Cavaliere and Pearsall was calculated solely on the disappearance of 2110 cm^{-1} peak, identically to that of this study.

Further, the identification of a two-step process is found in other studies[4, 5, 7, 14, 20, 21] that investigate the carbonyl substitution of transition metal clusters by $P(OR)_3$ ligands. Such investigations have found that, generally, carbonyl substitution is a first-order process that is zero order in ligand; substitution by phosphites occurs in two steps, while substitution by phosphines occurs in only one observable step[20]. Substitution of carbonyl ligands by phosphines is not investigated as part of this study as this introduces the possibility of C-H addition to the cluster by the R group of PR_3; this would cloud the kinetic data gathered by this current procedure and instrumentation set-up.

Synthesis of Intermediate, $Os_3(CO)_9I_2[P(OMe)_3]$ by Me_3NO

Due to the significant differences between Intermediate- and Product-fit k_2 values of both ligands, an attempt to synthesize the intermediate $Os_3(CO)_9I_2[P(OMe)_3]$ compound was made following the procedure modeled after the work of Shen, Shi, Gao, Shi, and Basolo[23]. This synthetic route employed vast excess of both Me_3NO and $P(OMe)_3$ in the original study, but dilutions were made to use stoichiometric amounts in this procedure as excess ligand was found to encourage formation of the disubstituted $Os_3(CO)_8I_2[P(OMe)_3]_2$. This synthesis is believed to occur through an attack of an already-coordinated carbon on CO by Me_3NO to produce CO_2(g), rather than the more standard carbonyl substitution that is thought to occur through an attack on the metal core by the incoming ligand to release CO(g), as demonstrated in Scheme 4.

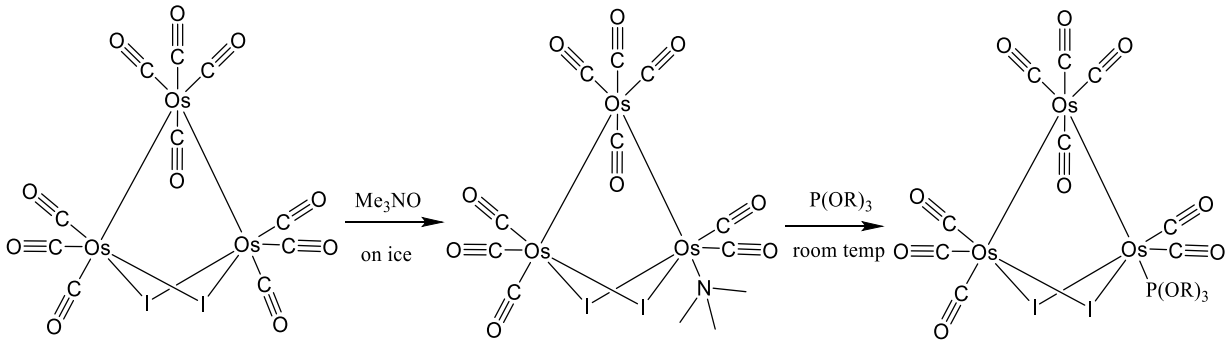

Scheme 4. Substitution of carbonyl by trimethylamineN-oxide (Me_3NO), adapted from Shen, Shi, Gao, Shi, and Basolo [*23*]. Me_3NO is thought to attack a coordinated carbon of CO to release CO_2 rather than CO. Me_3N is easily displaced by a second ligand, and this second step proceeds at room temperature; this is why the first step must be done on ice, to ensure that $P(OR)_3$ does not substitute too quickly in unwanted positions.

The desired product was confirmed by IR, shown below in Figure 29, and the indicative peaks match those that are intermediate in the overlays of Fig 21, most importantly that of 2097 and 2060 cm^{-1}. Figure 30 demonstrates confirmation of the identity of the intermediate from the kinetic overlays of Fig 21 by overlaying the synthesized $Os_3(CO)_9I_2[P(OMe)_3]$, taken in hexanes,

with the maximum intermediate height of a hexane reflux. This overlay confirms that the desired product of this synthesis does indeed match the proposed intermediate as determined by IR peaks.

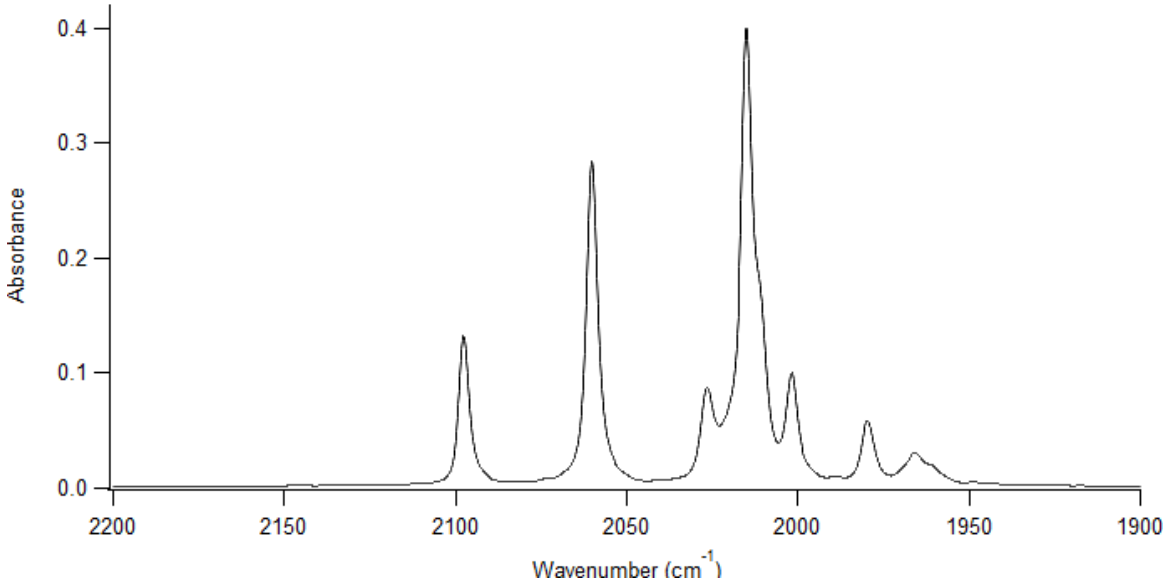

Fig 29. IR of monosubstituted intermedciate $Os_3(CO)_9I_2[P(OMe)_3]$ obtained by Me_3NO synthetic shortcut. Most important, indicative, peaks are 2097, 2060, 2026, 2015, 2002, 1979, and 1965 cm^{-1}, all of which match the starred intermediate peaks of Fig 21.

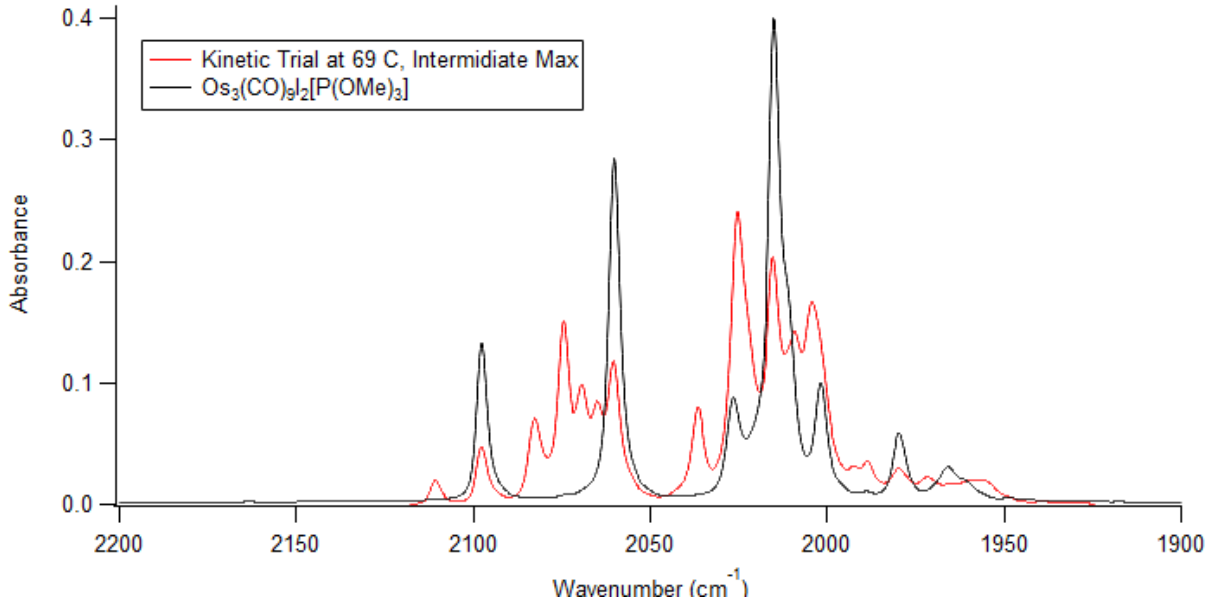

Fig. 30. Overlay of synthesized $Os_3(CO)_9I_2[P(OMe)_3]$ by Me_3NO shortcut (pink) onto the spectrum of maximum intermediate height from a kinetic reflux of $Os_3(CO)_{10}I_2$ with $P(OMe)_3$ (black). Both spectra were taken in hexanes. The black peaks directly correspond to the intermediate peaks within each kinetic reflux, shown in red, confirming the proposed structure of the intermediate compound obtained within these refluxes.

When refining this procedure, it was determined to be essential to prepare dilutions of both Me_3NO and phosphite ligand, as even one drop of $P(OMe)_3$ was found to be at least 33x excess. This excess of ligand drives the reaction to produce the disubstituted $Os_3(CO)_8I_2[P(OMe)_3]_2$ product rather than the desired $Os_3(CO)_9I_2[P(OMe)_3]$ intermediate. While this procedure did indeed produce the desired compound, this synthetic route led to a mixture of products that were often unable to be isolated by Prep-TLC. From a synthetic perspective, yes this is a means to an end. For the purposes of this study, however, this procedure is inefficient and was abandoned after three subsequent failed attempts.

Half-equivalence

The reaction of $Os_3(CO)_{10}I_2$ with $P(OR)_3$ consistently produced the disubstituted $Os_3(CO)_8I_2[P(OR)_3]_2$ final product after first producing a monosubstituted intermediate compound. Due to the tendency of the Me_3NO synthetic pathway to favor the disubstituted product, a preliminary investigation into the stability of the $Os_3(CO)_9I_2[P(OR)_3]$ compound was launched by way of an IR-monitored reflux with half-stoichiometric amounts. Instead of a reaction with just enough phosphite to produce the disubstituted final product, or a 1:2 ratio of cluster:$P(OR)_3$, a reflux was monitored by IR with 1:1 cluster:$P(OR)_3$ at 60 ^oC as this is a reasonable rate for this reaction; not too fast that it cannot be monitored cleanly, but not too slow that it would take several hours.

If the reaction ran to half-completion, thereby yielding a mixture of leftover starting material and disubstituted product, then this reaction would be thermodynamically driven; if the reaction produced a mixture of all three compounds, starting material, intermediate, and final

product, then it would be determined to be kinetically driven. Figure 31 presents the graph of peak heights of 2110 cm^{-1} (reactant), 2098 cm^{-1} (intermediate), and 2086 cm^{-1} (product) over time. Figure 31 displays that complete consumption of $P(OPh)_3$ occurs around 2000 seconds, or just about 33 minutes. The final solution contained a mixture of starting material, intermediate, and product indication that this reaction is kinetically driven.

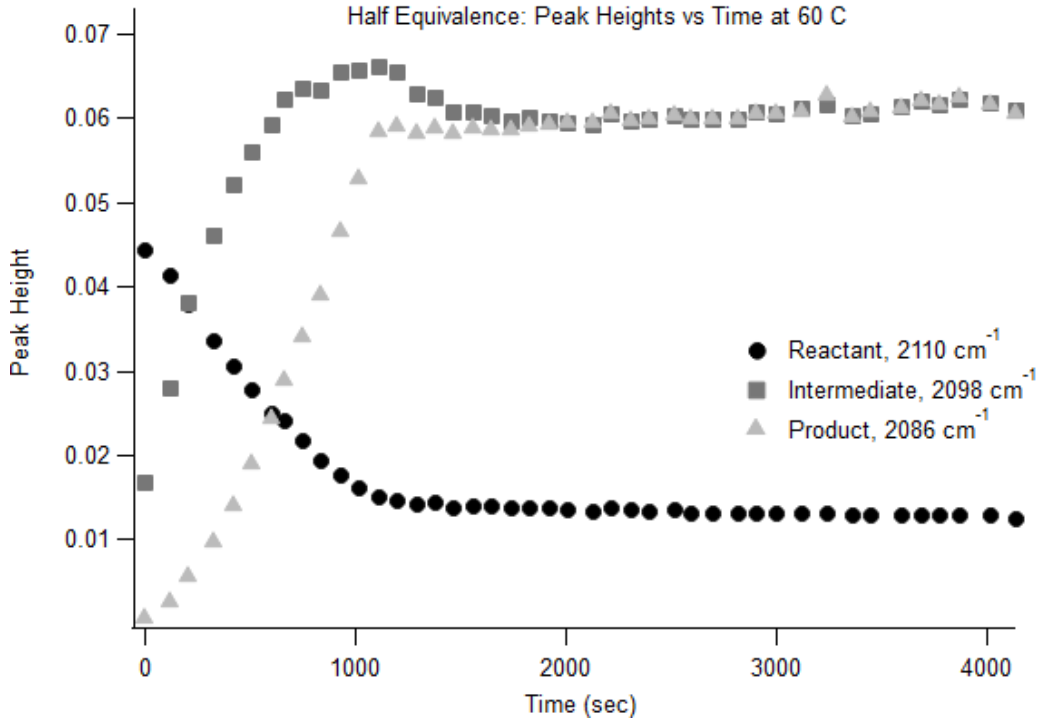

Fig. 31. Peak heights over time (sec) for reaction with 1:1 cluster:$P(OPh)_3$ at 60 °C. Black circle is reactant (2110 cm^{-1}), grey triangles are intermediate (2098 cm^{-1}), light grey squares are product (2086 cm^{-1}). Though change in peak height is equivalent to change in concentration, exact peak height does not equate to concentration at that time; thus, though intermediate and product achieve identical heights, they are not equivalent in concentration as maximum 2086 cm^{-1} is much stronger/taller than max 2098 cm^{-1}.

To then investigate the stability of these compounds in solution, the reaction vessel was taken off heat but allowed to cool to room temperature under nitrogen. Once cool, the nitrogen was stopped, and the reaction vessel capped immediately, effectively having pumped the flask full of nitrogen. This solution, containing reactant, intermediate, and product, was allowed to sit capped and undisturbed for a week. Figure 32 shows (a) TLC plates from the day of reaction against a TLC of the same solution a week later, (b) with a cartoon simplification to the right.

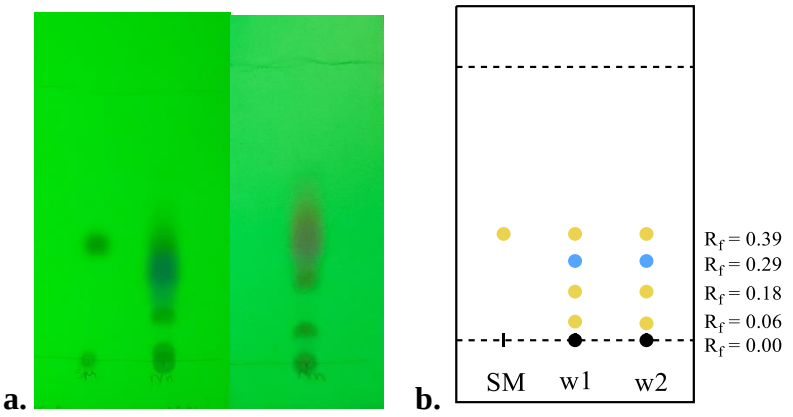

Fig 32. (a) picture of TLC in 20% dichloromethane/hexanes of $Os_3(CO)_{10}I_2$ (SM), half-equivalence reaction mixture once cooled to room temperature, and that same solution a week later (w2) in UV light, (b) cartoon depiction of each to simplify. Spots have been colored in the cartoon depiction according to their appearance in visible or UV light, thus identifying the yellow spots as Os_3 cluster derivatives $–(CO)_{10}$, $–(CO)_9$, and $–(CO)_8$ (R_f = 0.389, 0.178, 0.0618). The spot at R_f = 0.290 is invisible in visible light but appears blue in the UV lamp.

As the half-equivalence solution was spotted against starting material, $Os_3(CO)_{10}I_2$, the top-most spot can be confirmed to be unreacted starting material (avg R_f = 0.389). In visible light, the osmium compounds are a pale yellow; when the TLC place is held in visible light, three yellow spots are seen, indicating that these are the osmium compounds $Os_3(CO)_{10}I_2$ (starting material, R_f = 0.389), $Os_3(CO)_9I_2[P(OPh)_3]$ and $Os_3(CO)_8I_2[P(OPh)_3]_2$. While the identity of each cannot yet be confirmed, as these two products have yet to be isolated from one another, it is proposed that the upper spot of R_f = 0.178 is the monosubstituted $–(CO)_9$ intermediate while the lower yellow

spot at R_f = 0.0618 is thought to be $–(CO)_8$ as two $P(OR)_3$ groups would create a larger dipole across the osmium cluster, even if very slight.

When under UV light, most spots on a TLC plate appear somewhere in a range from deep orange to black. The exact shade of this color is correlated to the concentration of compound within that spot; more compound, higher concentration, darker and nearer-black spot. However, the spot at R_f = 0.290 appears blue in the UV lamp and bears no color in visible light. This compound is not seen in the starting material and is thus generated through these reactions, though it's identity remains unknown. This was at one point hypothesized to be the $P(OPh)_3$, as this UV-blue spot also appears in reactions run with excess phosphite but was confirmed to be something else when a TLC run against the $P(OPh)_3$ dilution in the same solvent system (20% dichloromethane in hexanes).

To investigate the possibility of a bimolecular pathway to produce $Os_3(CO)_8I_2[P(OR)_3]_2$, the same reaction mixture was brought to reflux in hexanes (69 ^oC). Should the additional heat energy encourage the production of $Os_3(CO)_8I_2[P(OPh)_3]_2$ as monitored by peak height, it would be assumed that such a shift would occur by a bimolecular pathway described in Scheme 5 where two molecules of intermediate collide to redistribute the $P(OR)_3$ ligands to produce the final product and some starting material.

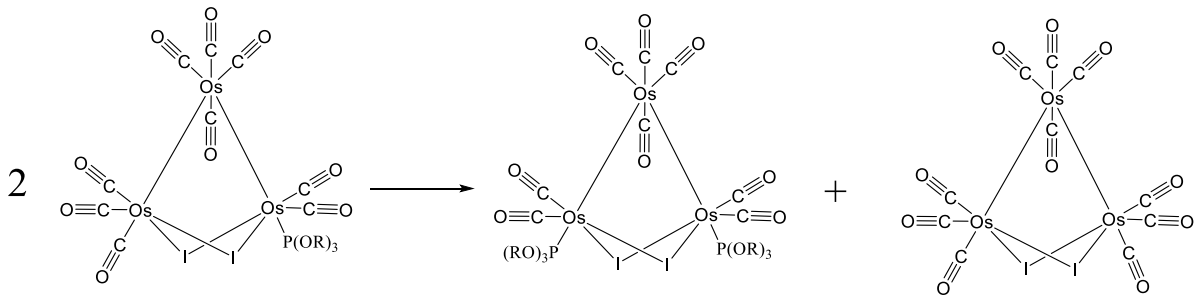

Scheme 5. Possible bimolecular pathway that would result in the observed equilibrium between $Os_3(CO)_9I_2[P(OR)_3]$ and $Os_3(CO)_8I_2[P(OR)_3]_2$. Increasing heat of reaction might result in a shift in equilibrium towards the disubstituted $-(CO)_8$ compound.

The IR spectra for this reaction showed no change in any peak height for a full reflux of 45 minutes, as this is the total time of trials at 69 ^oC should there be enough phosphite in solution. Since no change was observed, it can be concluded that the compounds $Os_3(CO)_9I_2[P(OR)_3]$ and $Os_3(CO)_8I_2[P(OR)_3]_2$ are stable in solution and do not interact to redistribute CO and $P(RO)_3$ ligands, thereby eliminating the possibility of a bimolecular side reaction described above.

Proposed Mechanism

Compiling the information confirmed and discovered throughout this study, an updated mechanism proposal is provided in Scheme 6. We now understand that there are two observable steps, the first of which results in the production of an intermediate compound $Os_3(CO)_9I_2[P(OR)_3]$ while the second produces the final product $Os_3(CO)_8I_2[P(OR)_3]_2$ from the observed intermediate. This observation agrees with various studies that investigate the kinetics of carbonyl substitution of trinuclear clusters with P-donors of the type $P(OR)_3$[14, 20, 21].

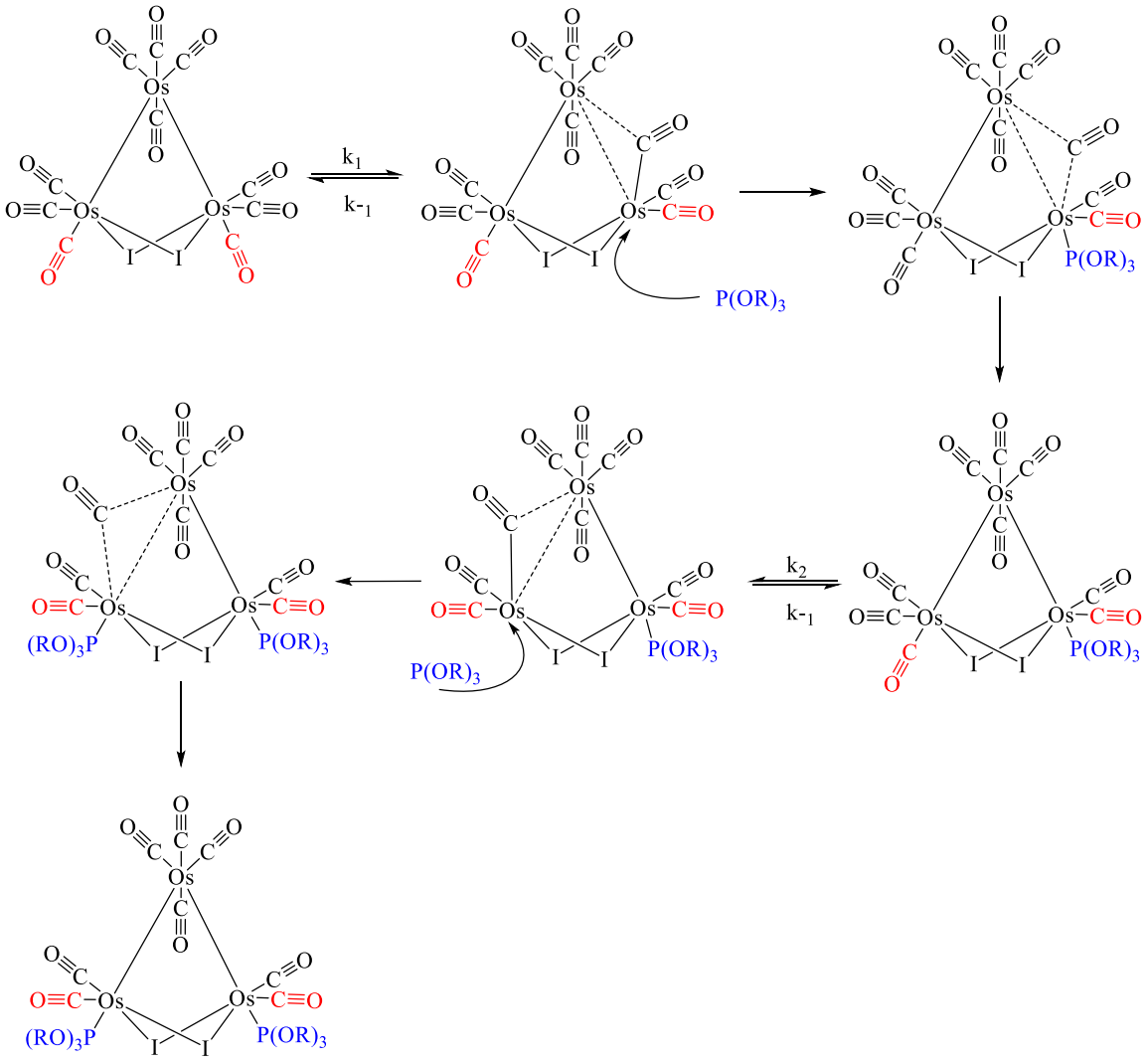

Scheme 6. Proposed mechanism from the data of this research. Rate limiting steps are thought to include the breaking of the Os-Os bond, which becomes partially stabilized by an adjacent carbonyl. The incoming $P(OR)_3$ then competes for back-donation from the metal atom, thereby weakinging the Os-C bond. This encourages the release of CO to then reform the Os-Os bond. This process then repeats to substitute the second trans carbonyl. The CO originally presumed to be leaving, marked in red, are not proposed to leave but rather to shift.

We propose that the rate-limiting step of these two observable steps is the breaking of the metal-metal bond, as per the calculations of Barnum and Pearsall[16] in conjunction with the thermodynamic work done here and in the investigation of Cavaliere and Pearsall[11], and also seems to concur with other published studies[24]. This bond is thought to break spontaneously, meaning

independently of ligand introduction, as the ligand identity and concentration was found to have no effect on this first order overall reaction.

It is proposed, then, that this broken bond is then partially stabilized by the surrounding CO ligands, thereby maintaining the 3D structure of this cluster and preventing the unravel into a near-linear form. This partial reconfiguration therefore provides enough space for an incoming ligand to attack the Osmium atom, rather than a true vacancy as previously assumed, and the "labile" CO, marked in red, are spread out to provide enough space for a nucleophilic attack. Once the $P(OR)_3$ has coordinated to the metal, the metal can contribute some of its electron density back onto the phosphorus as $P(OR)_3$ molecules in the same way that CO also accepts metal electron density through π-acceptance. The trans relationship of the now-coordinated $P(OR)_3$ and the still-coordinated CO results in competition between the two, as they both "want" the osmium's electron density to stabilize their own Os-L bonds. In effect, the coordination of $P(OR)_3$ weakens the CO trans to it, which is the CO currently proposed to stabilize the broken Os-Os bond, and thus it leaves.

This process results in the formation of $-(CO)_9$ intermediate and is then repeated to form $-(CO)_8$ as the final, and only, product of this reaction. This detail is supported by the kinetic data presented here, as the rates of k_1 and k_2 do not vary with the introduction of coordinated ligand. This is to say that the substitution of one carbonyl for a P-donor ligand does not appear to affect the electronic distribution of the molecule in such a way as to change the strength of the Os-Os bond, which would have resulted in a different value of k_2 as compared to k_1.

Additionally, the proposed mechanism, which is supported by the data reported herein, clarifies which CO ligands are leaving. It has been known within the Pearsall lab that triosmium clusters of the type $Os_3(CO)_{10}X_2$ will react to replace the carbonyls trans to the Os-Os bond,

supported by spectroscopic and crystallographic data compiled through the years. This work, however, proposes that the phrase “labile CO,” used to refer to these two CO trans to the Os-Os bond and indicated in red in Scheme 6, is a misnomer. These CO are not proposed to leave the cluster, but rather shift during the torsion necessary to stabilize the broken metal-metal bond; this allows for the incoming ligand, in blue, to attack trans to the metal-metal bond, but does not force the ”labile” CO to truly leave.

While the mechanism proposed here is in agreement with the reported data, further studies are necessary. It is critical that isotopic labeling be integrating into reproducing this work as this would allow for spectral tracking of the “labile” CO specifically in IR and NMR.

Discussion

Solvent Effects and Possible Catalysis

As kinetic investigations are somewhat material intensive, it is impossible to complete this entire study with one single bottle of 2-methylpentane. Upon receiving and opening a new bottle, an event that coincided with switching ligands, the rate of reaction was found to increase dramatically. It was initially assumed to be a result of differences in ligand, but this rate was found to decrease overtime with the addition of sieves to solvent. Shown in Table 13, the rate decreases over a period of three days as sieves were not added until after the first $P(OMe)_3$ reflux; in other words, molecular sieves were added between data points one and two.

Full Data of 300x P(OMe)3, Effect of Wet Solvent						
	2110 /cm		2097 /cm		2082 /cm	
	k1, /sec	**± std dev**	**k2, /sec**	**± std dev**	**k2, /sec**	**± std dev**
No Sieves, WET	1.32E-03	0.03	1.22E-03	0.04	1.46E-03	0.09
<24hr w sieves	1.32E-03	0.03	1.48E-03	0.04	2.38E-03	0.36
> 24hr, DRY	9.18E-04	0.01	1.08E-03	0.02	6.47E-04	0.62
DRY	9.47E-04	0.09	1.13E-03	0.02	5.22E-04	0.52
DRY	9.60E-04	0.12	1.09E-03	0.01	5.00E-04	0.33

Table 13. Full data set of 300x $P(OMe)_3$ refluxes. Molecular sieves were added after Reflux #1; Reflux #2 was collected the next morning, ~17 hours after addition of sieves. Reflux #3 was collected the following day, well over 24hr after sieves addition and therefore considered the first dry reflux of this set. This table therefore shows the overall affect of water on the rate, and a qualitative investigation of dryness over time. Standard deviations are reported to the same magnitude as the associated k.

Shown in Table 13, the rate decreases within the first three days of data collection; by day three, well after 24hr since the addition of sieves, the rate has dropped back to the expected value and is therefore the first "real" data point of the $P(OMe)_3$ investigation. This table not only captures the drying of solvent, effectively observing water leaving the solvent, but also demonstrates the effect of water on the rate of this reaction. This provides the first step into an investigation of

solvent effects that should be investigated in the future as it remains unclear why the introduction of water would increase the rate of reaction so dramatically.

It should be noted that the concentration of water impurity in these solvents, though presumed to be less than 1% per commercial regulations, is of the order of magnitude of the concentration of $Os_3(CO)_{10}I_2$ in solution for each kinetic trial. Assuming a maximum concentration of 1% water by volume, there is estimated to be 5.56×10^{-3} mols of water within the solvent of kinetic trials. If a full 20 mg of $Os_3(CO)_{10}I_2$ was used in that trial, there would be 1.81×10^{-5} mol of osmium compound in solution as well. Thus, the water present in the wet solvents used is comparable to the amount of substrate also in solution. While it is still possible that water serves a catalytic function, the concentration is on par with that of substrate—if not in 100x excess—it is unlikely that the observed activation is catalytic in function.

Some possibilities as to why the presence of less than 1% water in fresh solvents may encourage carbonyl substitution include possible disruption of the solvent shell surrounding the molecules when they are dissolved. This would allow incoming molecules to penetrate this solvent envelope with greater ease and speed, thus encouraging carbonyl substitution.

Additionally, it is possible that the presence of water stabilizes some transition state within the proposed mechanism. It is reasonable to assume that water encourages the donation ability of CO ligands by stabilizing the partially positive oxygen; this would begin to push electron density through the oxygen onto the carbon, thereby increasing the effective amount of electron density that the carbon can donate to the metal center in the proposed bridging transition state of this mechanism. Shown below in Figure 33, the proposed water stabilization of a nearby carbonyl would increase the stability of the bridging carbonyl transition state, indicated by a true “bond” for emphasis and clarity though this is not necessarily a full sigma bond, after the breaking of the Os-

Os bond. This increased stability of the transition state would shift the slow equilibrium of the proposed rate-limiting step to the right, driving the reaction forward.

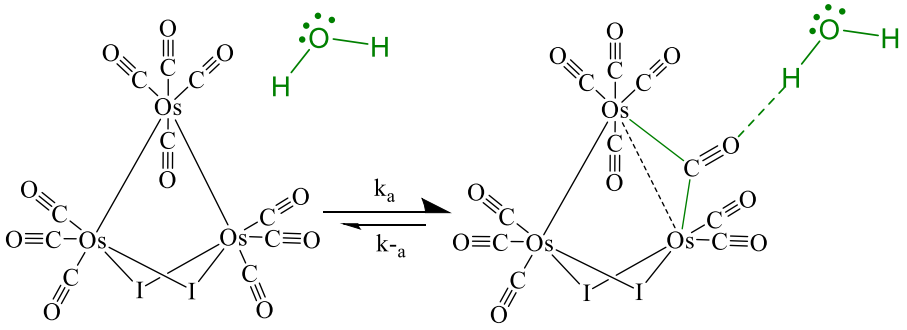

Fig 33. Proposed stabilization of the rate-limiting step by water in solvents. Because the water molecule increases the sigma donation ability of the carbonyl, the presence of minute concentrations of water in solvent may stabilize this bridging transition state in such a way that shifts the equilibrium in its favor, thereby speeding up the reaction.

While this stabilization of the transition state of the rate-limiting step may not be significant in larger-scale reaction conditions, such interaction of wet solvent and osmium substrate is noteworthy under these small-scale reactions wherein the concentration of water in commercially available reagents is on par with the concentration of starting material in solution.

Subsequent studies should investigate the rate and thermodynamic parameters, as described in this study, with carefully measured aliquots of water. Should the labialization of this substitution by water be due to disruption of the solvent shell, these effects would be seen in the entropy of transition. In any case, the observed effects on rate due to the presence of water indicates that future studies should distill solvents. Though molecular sieves are used to dry commercially obtained solvents, they are not absolute and thus some minute quantity of water may still be present in solvent. It is possible, then, that the kinetic data reported here is simply a plateaued water-driven rate of reaction rather than the true rate of carbonyl substitution, further supporting the need for distilled solvents for future studies.

Kinetic Isotope Effect

The kinetic isotope effect describes the change in observed rate when performing a reaction with isotopic equivalents. This sheds light onto the rate determining step(s) of that mechanism. Since the isotope has a different effective mass than the abundant or original compound, the zero-point energy of the isotope-substituted bond of that compound would be different. This is to say that, though the strength of the bond does not change—as there is no chemical difference between an abundant atom and its isotope—it would require more energy to vibrate or break that bond. Should that altered bond be involved in the rate-limiting step, then, a change in rate constant k would appear as observed by the ratio of abundant or normal k over isotopic k.

The rate constant k can be defined as

$$k = Ae^{\frac{-Ea}{RT}} \tag{20}$$

where A is the preexponential factor, E_a is the activation energy, R is the universal gas constant, and T is the temperature of the reaction recorded in Kelvin. Comparing the ratio of k_a, for abundant, and k_i, for isotope, would result in the expression

$$\frac{k_a}{k_i} = \frac{Ae^{\frac{-Ea}{RT}}}{Ae^{\frac{-Ea}{RT}}} = e^{\frac{-(Eaa-Eai)}{RT}} \tag{21}$$

such that the negative quantity of the difference in activation energies, E_{aa} and E_{ai}, is equivalent to the difference in zero-point energies of the isotopic bond itself.

The zero-point energies are calculated by approximating the bond in question as a harmonic oscillator, which can be further simplified to a mass on a spring. The vibration of that mass on a spring can be considered equivalent to the stretching of the bond itself, and represented by the equation

$$\tilde{\nu} = \frac{1}{2\pi}\sqrt{\frac{k}{\mu}} \quad \textbf{(22)}$$

where $\tilde{\nu}$ is the frequency of vibration, k is the spring constant from Hooke's law, and μ is the combined effective mass of that bond. Thus, an isotope that increases the effective mass will decrease the frequency of vibration, which in turn lowers the zero-point energy of that bond. Since this isotope-doped bond sits at a lower zero-point energy than the abundant equivalent, it requires more energy to vibrate or break it and would result in a change in rate constant. Calculating these values for any isotopic equivalent and finding the ratio of the resulting rate constants will give a ratio of an expected change in observable rates, should the bond in question be involved in the rate-limiting step.

Conducting such an investigation with ^{13}C carbonyls would shed light onto whether the release of the Os-CO bond is involved in the rate limiting observable steps. With the current mechanism proposal, it is not expected that this bond is involved in the rate-limiting step. Thus, it is expected that there will be no change in the observed rates with the isotopic equivalent of these clusters, but such an investigation should still be done to confirm the current proposed mechanism.

Conclusions

- Carbonyl substitution of triosmium clusters $Os_3(CO)_{10}I_2$ by $P(OR)_3$ P-donor ligands is a two-step process as observed with IR spectroscopy. Both steps were found to be first order in cluster, zero order in ligand—even in stoichiometric conditions. Ligand identity ($P(OMe)_3$ vs $P(OPh)_3$) was not found to significantly affect the rate of either step. Rate-limiting steps are thought to be the breaking of the metal-metal bond, evidenced by the enthalpy of transition, which is of the order of magnitude of an Os–Os bond, and that incoming ligand does not affect the observed rate-limiting steps.
- The proposed mechanism, which is consistent with the collected data, suggests that the broken Os–Os bond is partially stabilized by an adjacent carbonyl. This creates enough space between the bound carbonyls for an incoming ligand, rather than creating a vacant site by the dissociation of a bond. Once the $P(OR)_3$ is bound, the Os–carbonyl bond trans to it is weakened due to the competing back-donation between the carbonyl and the $P(OR)_3$ ligand. It is this carbonyl that is proposed to be the one leaving in both rate-limiting steps to produce the final compound $Os_3(CO)_8I_2[P(OR)_3]_2$. This is to say that though carbonyl substitution only occurs at the position trans to the Os–Os bond, those carbonyls are not though to leave during this reaction. Isotopic labeling is suggested for future studies to confirm this proposal.
- The compounds observed throughout these substitution reaction trials were isolated by stepwise gradient column chromatography. These compounds, $Os_3(CO)_{10}I_2$, Os3(CO)-$_9I_2[P(OR)_3]$, and $Os_3(CO)_8I_2[P(OR)_3]_2$, were refluxed at temperatures up to 69 ^oC and found to be stable in solution, thereby eliminating the bimolecular collision as a possible route to synthesis of $Os_3(CO)_8I_2[P(OR)_3]_2$.

- Some solvent effects were observed, suggesting that water may play a catalytic role in this carbonyl substitution mechanism. While fresh, commercially obtained solvents would have less than 1% water contaminant by volume, this concentration is stoichiometric with the osmium cluster in solution and was found to greatly increase the rate of carbonyl substitution. Molecular sieves were used to keep solvents dry, but, as these are not absolute, future studies should distill solvents prior to use.

Spectral Appendix

All IR were taken in a 0.2mm NaCl liquid cell with hexanes solvent, as CH_2Cl_2 was found to broaden and aggregate overlapping peaks, often misattributing "purity" to some chromatographic fractions during column isolation. Hexanes was found to give the best clarity of IR spectra. Peaks have been labeled with their relative intensities, strong (s), moderate (m), or weak (w). Wavenumbers are presented to the nearest whole value, (0.6 – 0.9 → 1.0, 0.1 – 0.5 → 0.0), though it should be noted that wavenumbers did not shift more than 0.3 cm^{-1}. This is to say that, in the case of $Os_3(CO)_{10}I_2$, for example, the lowest frequency peak was *always* 1988.7-1988.9 cm^{-1}, but it presented as 1989 cm^{-1} for clarity and simplicity.

All ^1H NMR were taken in $CDCl_3$ solvent, and TMS standard, taking 128 scans in a 400 MHz NMR. Unfortunately, ^{31}P NMR could not be obtained as the final, isolated concentrations of $–P(OR)_3$ derivative compounds were not high enough to be distinguished from baseline in an isotopic NMR spectrum.

Triosmium dodecacarbonyl, $Os_3(CO)_{12}$

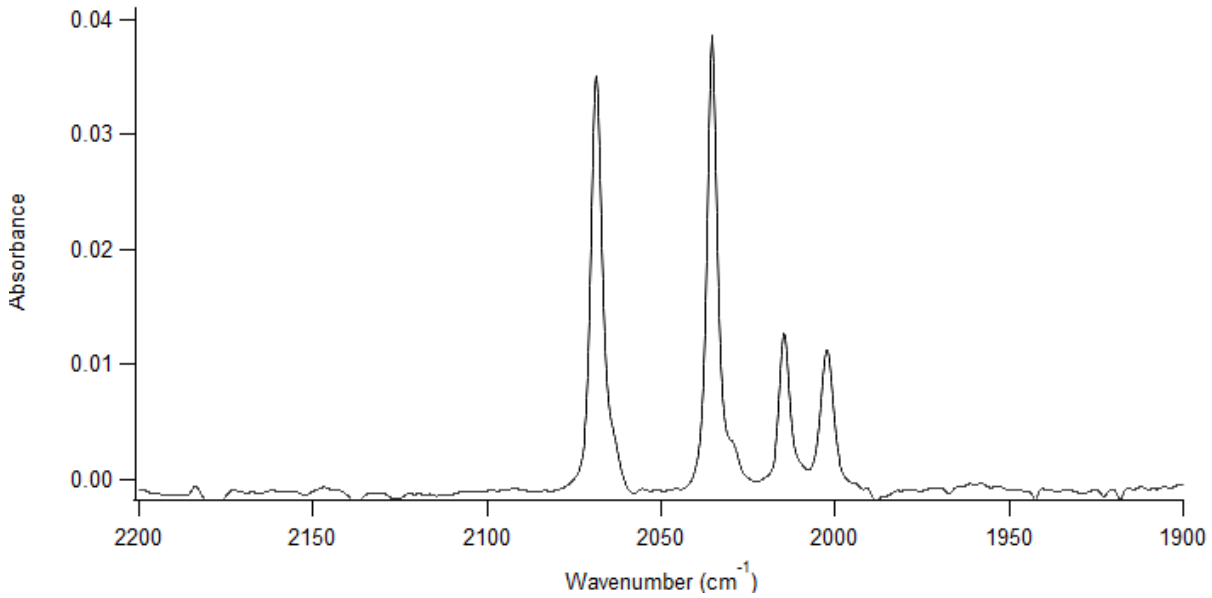

$Os_3(CO)_{12}$ in hexanes. Starting material for synthesis of $Os_3(CO)_{10}I_2$. Peaks at 2069(s), 2035(s), 2015(m), and 2002(m) cm^{-1}

Diosmium hexacarbonyl diiodide, $Os_2(CO)_6I_2$

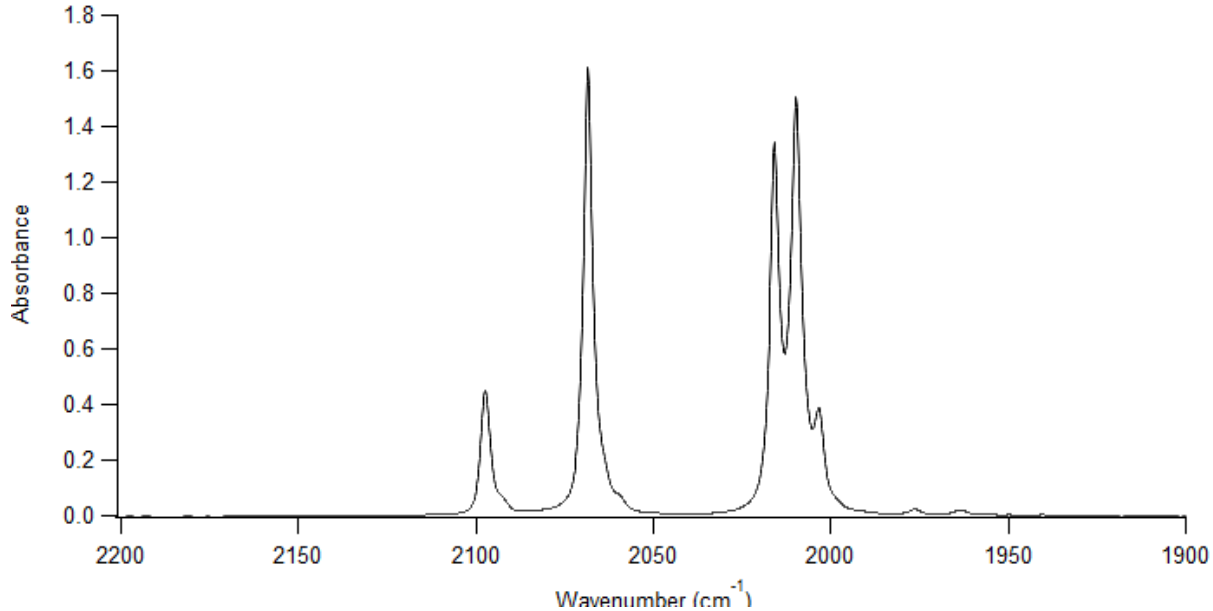

$Os_2(CO)_6I_2$ in hexanes. Byproduct from microwave synthesis. Peaks at 2097(m), 2068(s), 2016(s), 2010(s), and 2003(m) cm^{-1}

Triosmium decacarbonyl diiodide, $Os_3(CO)_{10}I_2$

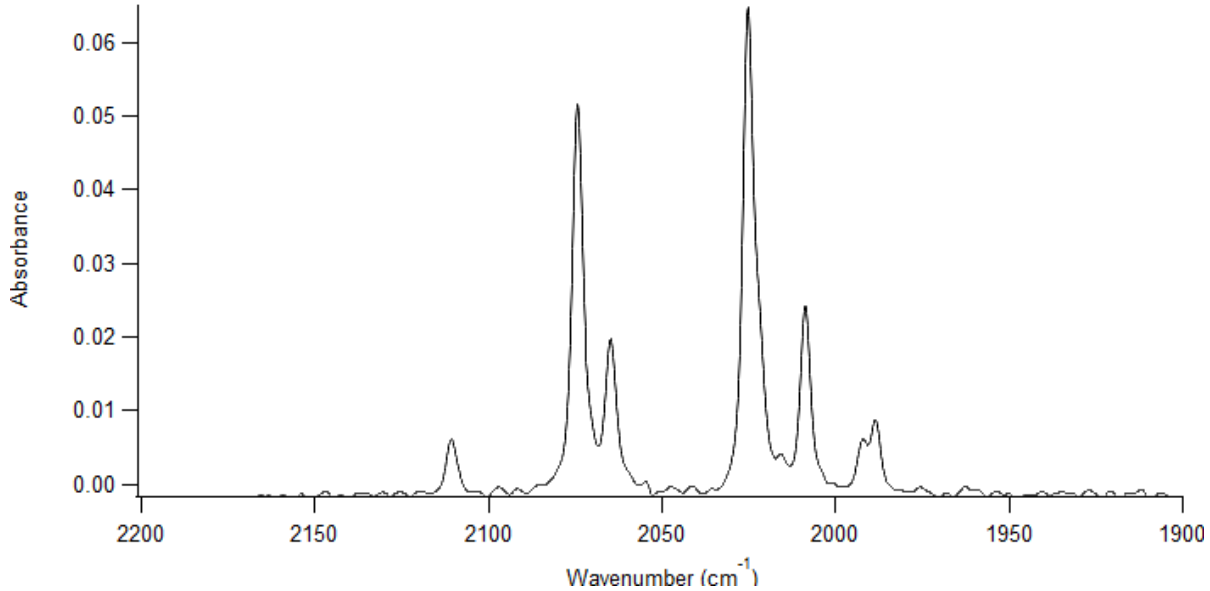

$Os_3(CO)_{10}I_2$ in hexanes. Peaks at 2010(w), 2074(s), 2065(m), 2025(s), 2009(m), 1992(w), and 1989(w) cm^{-1}

$Os_3(CO)_9I_2[P(OMe)_3]$

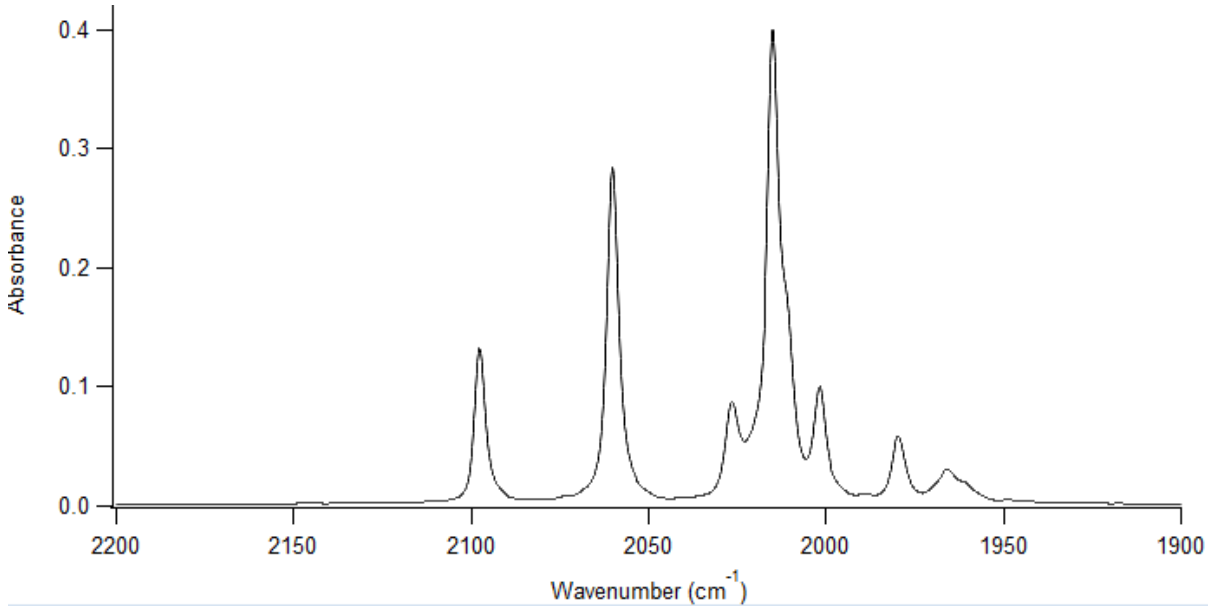

$Os_3(CO)_9I_2[P(OMe)_3]$ in hexanes from Me_3NO synthetic "shortcut." Peaks at 2097(m), 2060(s), 2026(w), 2015(s), 2001(w), 1980(w), and 1966(w) cm^{-1}

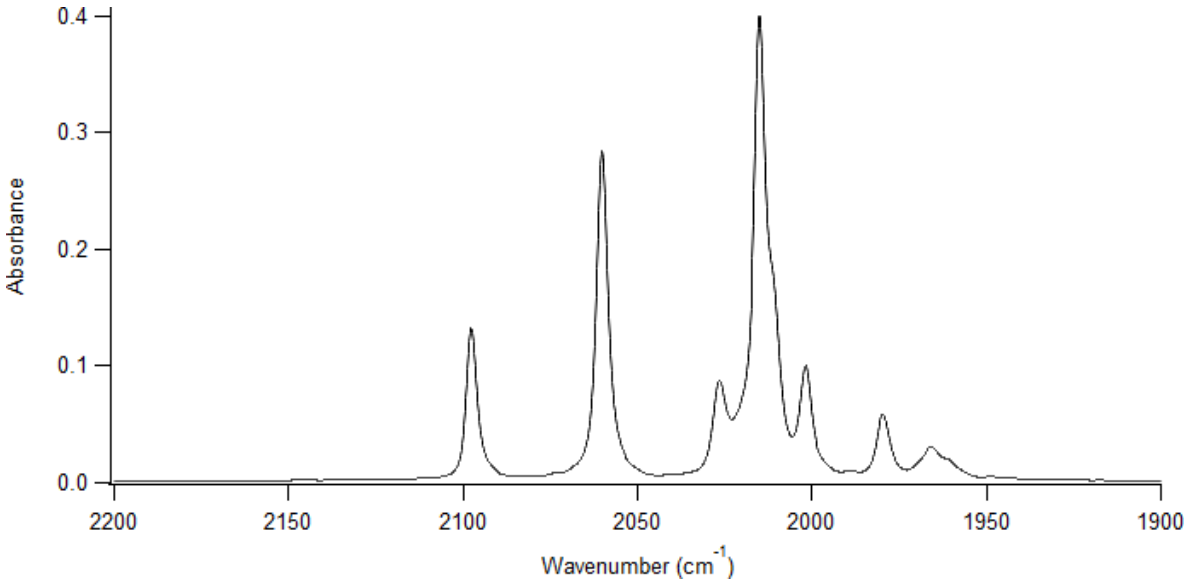

$Os_3(CO)_9I_2[P(OMe)_3]$ in hexanes. Intermediate compound of kinetic trials. Peaks at 2097(m), 2060(s), 2026(w), 2015(s), 2001(w), 1980(w), and 1966(w) cm^{-1}

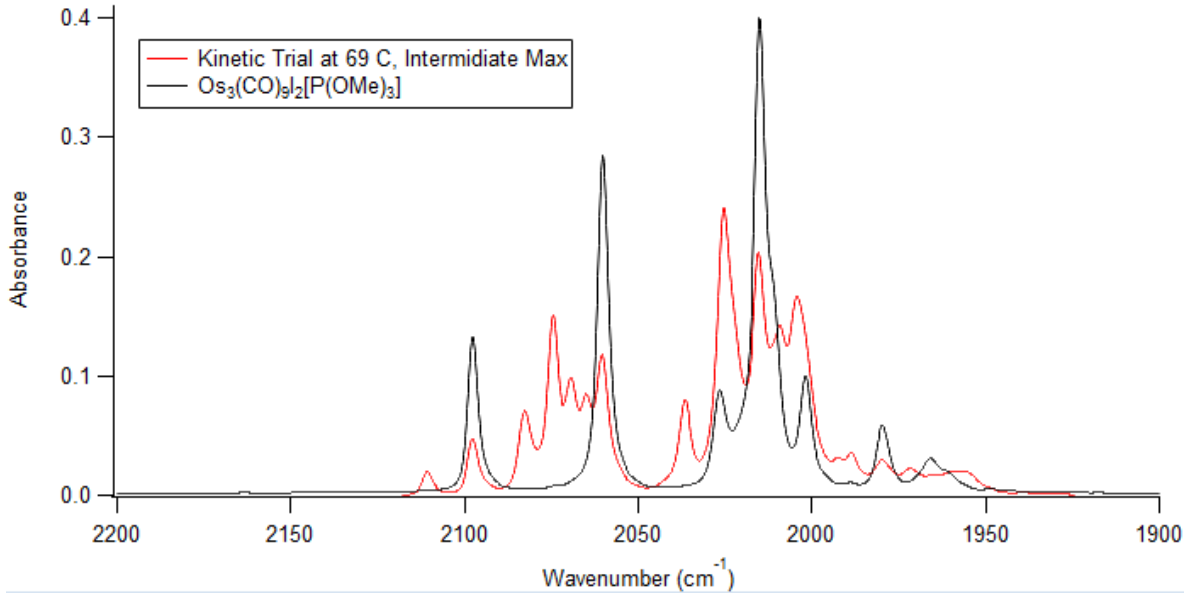

Spectral overlay of $Os_3(CO)_{10}I_2[P(OMe)_3]$ by synthetic "short cut" taken in hexanes, shown in black, against kinetic trial run in hexanes at intermediate max height. This confirms that the intermediate compound observed in kinetic trials is indeed this monosubstituted cluster.

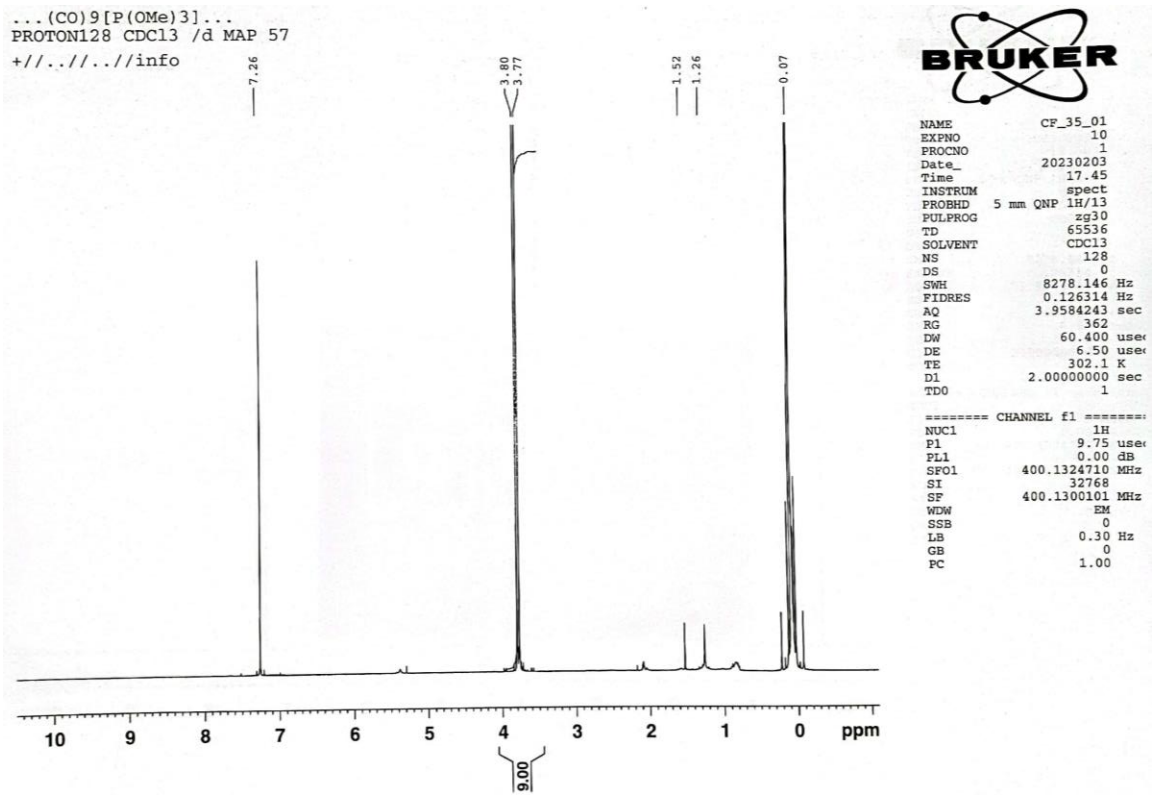

$Os_3(CO)_9I_2[P(OMe)_3]$ ^1H NMR in $CDCl_3$. Intermediate compound of kinetic trials. $P(OMe)_3$ appears as a doublet at 3.80 and 3.77 ppm.

$Os_3(CO)_8I_2[P(OMe)_3]_2$

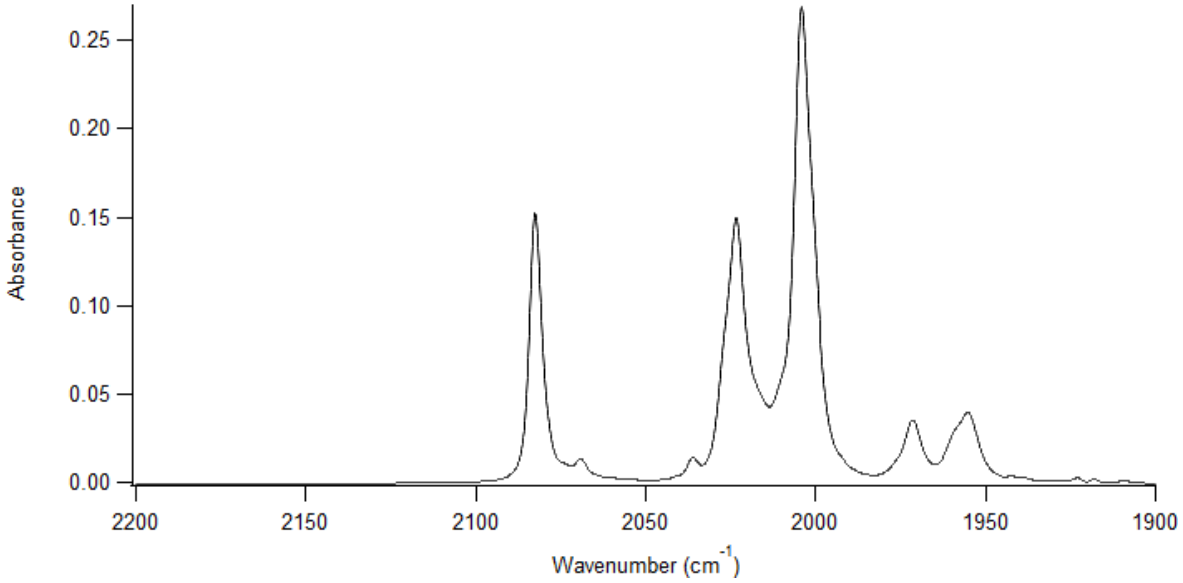

$Os_3(CO)_8I_2[P(OMe)_3]_2$ in hexanes. Final product of kinetic trials. Peaks at 2082(s), 2023(s), 2004(s), 1971(w), and 1955(w) cm^{-1}

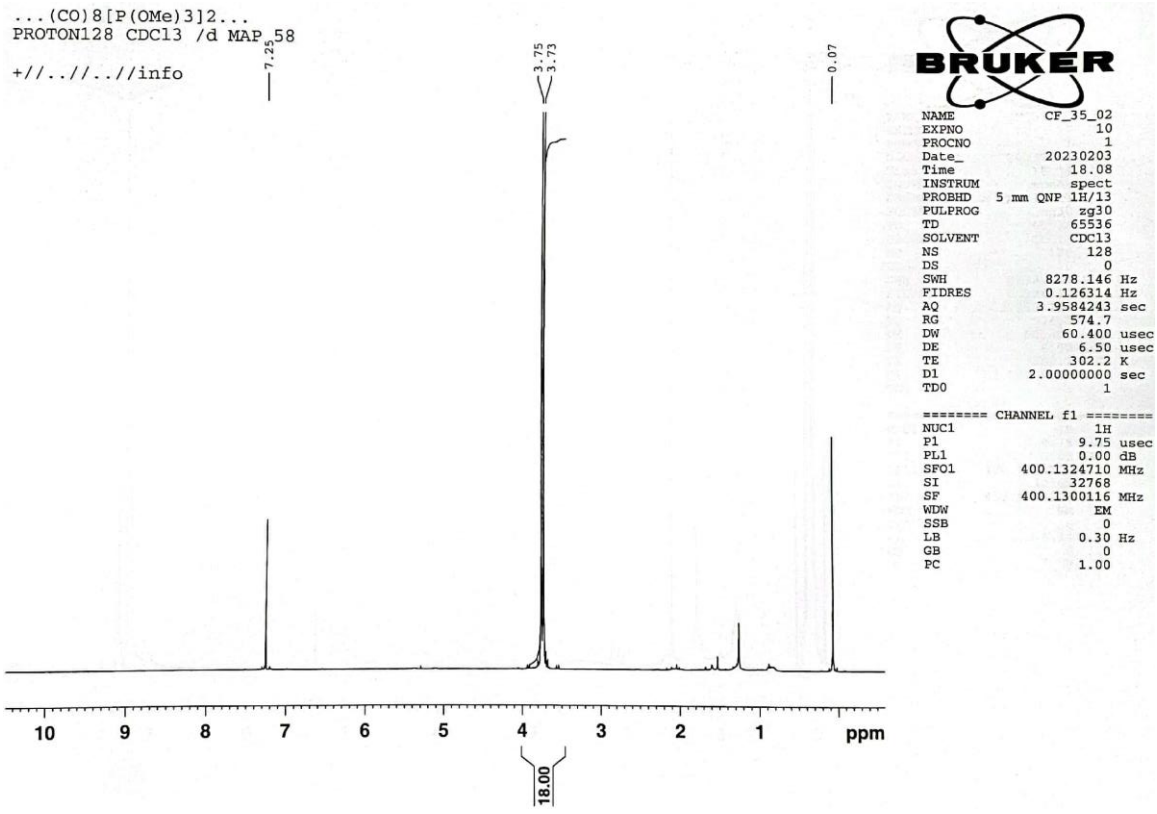

$Os_3(CO)_8I_2[P(OMe)_3]_2$ ^1H NMR in $CDCl_3$. Final product of kinetic trials. P(OMe)3 appears as a doublet at 3.75 and 3.73 ppm.

$Os_3(CO)_9I_2[P(OPh)_3]$

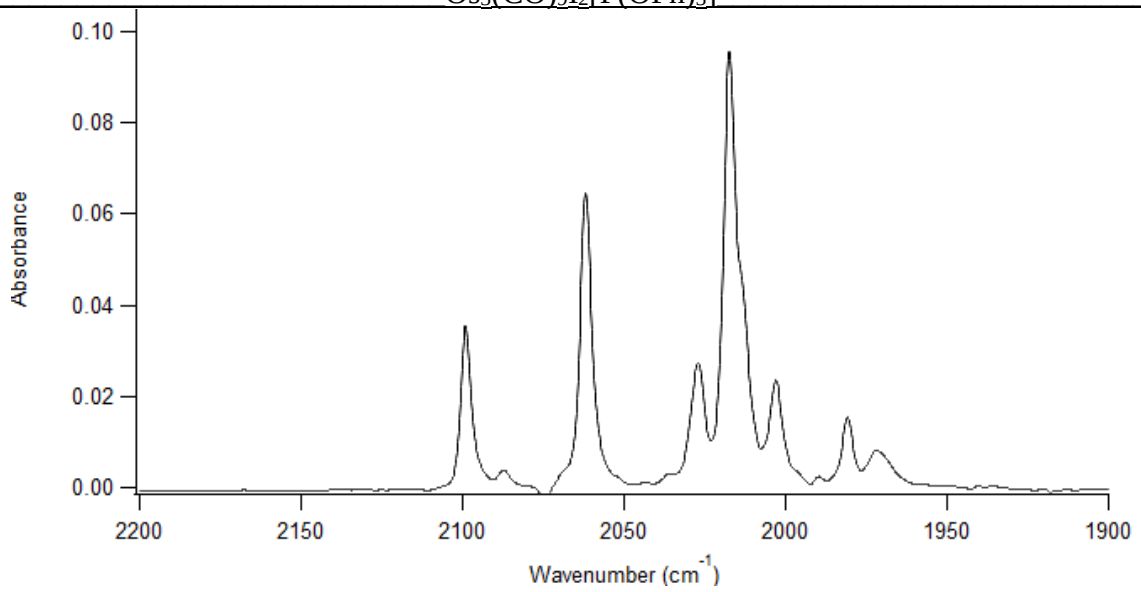

$Os_3(CO)_9I_2[P(OPh)_3]$ in hexanes. Intermediate from kinetic trials Peaks at 2099, 2061, 2027, 2017, 2002, 1980, and 1971 cm^{-1}.

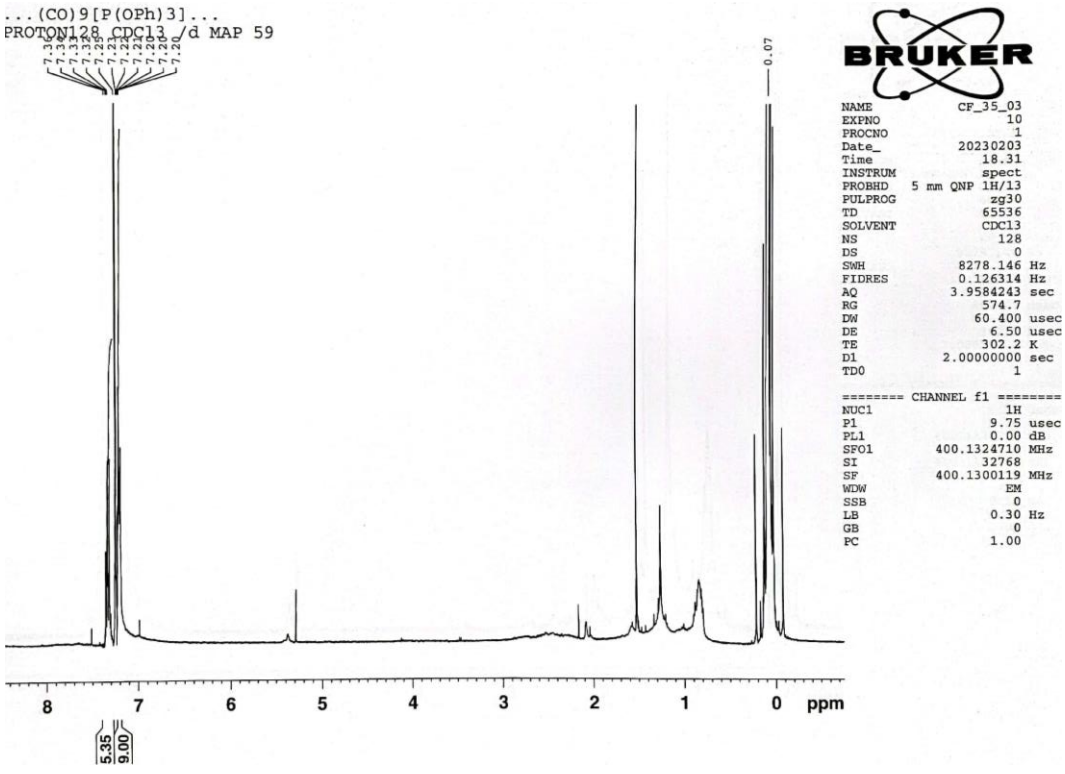

$Os_3(CO)_9I_2[P(OPh)_3]$ ^1H NMR in $CDCl_3$. Intermediate from kinetic trials. $P(OPh)_3$ appears as multiplets between 7.20 and 7.36 ppm. Note: $CDCl_3$ solvent peak appears at 7.25 ppm in this spectrum, splitting the peaks of interest

$Os_3(CO)_8I_2[P(OPh)_3]_2$

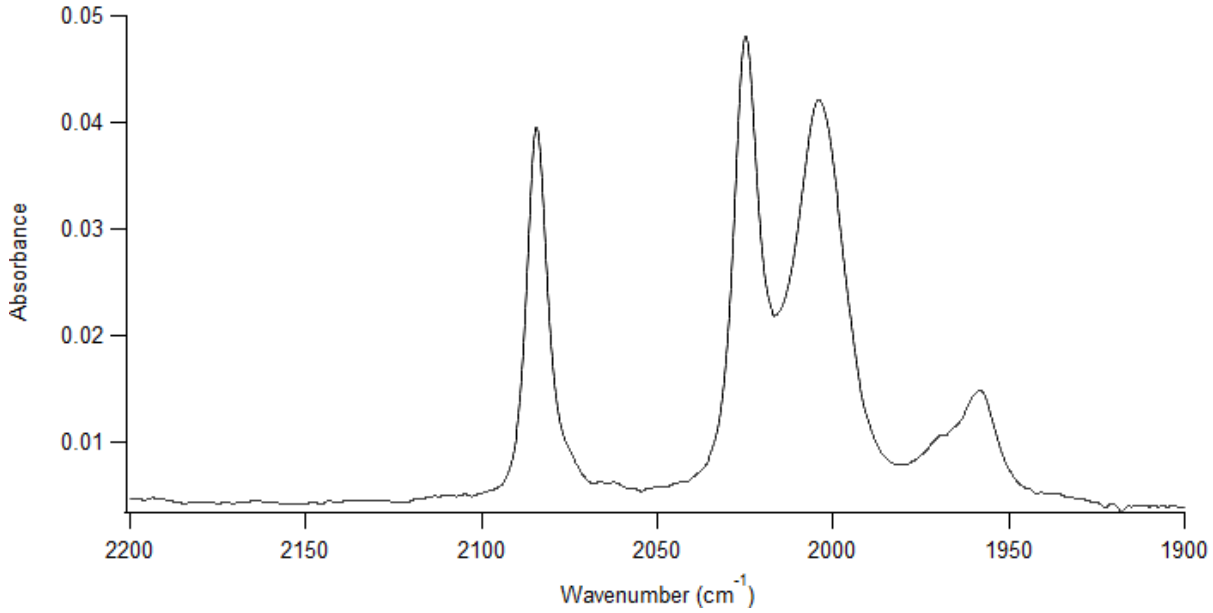

$Os_3(CO)_8I_2[P(OPh)_3]_2$ in hexanes. Final product of kinetic trials. Peaks at 2087(s), 2027(s), 2010(s), 1974(w), 1965(w) cm^{-1}

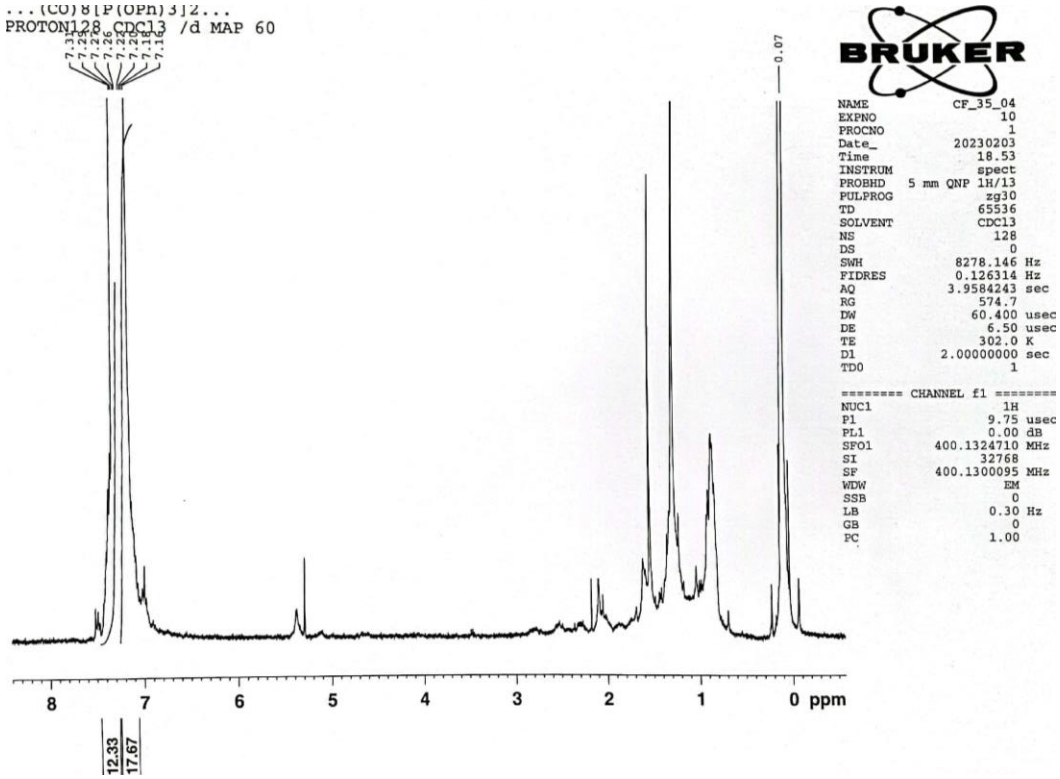

$Os_3(CO)_8I_2[P(OPh)_3]_2$ ^1H NMR in $CDCl_3$. Final product of kinetic trials. $P(OPh)_3$ appears as multiplets between 7.16 and 7.31 ppm. Note(s): $CDCl_3$ appears at 7.26 in this spectrum, splitting the peaks of interest. Additionally, the concentration of this sample is so minute, impurity peaks were augmented due to appropriate scaling of peaks of interest. A good demonstration of this effect is seen in the size of the spin-coupling peaks surrounding the TMS standard (-0.07).

References

1. Cotton, F. A; Wilkinson G. Organometallic compounds in homogenous catalytic reactions. In *Advanced Analytical Chemistry*, 5th ed. Wiley, New York, **1988**

2. Klein, D. R. Aldehydes and Ketones. In *Organic Chemistry as a Second Language*, 4th ed. Wiley: Hoboken, NJ, 2021; 904-957.

3. Obligacion, J. V.; Chirik, P. J. Earth-abundant transition metal catalysts for alkene hydrosilation and hydroboration. *Nature Reviews Chemistry* **2018** *iss*(2), 15-34. https://doi.org/10.1038/s41570-018-0001-2

4. Bunten, K. A; Farrar, D. H; Poë, A. J; Lough, A. J. Chelation Kinetics of Bidentate Phosphine Ligands on Pentacoordinate Ruthenium Carbonyl Complexes *Organometallics* **2000** *19* (18), 3674-3682. DOI: 10.1021/om000289t

5. Poe, A.; Sekhar, V. C. "Substitution and fragmentation kinetics of $Os_3(CO)_{12}$, $Os_3(CO)_{11}$(P-n-Bu_3), and $Os_3(CO)_{10}$(P-n-$Bu_3)_2$" *Inorganic Chemistry* **1985** *24* (25), 4376-4380 DOI: 10.1021/ic00219a035

6. Chen, L. and Poe, A. J. Systematic substituent effects on dissociative substitution kinetics of ruthenium carbonyl, Ru(CO)4L, complexes (L = phosphorus, arsenic, and antimony donor ligands). *Inorganic Chemistry* **1989** *28* (19), 3641-3647. DOI: 10.1021/ic00318a006

7. Shen, J. K; Basolo, F. Intramolecular activation of metal carbonyl cluster complexes. Kinetics and mechanism of ligand substitution reactions of $[Os3(CO)10LX]^-$ (L = PPh3, CO; X = Cl, Br, I, NCO). Organometallics **1993** 12 (8), 2942-2946 DOI: 10.1021/om00032a015

8. Parker, M; Pearsall, M. Reactions of and synthetic approaches to $Os_3(CO)_{10}(OEt)_2$ and the kinetics of osmium carbonyl clusters using triphenyl phosphite. Honors Thesis, Drew University, Madison, NJ. **2007**

9. Schmitt, L; Pearsall, M. Steric effects on the reactions of trisomium decacarbonyl bisethoxide and carboxylic acids. Honors Thesis, Drew University, Madison, NJ. **2013**

10. Baum, B. E.; Pearsall, M. An investigation of the kinetics of the disubstitution reaction of triosmium complexes of type $Os_3(CO)_{10}(\mu^2\text{-}X)_2$ (X = Cl, Br, I, OMe, OEt, OiPr, OtBu, OPh) with trimethyl phosphite. Honors Thesis, Drew University, Madison, NJ. **2004**

11. Cavaliere, V; Pearsall, M. Substitution Kinetics of Dihalo-bridged Triosmium Complexes. Honors Thesis, Drew University, Madison, NJ. **2006**

12. Bradford, J; Pearsall, M. A Kinetic Analysis of the Ligand Substitution reaction of Os3(CO)10I2 and P(OC6H5)3. Unpublished Results, Drew University, Madison, NJ. **2020**

13. Farrar, D. H.; Hao, J.; Poë, A. J.; Stromnova, T. A. The Aryl Effect in Disubstituted Dimanganese and Dicobalt Carbonyls. Organometallics **1997**, 16 (13), 2827–2832.

14. Bunten, K. A.; Farrar, D. H.; Poë, A. J. Potential Energy Surfaces in Transition States for Associative Reactions of Metal Carbonyl Clusters: Reactions of Rh4(CO)12 with P-donor Nucleophiles. *Organometallics* **2003,** *22* (17), 3448-3454. DOI: 10.1021/om030071h

15. Tolman, C. Steric Effects of Phosphorus Ligands in Organometallic Chemistry and Homogenous Catalysis. *Chem Rev* **1977** *77* (3), 313-348. DOI: 10.1021/cr60307a002

16. Barnum, T. J.; Pearsall, M. Synthesis and Theoretical Analysis of Dibridged Triosmium Carbonyl Clusters. Honors Thesis, Drew University, Madison, NJ. **2013**

17. Sommerhalter, R. E; Pearsall, M. New synthetic approaches to triosmium decacarbonyl bisethoxide and the systematic design of linked triosmium clusters via bridging diols. Honors Thesis, Drew University, Madison, NJ. **2016**

18. Steigel, A.; Sauer, J.; Kleier, D. A. ; Binsch, G. Nitrogen analogs of cycloheptatrienes and narcaradiences: A nuclear magnetic resonance study of their thermodynamic and kinetic properties. *Journal of the American Chemical Society 94*(8): 2770-2779. **1972**

19. Morse, P. M.; Spencer, M. D.; Wilson, S. R.; Girolami, G. S. A static agnostic α-CH···M interaction observable by NMR spectroscopy: Synthesis of the chromium(II) alkyl $[Cr_2(CH_2SiMe_3)_6]^{2-}$ andits conversion to the unusual "windowpane" bis(metallacycle) complex $[Cr(k^2C,C'\text{-}CH_2SiMe_2CH_2)_2]^{2-}$. *Organometallics* 13, 1646-1655. **1994**

20. Poe, A; Twigg, M. M. Reaction mechanisms of metal-metal bonded carbonyls. IX. Reaction of tributylphosphine with doceacarbonyltriruthenium and tetracarbonyl(tributylphosphine)ruthenium. *Inorganic Chemistry* **1974** *13*(12), 2982-2985.

21. Brodie, N. M. J; Poë, A. J. Systematic substitution kinetics of the clusters $Ru_3(CO)_{11}L$ and $Ru_3(CO)_{10}L_2$ (L = P-donor ligands): The unimolecular path. *Canadian Journal of Chemistry* **73**(7): 1187-1195. https://doi.org/10.1139/v95-146

22. Willson, B; Pearsall, M. Microwave synthesis of $Os_3(CO)_{10}I_2$; Method development. Unpublished results, Drew University, Madison, NJ. **2021**

23. Shen, J., Shi, Y., Gao, Y., Shi, Q., and Basolo, F. Oxygen atom transfer reactions to metal carbonyls. Kinetics and mechanism of CO substitution reactions of M3(CO)12 (M = Fe, Ru, Os) in the presence of (CH3)3NO. *Journal of the American Chemical Society* **1988** *110* (8), 2414-2418 DOI: 10.1021/ja00216a013

24. Jackson, R. A., Poe, A. Reactions mechanisms of metal-metal bonded carbonyls (18) Kinetic measurement of the strengths of some metal-metal bonds. *Inorganic Chemistry* **1978** 17(4), 997-1003.

25. Einstein, F. W. B.; Jones, T.; Tyers, K. G. Structure of 1,1,1,1,2,2,2,3,3,3-decacarbonyl-2,3;2,3-di-μ-chloro-*triangulo*-triosmium. In *Cambridge Structural Database*; CCDC, uploaded May 05, 1988. https://www.ccdc.cam.ac.uk/structures/Search?Ccdcid=1158634&DatabaseToSearch=Published

26. Pearsall, M. Crystal structures of some trisomium carbonyl clusters. Unpublished results, Madison, NJ, **2013**